DEVELOPMENT OF A PLASMONIC BIOSENSOR FOR DETECTION OF EXOSOMES

A Thesis Submitted to
the Graduate School of
İzmir Institute of Technology
in Partial Fulfillment of the Requirements for the Degree of

DOCTOR OF PHILOSOPHY

in Chemical Engineering

by
Damla TAYKOZ

July, 2020
İZMİR

ACKNOWLEDGMENTS

I would love to thank my advisor, Dr. Volga Bulmuş for her help. She has set an example of excellent researcher, mentor, and instructor to me**.** I have learned so much from her during this process. I also thank my co-advisor Dr. Cumhur Tekin for the discussions as well as my scientific committee Dr. Sacide Alsoy Altınkaya and Dr. Başak Sürmeli during these 4 years.

Some part of this thesis took place in University of Washington (UW), Seattle, USA thanks to the scholarship 2214/A from the Scientific and Technological Research Council of Turkey. I also would like to thank two NIH grants NIBIB P41 EB002027 and NIH Grant# 61-1140 (Placentomics). I would love to thank Dr. Patrick Stayton as well as his research team; Selvi Srinivasan, Debashish Roy, Clare LeGuyader and Ciana Lopez for their help and friendships during the times of Seattle-freeze. I am very grateful to Dr. James Lai for his precious ideas and discussion as well as his help with some of the experiments. I would like to thank Dr. Lara Gamble and Dr. David Castner for valuable discussions and letting me use their facilities. I also thank to the staff of Molecular Analysis Facility of UW; Scott Braswell, Samantha Young and Micah Glaz for their help and guidance with the experiments and Corin Shelley-Reuss with my life in Seattle. Also, I would like to thank Winston Ciridon for everything; Zirui Fu for HPLC experiments, Lucia Vojtech for semen exosome samples. Finally, I would like to express my gratefulness to "güzel arkadaşım" Rebekah Perkins for being there for me every time I need, as well as Pablo, Eva, Yi, Aiwen, Hollis, Catrina, Miguel and Lindsay.

Also, I would like to thank the staff of Biotechnology and Bioengineering Research and Application Center, IZTECH, especially Yekta Günay Oğuz for DLS, zeta and FTIR experiments and Özgür Okur for motivation talks and special recipes. I am grateful to Dr. Devrim Pesen Okvur, Dr. Özden Yalçın Özuysal and Dr. Aslı Kısım for providing me cancer exosome samples. I would like to thank to members of Sürmeli Lab: Gülce Güralp and Tuğçe Sakallı for their help with SDS experiments.

I would like to thank to current and ex-members of Bulmuş group; Aysel Tomak, Gürbüz Dursun, Cansu Söylemez, Ecem Önal, Sinem Toksabay, Fazilet Gürer, Aytaç Gül for everything as well as members of other research teams İlayda Özkan, Çağlar Ersanlı and Sedef Tamburacı. Even though when we were at three different continents in three different time zone, Aykut Zelçak and Esra Aydınlıoğlu listened, understood, and helped me during this PhD. Sibel Değer and Seren Şen also listened me constantly and gave me precious ideas, thanks to them.

Although we have met outside of a research purpose, Seda Duman, İrem Pehlivanoğlu, Cem Bakkal and Bahadır Ayaz listened me very carefully and constantly and cheered me up all the time that helped me to keep my mental health together.

There are not enough words for how to thank Ceren Süngüç, Mehmet Çağlıyangil, Babto from losbabtos (Hakan Mehmet Doğan), Ece Akça Doğan and Çağlar Aktepe for constantly checking me if I am doing OK, being there for me and giving me precious ideas even though I am not acting on them. My ex-flatmate Çiğdem Kahraman Bıyıklı is also responsible for this thesis to happen and little Tomris Bıyıklı is responsible for keep me going. Last two years of the thesis was the hardest part, and Meltem Şan was exposed to all my breakdowns and embraced them and walked me through this door in the end of the thesis although “it was the end, my friend”.

Finally, I thank all my family for supporting me during all my education for 26 years. I dedicated this thesis to my aunt, Asuman Eren Küçük, who recently passed away with all her interest about this work and her proud on me with getting my PhD degree. Special thanks go to my dear mother Armağan Taykoz; my dear father Fikret Taykoz; my only and dearest sister Merve Taykoz and another sister to me Vahide Segah Üney for letting me through these days. They are the most patient, honest, and loving people in my life.

ABSTRACT

DEVELOPMENT OF A PLASMONIC BIOSENSOR FOR DETECTION OF EXOSOMES

Aim of this work was to develop Localized Surface Plasmon Resonance (LSPR) surfaces for quantitative detection of exosomes. For this aim, gold nanorods (AuNRs) with a mean diameter of 40 nm and an aspect ratio of 2.9 were synthesized and characterized. PEGylation of cetrimonium bromide (CTAB) stabilized AuNRs was investigated using PEGs with three different molecular weights. PEGylated AuNRs were further self-assembled on silanized glass slides. Surface functionalization of AuNR patterned slides was performed using alkane thiol molecules having carboxylic acid and hydroxyl functional groups. Specific antibodies (Ab) were conjugated to surface following two different methods, i.e. click and NHS/EDC chemistry. To perform click chemistry strategy, ImmuneLink® was conjugated with Abs and the final conjugate was used to functionalize surfaces prepared beforehand using azide bearing molecules. Orientation of the antibodies on AuNRs patterned surfaces was investigated with LSPR in comparison with conventional EDC/NHS chemistry. The click-chemistry strategy proved to provide conjugation of antibodies through Fc regions exposing Fab regions better for antigen recognition. Finally, surfaces functionalized with a variety of antibodies via click chemistry were used to detect a pregnancy-associated protein, PLAP, and exosomes obtained from human semen samples with pre-determined exosome concentrations. LoD of biosensor surfaces was found to be between 10^3-10^4 exosomes/mL and 5 ng/mL (86 pM) PLAP. Samples having an unknown concentration of exosomes were further analyzed using newly developed LSPR biochips and exosome concentration was determined as 10^8 exosomes/mL for MCF-7 cell line and 10^7 exosomes/mL for MDA-MB-231 cell line, in accord with the relevant literature.

ÖZET

EKSOZOM TAYİNİ İÇİN PLAZMONİK BİYOSENSÖR GELİŞTİRİLMESİ

Bu çalışmanın amacı, farklı kaynaklardan eksozomların nicel tayini için lokalize yüzey plazmon rezonans (LSPR) yüzeyleri geliştirmektir. Bu amaçla, ortalama 40 nm çapında 2.9'luk boy:en oranına sahip altın nanoçubuklar sentezlenmiş ve karakterizasyonları yapılmıştır. Ardından, altın nanoçubukların cam yüzeyler üzerinde kendiliğinden organizasyonları çeşitli deneyler ile optimize edilmiştir. Paralelinde, sitrinum bromür (CTAB) ile stabilize edilmiş altın nanoçubukların üç farklı molekül ağırlığındaki PEGler ile PEGilasyonu ayrıntılı olarak incelenmiş ve altın nanoçubukların PEGilasyonu için optimum koşullar LSPR, zeta potansiyel ölçümü ve XPS kullanılarak belirlenmiştir. PEGlenmiş altın nanoçubukların silanlanmış mikroskop lamları üzerinde kendiliğinden organizasyonu sağlanmış ve sonuçlar LSPR, XPS ve zeta potansiyel ölçümü ile onaylanmıştır. Altın nanoçubukların yüzeyleri, karboksilik asit ve hidroksil fonksiyonel gruplarını içeren küçük alkan tiyol molekülleri kullanılarak fonksiyonelleştirilmiştir. Bu, XPS, FTIR ve zeta potansiyel ölçümleri ile doğrulanmıştır. İlgili spesifik antikorlar EDC/NHS kimyası ve klik kimyası kullanılarak yüzeylere bağlanmıştır. Klik kimyası için, ImmuneLink ® molekülü spesifik antikorlar ile konjuge edilmiş ve bu konjugatlar önceden azid ile fonksiyonelleştirilmiş yüzeylere bağlanmıştır. Bu fonksiyonelleştirme XPS, LSPR ve FTIR ile gösterilmiştir. Altın nanoçubuk desenine sahip yüzeyler üzerindeki antikorların yönlenmesi, EDC/NHS kimyası ile fonksiyonelleştirilmiş yüzeylerle karşılaştırmalı olarak LSPR ile kontrol edilmiştir. Klik kimyası ile hazırlanmış yüzeylerde antikorların Fc bölgelerinden bağlanma sağlayarak antijen tanımaya yönelik Fab bölgelerini açıkta bırakacak şekilde yönlendiği kanıtlanmıştır. Son olarak yüzeyler, farklı antikorlar ile modifiye edilerek, hem hamilelik sırasında ortaya çıkan protein, PLAP, hem de konsantrasyonu önceden belirlenmiş olan insan sperm eksozomları ile test edilmiştir. Yüzeylerin tanıma alt limiti 10^3 -10^4 eksozom/mL ve 5 ng/mL (86 pM) PLAP olarak bulunmuştur. Son olarak, hazırlanan LSPR biyoçipler, insan meme kanseri hücre kültürleri içinde bilinmeyen konsantrasyondaki eksozomların nicel tayini için kullanılmıştır. Eksozom konsantrasyonları MCF-7 hücre kültürü için 10^8 eksozom/mL ve MDA-MB-231 hücre kültürü için 10^7 eksozom/mL olarak bulunmuştur.

to my aunt Asuman Eren Küçük

TABLE OF CONTENTS

LIST OF FIGURES

Figure	**Page**

<u>Figure</u> **<u>Page</u>**

ABBREVATIONS

SYMBOL	DESCRIPTION
EVs	Extracellular vesicles
MVs	Microvesicles
Ex	Exosomes
LoD	Limit of detection
APTES	3-Aminopropyl)triethoxysilane
MPTMS	3-Mercaptopropyl)trimethoxysilane
PEG	Polyethylene glycol
AuNRs	Gold nanorods
PLAP	Placental alkaline phosphatase
5K PEG	Molecular weight 5000 Da PEG
2K PEG	Molecular weight 2000 Da PEG
1K PEG	Molecular weight 1000 Da PEG
5K PEGylated AuNRs	5000 Da PEG stabilized gold nanorods
2K PEGylated AuNRs	2000 Da PEG stabilized gold nanorods
1K PEGylated AuNRs	1000 Da PEG stabilized gold nanorods
PBS	Phosphate buffered saline
COOH	11-Mercaptoundecanoic acid
OH	11-Mercapto-1-undecanol
N3	Bis(11-azidoundecyl) disulfide
BN3	Before azide functionalization of the surface
AN3	After azide functionalization of the surface
DBCO	Dibenzocyclooctyne
λ_{max}	Maximum wavelength
RIU	Refractive index unit
IL	ImmuneLink^{TM}
Ab	Antibody
DBCO-IL-Ab	DBCO carrying ImmuneLink^{TM} conjugated with antibody

CHAPTER 1

INTRODUCTION

Extracellular vesicles (EVs) are defined as vesicles that are released from the cell membranes. They can be in three different forms as exosomes, microvesicles and apoptotic structures. All these types of vesicles play an important role for cell-cell interactions through their protein and RNA contents. Recently, the important role of EVs have been discovered during formation and progress of diseases (Raposo and Stoorvogel 2013). EVs are mostly found in biological fluids such as blood, saliva and urine (Thakur et al. 2017). The role of EVs for the detection and treatment of a disease has gained more and more attention during recent years (Munson and Shukla 2015). Exosomes (Ex), which are subtypes of EVs, have nanoscale sizes (40-120 nm) and have densities of about 1.12-1.19 g/mL. Ex have roles in translation, angiogenesis, proliferation, metabolism and apoptosis activities of the cells (Mitchell et al. 2015). Purified Ex exist in concentrations around 10^9-10^{12} particles/mL in all body fluids and exosomes bearing disease-specific protein markers are found to increase in concentration throughout diseases (Fernando et al. 2017). In conclusion, detection of EVs including Ex emerged to have great potential either in normal or disease related biological processes.

Exosomes are known to have an enriched amount of tetraspanin proteins (CD9, CD63, CD81) on their membrane which segregate them from other generic plasma and lysosomal membrane proteins (Pegtel and Gould 2019). Most of the techniques for the separation of exosomes focus on isolation of exosomes using their tetraspanins. There are several techniques for the detection of exosomes. These can be listed as follows: molecular imaging techniques (Gangadaran, Hong, and Ahn 2017), nanoplasmon-enhanced scattering (nPES) (Liang et al. 2017), normal or microarray based plasmonic techniques (Grasso et al. 2015; Im et al. 2014; Rupert et al. 2014), fluorescently labelled exosome detection via a standard plate reader through microfluidic chips (Kanwar et al. 2014), using calorimetric methods with alternating current electrohydrodynamics in microsystems (Vaidyanathan et al. 2014), graphene oxide microfluidic platforms working with enzyme-linked immunosorbent assay (ELISA) principle (Zhang, He, and Zeng 2016) and conventional methods like ELISA or polymerase chain reaction (PCR). There have been also a number of studies reported to improve methodologies for the isolation of EVs (Liga et al. 2015). Among these isolation studies, two articles reported the detection of genetic material from exosomes using Localized Surface Plasmon Resonance (LSPR). These studies focused on exosome material detection (already isolated) such as RNAs (Joshi et al. 2015; Shao et al. 2015). The studies about direct detection of exosomes via LSPR is based on creating self-assembled gold nano-island (SAM-AuNIs) surfaces and distinguishing cancer exosomes from other exosomes (Thakur et al. 2017) and creating gold nanopillars to detect exosomes (Raghu et al. 2018). Raghu et. al. successfully detected exosomes with a limit of detection (LoD) of 10^5 particles/mL using CD63 proteins on exosomes that are derived from MCF7 breast adenocarcinoma cells. Thakur et. al. found a LoD of 0.194 µg/mL for A549 cancer cell derived exosomes using CD9 proteins. A recent study using LSPR to detect exosomes via anti-CD63 antibodies showed a limit of detection of 1 ng/mL (Lv et al. 2019) (calculated as approx. between 10^7-$2x10^6$ particles/mL with calculation of assuming all exosome diameters are same and between 50-100 nm along with an average density of 1.2 g/mL (Konoshenko et al. 2018)).

LSPR method has been widely used for detection of biomolecules because it has high sensitivity to short range environmental changes compared to bulk changes (SPR). This phenomenon is explained by the shorter electromagnetic decay length (EM) of nanoparticles in LSPR compared to metal coatings in SPR. EM of nanoparticles is 40-50 times lower than metal coatings and this enables the application of the LSPR technique to smaller volumes (Haynes, McFarland, and Van Duyne 2005). Furthermore, incorporation of nanoparticles to a sensing system has the advantage of flexibility in designing the experiments such as application to smaller volume of analytes, ease of alteration for the size and shape of the nanoparticles which finally yields to enhanced response, etc. (Sherry et al. 2005). In summary, the LSPR technique has advantages over the SPR technique by means of design flexibility and small volume detections.

The aim of this thesis is to develop LSPR biosensor surfaces with enhanced sensitivity for quantitative detection of exosomes. For this aim, different types of glass wafers were first silanized with different types of silane bearing molecules. Separately, gold nanorods (AuNRs) were prepared via seed-mediated synthesis method and PEGylated using three different molecular weight PEGs (1 kDa, 2 kDa and 5 kDa). These PEG-stabilized AuNRs were then self-assembled on silanized glass wafers with different methodologies via bottom-up surface development technique. The AuNRs patterned surfaces were checked for their sensitivity via LSPR. The results were supported with

SEM and XPS experiments. After the optimization of the methodologies to obtain repeatable and homogeneous AuNR patterned glass wafers, the study continued with the surface functionalization of AuNRs on glass wafers with antibodies. Different than the current methods applied in literature, surfaces were not plasma-treated and PEG molecules were deliberately kept around AuNRs for further modifications. Two different methodologies have been investigated to bind antibodies to AuNRs patterned surfaces for LSPR detection; the conventional EDC/NHS chemistry and click chemistry using ImmuneLink® reagent. The click chemistry strategy was utilized to ensure the conjugation Ab molecules through their Fc region to the surfaces, and hence to enhance the sensitivity and limit of detection (LoD) of the prepared surfaces. In this strategy, a commercialized protein-G fragment (Immunlink®) was introduced to the surfaces via click chemistry. LSPR characterization of Ab-functionalization was further supported by zeta-potential experiments, FTIR and RAMAN spectroscopies Antibodies conjugated to the surfaces included rabbit anti-mouse IgG antibodies, mouse anti-human CD63 antibodies and recombinant anti-PLAP antibodies.

Finally, surfaces functionalized with different antibodies were first used to detect, anti-mouse IgGs and a pregnancy-associated protein, PLAP for validation of the surfaces. At the final step, exosomes obtained from human semen samples with pre-determined exosome concentrations were used to identify the LoD and linearity of the surfaces for quantitative detection of exosomes. Human breast cancer cell culture samples having an unknown concentration of exosomes were further analyzed using the newly developed LSPR biochips and the exosome concentrations in unknown samples were determined. All results are presented and discussed in Chapter 4: Results and Discussion.

The innovation and contribution of this thesis to literature are as follows:

(i) In contrast to the literature, PEG molecules around AuNRs were deliberately maintained on the AuNRs patterned surfaces and antibodies were successfully conjugated to the PEGylated surfaces. The results proved that this uncommon methodology inhibited all non-specific binding events in the detectable range.

(ii) To the best of the author’s knowledge, ImmuneLink, which is a relatively new, Fc-specific protein was used for the first time in literature, to functionalize AuNRs patterned glass surfaces with antibodies. This methodology led to LSPR detections with higher sensitivity as it ensured the conjugation of antibodies to the surface through their Fc regions.

(iii) A calibration curve with pre-quantified human semen exosome samples in a wide concentration range was prepared. LoD between 10^3-10^4 exosomes/mL which, to the best of the author's knowledge, is the lowest limit of detection in the literature so far for the LSPR-based surfaces prepared via bottom-up nanoparticle patterning.

(iv) To the best of the author's knowledge, placental alkaline phosphatase (PLAP) detection via an LSPR-based system was performed for the first time in the literature. LoD of 86 pM for PLAP detection was determined. A calibration curve with placental alkaline phosphatase (PLAP) was constructed for the first time in literature.

CHAPTER 2

LITERATURE REVIEW

In this part of the thesis, information about exosomes; definitions; the role of exosomes in biological functions; isolation and quantification techniques for exosomes; LSPR theory and its biological applications, and finally exosome detection via LSPR method have been discussed.

2.1. Definition and Biological Content of Exosomes

Membranous vesicles were first discovered 50 years ago with the assumption of being a waste product that were released from cell through their cell membrane. This was followed by the first discovery of exosomes (Harding, Heuser, and Stahl 1983), 37 years ago, and the first exosome definition came out with the study in 1987 (Johnstone et al. 1987). However, ‘exo’vesicles have been ignored due to the fact about being a waste product from cells until the last decade (Edgar 2016).

Exosomes can be defined as endocytic compartments that are released from cell membranes after endocytic pathway (Raposo and Stoorvogel 2013) and thus exosomes are different than other extracellular vesicles which are microvesicles (MVs) and apoptotic bodies by means of genetic material presence (Osaki and Okada 2019). Exosomes have roles in cell-cell communication along with their ability to carry proteins, lipids, RNA and DNA contents between cells to develop several diseases (Raposo and Stoorvogel 2013). Since exosomes are released by all eukaryotic cells, their content is significantly different depending upon the originated cell type and its current state such as differentiated, stimulated or stressed (Zhang et al. 2019). Their densities are between 1.13 g/mL (B cell-derived) (Bobrie et al. 2011) and 1.19 g/mL (epithelial cell-derived) (Zakharova, Svetlova, and Fomina 2007). The identified contents for exosomes so far are 4400 proteins, 1639 mRNAs, 194 lipids and 764 miRNAs showing the complexity and diversity of exosomes along with their potential (Zhang et al. 2019).

Tetraspanin proteins (CD9, CD63 and CD81) which are responsible from penetration, invasion and fusion are identified as exosomal markers along with stress response proteins (HSP70, HSP90), exosome release proteins (Alix, TSG101) and membrane transport proteins (annexins and Rab) (Vlassov et al. 2012). miRNAs such as miR-1, miR-29a, miR-126, miR-214 and miR-320 are found to exist in exosomes and they are responsible from angiogenesis, hematopoiesis, exocytosis and tumorigenesis through cell-cell communication by exosomes. A summary of exosome content and their known functions can be seen in Figure 2.1.

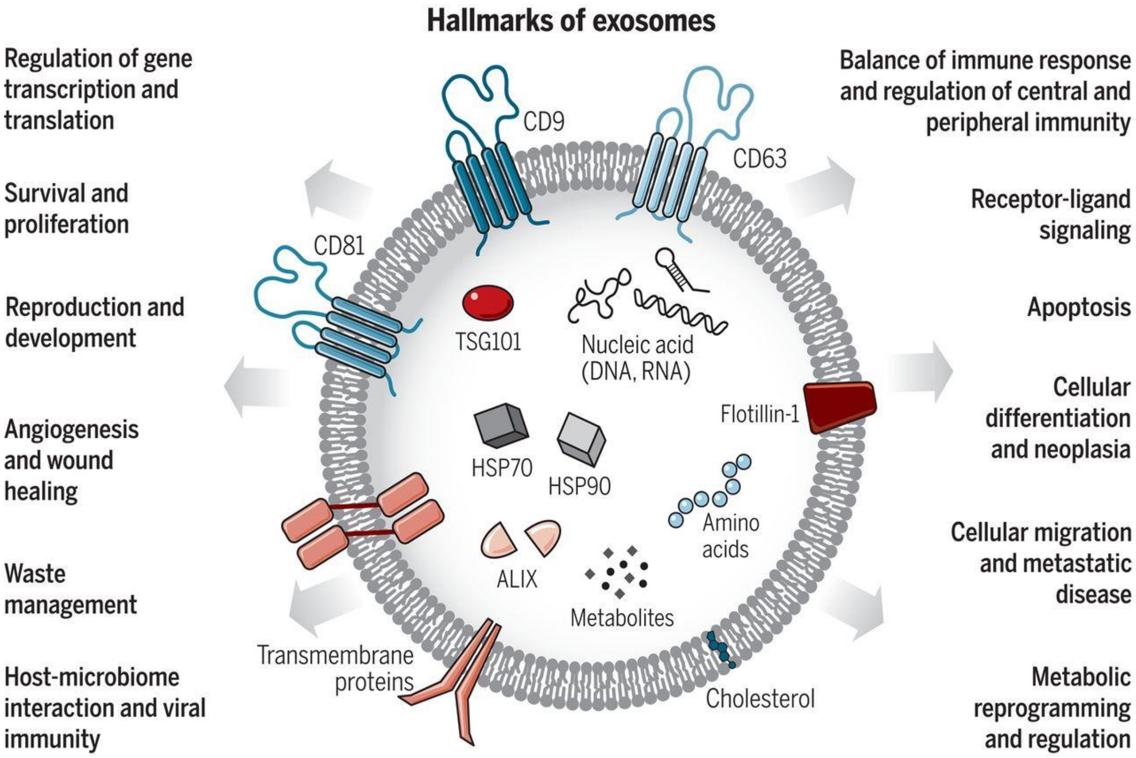

Figure 2.1. The key components and important roles of exosomes in biological functions (Kalluri and LeBleu 2020)

All these properties make exosomes a great candidate as a biomarker for detection of a disease as well as a great therapeutic agent for drug delivery purposes while known unknowns still remain to be challenged (Margolis and Sadovsky 2019).

2.2. The Important Roles of Exosomes in Biological Functions

Exosomes are known to have association with biological functions and conditions such as cardiovascular diseases, pregnancy, central nervous system related diseases, viral pathogenicity, cancer progression and immune responses and so forth (Figure 2.1). These exosomes are found to be responsible either promoting a disease or restraining it. Exosomes can be engineered as targeted drug delivery agents with the ability of delivering siRNAs, antisense oligonucleotides, diverse therapeutic payloads such as chemotherapeutic agents and immune modulators to a desired target through their membrane proteins. While the lipid bilayer structure of exosomes enhances the pharmacokinetic properties, their natural contents may enhance the bioavailability with lowering the immune reactions. Along with their potential therapeutic agent applications, exosomes can be used as biomarkers for disease detection. Exosomes can be found in all biological fluids and they can be easily used as liquid biopsy markers. Furthermore, response to a treatment and disease progression can also be determined via exosomes through their multicomponent analysis (Kalluri and LeBleu 2020; Rahmati et al. 2019; Zhang et al. 2019; Gurunathan et al. 2019; Latifkar et al. 2019; Margolis and Sadovsky 2019).

Exosomes are produced/consumed during the endocytic pathway thus they have the different content and/or membrane bound proteins than other extracellular vesicles. When the late endosome fuses with plasma membrane, exosomes are released outside of the cell or uptaken exosomes are consumed during endocytic pathway and released outside of the cell. Exosomes may vary in size, content and functionality depending upon the source and/or cell origin. The function of exosomes largely depend on their uptake mechanism by the recipient cell (Mulcahy, Pink, and Carter 2014). There are different discovered uptake mechanisms of different cell types for exosomes such as macropinocytosis for human pancreatic cancer cells (Kamerkar et al. 2017), fusion through cell membrane for human melanoma cells (Parolini et al. 2009), clathrin-dependent uptake for neurosecretory cells (Tian et al. 2014). A major drawback for exosomes is the mechanism on action of externally produced and administrated exosomes is still unknown since it will vary depending upon the nature of the cargo exosome and the metabolic status of the recipient cells (Kalluri and LeBleu 2020). The roles of exosomes in different biological functions have been extensively researched and the discoveries so far have been summarized in this section.

Exosomes are known to have roles on many biological functions as well as development of tissue homeostasis (Latifkar et al. 2019). This interesting property of exosomes creates a great potential for applications in regenerative medicine. Stem cells or tissue specialized cells that are differentiated from stem cells are used for transplantation for tissue regeneration and mesenchymal stem cells (MSCs) are considered to be the best stem cell type (Kassem, Kristiansen, and Abdallah 2004). Researchers showed that just the conditioned medium of MSCs was successful to maintain the effects of grafted cells (Timmers et al. 2011) and later more studies have been accomplished on the success of the MSCs derived exosomes in regenerative medicine (Arslan et al. 2013; Teng et al. 2015). Nowadays, exosomes are used in cosmetics such as skin rejuvenation treatments, hand creams, skin whitening and sun tanners.

Exosomes play important roles within immune responses such as restraining and/or activating the activity of B cells, CD8+ and natural killer cells along with increasing the activity of regulatory T cells and suppressing the differentiation of monocytes through their ability to be translocated into any cell type (Rahmati et al. 2019). Also exosomes found to influence the immune response through their ability to transfer DNA or RNA content which will consequently influence gene expression and signal pathways (Montecalvo et al. 2012). Exosomes that are derived from bacteria found to have roles on health and disease stages in hosts (Ahmadi Badi et al. 2017) and they have roles on inflammation either directly or transferring of RNA/DNA content through another recipient cell in host immune system in bacterial infections (Sisquella et al. 2017). They are used as bio-machineries by viruses which eventually promotes the viral infection (Crenshaw et al. 2018) while multiple viruses can be packaged in exosomes which will cause a viral genetic cooperativity (Altan-Bonnet 2016). As a result, different cell types including cancer cells, immune cells (B cells and dendritic cells), epithelial and mesenchymal cells release exosomes with different contents that can have different influences as the proliferation or cytotoxic activity of recipient cells of both the nonspecific and adaptive immune system (Kalluri and LeBleu 2020).

The role of exosomes have been discovered on metabolic diseases such as obesity (Castaño et al. 2018), cachexia (Chitti, Fonseka, and Mathivanan 2018), insulin resistance (Javeed et al. 2015), muscle wasting (Zhang, Liu, et al. 2017) along with neurodegenerative diseases such as Parkinson’s disease (Yuan and Li 2019) and Alzheimer’s disease (Rajendran et al. 2006) via enhancing or limiting the aggregation of proteins in the brain (Budnik, Ruiz-Cañada, and Wendler 2016; Quek and Hill 2017; Levy 2017).

2.2.1. Exosomes in Cancer

The roles of exosomes during cancer progression are very complex and exosomes alter many numbers of cancer related functions (Hanahan and Weinberg 2011; Kalluri and LeBleu 2020). Cancer progression is known to be modulated by immune modulating exosomes that are released from tumor cells as well as they are suspected to be responsible of enabling the spread of metastasis colonization in other organs and further prompt inflammation (Hoshino et al. 2015). Other researchers such as Nabet et. al. has showed that activated (unshielded) RNA (damage-associated molecular pattern (DAMP)) containing exosomes have roles on signaling the stimulation and inflammation in breast cancer (Nabet et al. 2017). On the other hand, Gao et. al. has showed the innate immunity functions, which reduces the defense against viral factors, can be suppressed by lung cancer related exosomes (Gao, Wang, et al. 2018). These controversy studies showed that the functions of exosomes may differ from cell type to cell type as well as with their interaction site. Thus it is not certain whether these effects are model specific and if they have the same effects in humans (Kurywchak, Tavormina, and Kalluri 2018).

Researchers still putting extensive effort to understand the exosome production related inhibitors, differentiation and tracking of exosomes in cancer either by experimentally or theoretically. These accumulating efforts lead to many applications both in therapy and detection of cancer related diseases (Kurywchak, Tavormina, and Kalluri 2018).

2.2.2. Exosomes in Reproductive Systems of Mammalians

Mammalian reproductive systems requires accurate and finely adjusted dynamic communication between cells. Exosomes have important responsibilities for this communication both for male and female reproductive systems. While seminal plasma exosomes have been found to have roles on sperm maturation (Sullivan et al. 2005), also enriched amount of microRNAs (let-7a, let-7b, miR-148a, miR375, miR-99a) in seminal plasma exosomes showed genital-resident immunity which prevents sperms from genital immune system throughout female reproductive tract (Vojtech et al. 2014). Also it has been discovered that seminal plasma exosomes inhibit HIV-1 infection (Madison, Jones, and Okeoma 2015) via blocking early protein of the disease: transcriptional activator (Tat) (Welch et al. 2018).

The placenta is the most important environment for the fetus growth and the survival and all maternal-fetus interactions are controlled within (McNanley and Woods 2008; Linzer and Fisher 1999). Hence, placental exosomes are responsible for cell-cell communications between placental and maternal body and along with preparation of maternal organs for metabolic changes (Burnett and Nowak 2016). The role of exosomes during pregnancy starts from as early as the first trimester and increases until term (Jin and Menon 2018). Since they carry the cell specificities, placental exosomes are expected to provide unique information during pregnancy (Pillay et al. 2016).

Placental-type alkaline phosphatase (PLAP) was found to be a unique marker for placental exosomes (Mincheva-Nilsson and Baranov 2014; Sabapatha, Gercel-Taylor, and Taylor 2006). This placental-type alkaline phosphatase is different from alkaline phosphatase that presents in all tissues with lack of last 24 amino acids and increased chemical resistance, heat stability with high specificity (Salomon et al. 2014). The different roles of placental exosomes during normal pregnancies are maternal-fetal communication (Chang et al. 2017), gene information transfer (Mitchell et al. 2015), providing immunosuppression of maternal body by inhibition of the T-cells (Gercel-Taylor et al. 2002) and regulation of cell migration as well as angiogenesis (Salomon et al. 2014; Sabapatha, Gercel-Taylor, and Taylor 2006). Also it has been reported that the number of placental exosomes starts to increase starting from the 6th week of gestation and reach to maximum number at term (Salomon et al. 2013). Hence, detection of placental exosomes and their cargo contents can be a novel liquid biopsy technique that will provide information about placental function (Jin and Menon 2018). Moreover, PLAP exosomes are suspected to play important roles during pathological pregnancies (van der Post et al. 2011). During pregnancy associated disfunctions such as preeclampsia, gestational diabetes, and preterm birth, the quantity and content of the exosomes can be directly linked to the disfunctions. Also, it is known that the number of placental exosomes increases during pregnancy related disfunctions such as preeclampsia

(Krishna and Bhalerao 2011; Salomon et al. 2014; Mitchell et al. 2015). Interestingly, PLAP exosomes observed in some gynecologic cancer types (Leitner et al. 2001).

2.2.3. Potential of Exosomes in Clinical Applications

The role of exosomes in cell-cell communication and promotion of metastatic niches have great impact on cancer development. Additionally, after the formation of metastatic environments, tumor derived exosomes begin to actively secrete. These exosomes further regulate the cancer progression by effecting immune system along with promoting angiogenesis (Tai et al. 2018) along with reprogramming the energy metabolism of tumor cells (Wu et al. 2019). Thus, exosomes can both serve as diagnosis targets and therapeutics during cancer progress. In cancer related studies interruption of biogenesis, secretion or uptake of exosomes result as cancer regression and had been reported in many studies (Escrevente et al. 2011; Baietti et al. 2012; Ostrowski et al. 2010; Tian et al. 2014).

Exosomes can also be used as potential therapeutics due to their biocompatibility and enhanced stability in clinical applications (Gurunathan et al. 2019). The therapeutic potential of mesenchymal stem cells (MSCs) derived exosomes have been studied in liver, lung, kidney, neural in juries and cardiovascular diseases as well as wound healing (Yamashita, Takahashi, and Takakura 2018) and MSCs derived exosomes found to be safer than of MSCs (Sun et al. 2016).

The role of exosomes during HIV infections is still a debate and more research needs to be done. While some studies showing the role of exosomes on HIV infection with regulating the virus functioning (Welch, Stapleton, and Okeoma 2019) and some other exosomes i.e. semen and breast milk can inhibit HIV infection as well as its replication by exosomal cargos (Teow et al. 2016; Madison, Jones, and Okeoma 2015), on the other hand semen exosomes are suspected to be responsible from HIV activity (Madison, Roller, and Okeoma 2014). Based on these findings, exosomes are studied as successful drug delivery vehicles in gene therapy for HIV infections by delivering RNAs (Yong, Jing, and Yi 2018). Some studies also showed the promotion of cancer by exosomes derived from HIV infected cells (Chen et al. 2018).

Despite of the great potential of exosomes as therapeutics, there are several drawbacks for development of a therapeutic from an exosome. These drawbacks are: i) lack of large-scale production, ii) lack of high quality and uniform production and iii) lack of information about storage conditions (Yamashita, Takahashi, and Takakura 2018). Research still focus on these subjects to overcome the problems. For example, a recent study showed that 5-10 fold exosome production can be achieved in a bioreactor (Watson et al. 2016).

2.3. Exosome Isolation and Quantification Techniques

During the last decade, the great potential of exosomes for clinical utilization created various isolation and quantification methods to have the maximum yield along with purity and reproductivity for exosomes. While the first separation methodology, which is ultracentrifugation, remains to be the classical ‘conventional’ isolation method, there are several commercial exosome isolation kits on the market based on different principles along with novel methodologies with high throughput and purity. All these different isolation and quantification techniques yields different efficiencies that ultimately depend on the purpose of the application.

2.3.1. Isolation

The most common and applied methodology for exosome isolation is ultracentrifugation with differential centrifugation technique (Jeppesen et al. 2014). The principle of this methodology is basically depending on the differences in physical properties of the exosome containing sample. Briefly, the exosome containing sample is centrifuged to remove other materials in the sample (cells, macromolecular proteins) and this is followed by ultracentrifugation 100 000 g for an hour to obtain exosomes in supernatant. This purification can be followed by a size exclusion chromatography to obtain well-defined and more pure exosome samples. The drawbacks for this methodology are that it is time-consuming, requires expensive instruments and it is labor-intensive along with loss of exosomes during the purification steps that reduces the yield (Li et al. 2017). Also, the complete isolation of exosomes from other apoptotic bodies is impossible with this methodology and exosome clusters might be formed during ultracentrifugation along with the presence of larger vesicles (Zhang, Yu, et al. 2017;

Oksvold, Neurauter, and Pedersen 2015). The application of ultracentrifugation methodology is depends on the purpose of the research since RNA content of exosomes purified from cell culture do not effected from this method (Yu et al. 2018). However, application of this method to clinical samples alters the final protein content of the sample with non-specifically bound proteins and protein aggregates (Zhang et al. 2019). This methodology can yield to 10^{10}-10^{12} exosome particles/mL which is confirmed by nanoparticle tracking analysis (NTA) (Jeppesen et al. 2014).

The isolation of exosomes has been studied with the use of immunomagnetic beads that are conjugated with relevant exosome tetraspanin antibodies (Tauro et al. 2012) even though these magnetic beads (i.e. anti-CD63 conjugated dynabeads®) can be found commercially, it still requires pre-enrichment of exosomes via ultracentrifugation. Comparing to conventional centrifugation methodologies, immunoaffinity capture beads showed better exosome yields and thus twofold amount of exosome related proteins (Tauro et al. 2012; Konadu et al. 2016). The exosome-magnetic bead conjugates are found to be suitable for flow cytometry and electron microscopy experiments since sample volume is quite low (Pedersen et al. 2013).

Another commercialized exosome isolation technique is based on a polymeric precipitation reagent that created meshes while polymerization process and captures exosomes that have the size range of 60-180 nm. Even though this methodology is easy to apply (requires one step of basic centrifuge), it may still precipitate some contaminants such as lipoproteins and it is applicable to small number of samples and an expensive kit (Alvarez et al. 2012). A comparative study upon exosome isolation using commercially available exosome isolation kits (precipitation principle) (de Hoog et al. 2013; Oksvold et al. 2014; Barile et al. 2014), ultracentrifugation method, immunomagnetic beads and size exclusion chromatography method studied and results showed that commercial kits along with size exclusion principle isolation showed better results by means of total protein amount while Invitrogen kit showed the best results. Also, the size distribution and zeta potential of the isolated exosomes with different techniques showed different results showing that the methodology is important for the downstream of the applications (Patel et al. 2019).

2.3.2. Quantification, Physical and Biochemical Characterization

The determination of size for exosomes as well as their quantification is commonly studied with dynamic light scattering (DLS), nanoparticle tracking analysis (NTA) and high-resolution imaging (Hartjes et al. 2019). Thus, the number of exosomes and/or exosomes that have a specific marker on them is important for detection of a disease or progress of a disease. The quantification and/or presence of exosomes in the relevant sample has been studied via different detection methodologies including either semi-quantitative or quantitative methods.

Electron microscopy techniques remain the most common methodology for the exosome characterization and quantification while preparation of the sample still a debate. The main limitation about this technique is the necessity of the vacuum during imaging requires drying or the fixation of the sample which ultimately lead to misinterpretation of the representative population of the sample (Hartjes et al. 2019; Théry et al. 2006).

DLS is also commonly used for the size determination of the exosome samples because of its simplicity and time effectiveness (Palmieri et al. 2014). The limitation with the DLS technique is the assumptions on the monodispersity of the sample which is more suitable for pre-processed biofluids (Habel et al. 2015).

NTA allows to analyze polydisperse samples because of Brownian motion estimation of the particles which leads to estimation of size of an individual particle (Dragovic et al. 2011). While the presence of other impurities in the biological samples remain a constraint for this technique, it is still the standard quantification technique for exosome analysis (Carnell-Morris et al. 2017; Dragovic et al. 2011). Additionally NTA has a limited range of detection for particles that are between 10^7-10^9 particles/mL (Koritzinsky et al. 2017).

Flow cytometry is another method for the quantification of exosomes. A typical analysis requires the fluorescence label of the biological sample and polystyrene beads are the calibration standard for this technique. This constraint leads to detection of larger extracellular vesicles (>500 nm) while the homogeneity for degree of fluorescence labelling remains as a question (Nolan and Jones 2017; Ayers et al. 2011). Researchers are still working on the improvements of flow cytometry technique which will be consequently applicable on exosomes (Pospichalova et al. 2015; Mastoridis et al. 2018).

Biochemical characterization of exosomes has great potential on diagnosis purposes. Exosomes known to have genetic cellular contents such as DNA and RNAs which can give insights on several physiological or pathological conditions (Yuana, Sturk, and Nieuwland 2013). Immunoblotting is one of the common methodologies for detection of exososomal protein content. Simply, the method involves lysing of exosomes and then determination of the proteins either by SDS-PAGE or dot blot assay. This methodology provides fast and simple protein detection however, it is semi-quantitative, and it has limitations on individual exosome analysis. Also, the assay requires large amount of sample and time consuming sample processing (Hartjes et al. 2019).

Immunosorbent assays can be used for determination of a surface protein that present on exosome membranes. Simply, the assay surface is modified with a tetraspanin antibody to be able to capture exosomes and following washing steps allow to remove contaminant proteins that present in the sample. This step is followed by introducing a labelled antibody of interest to the captured exosomes and quantification of the label of interest (Hartjes et al. 2019). This method provides the analysis of complex body fluids without any prior processing and one of this assay type (time-resolved-fluorescence immunoassay (TR-FIA)) can provide detection of exososomal cargo proteins (Salih et al. 2016). Based on immunosorbent type assay, researchers developed a microfluidic platform to isolate and quantify exosomes from complex biological fluids as well as their protein content (Kanwar et al. 2014). In this study, researchers coated the microfluidic chamber with anti-CD63 antibodies and captured the fluorescently labelled exosomes and quantified them. Also, they compared the number of exosomes in cancer and healthy patients. Further, they demonstrated the RNA profiling ability of their system by recovering exosomes. For this type of research, the number of capture antibodies can be increased and surface protein profiling of exosomes can be enhanced (Jørgensen, Bæk, and Varming 2015).

2.4. LSPR Theory and Biosensor Applications

Plasmonic behavior is defined as interaction between free electrons of a metal atom and incident light. The oscillating free electrons of the metals create a dipole on the surface of the material, and they tend to migrate to their initial state (Jatschka et al. 2016). Localized surface plasmon resonance (LSPR) is defined as the frequency of the oscillation of the electrons around a nanoparticle that is created by the incident light. Different from surface plasmon resonance (SPR), LSPR occurs around nanoparticles which are smaller in size than the incident light. Although the SPR technique is more sensitive to refractive index changes in bulk solution, LSPR provides comparable sensitivity to refractive index within short-range changes. Consequently, analyte detection in low volume is an advantage for LSPR technique (Willets and Van Duyne 2007).

There are several techniques to create metallic nanoparticle patterned surfaces for LSPR from bottom-up to top-bottom lithographic techniques. The most common metallic materials that bear plasmonic properties are gold (Au) and silver (Ag). Au and Ag particles are well-known for their biocompatible properties and ease of surface modification with biomolecules (Alaqad and Saleh 2016). Furthermore, gold nanoparticles have advantages by means of high surface area, low toxicity compared to silver, and better chemical stability in aqueous solutions (Chen et al. 2008; Khan et al. 2014).

$$Response\ (\lambda_{max}) = m\ \Delta n \left(1 - exp\ (-\ \frac{2d}{l})\right) \tag{1}$$

where; λ_{max}: LSPR response, m: refractive index sensitivity of gold nanorods, Δn: change in refractive index, d: adsorbate layer thickness, l: electromagnetic decay length.

The plasmonic response of nanoparticles occurs with an excitation that is created by an electrical field. The electron cloud around the particles starts to oscillate by the excitation and thus creates an electrical field around them. Accordingly, EM of a nanoparticle depends on its size and shape (Duque, Blandón, and Riascos 2017). It should be noted that EM decay length of nanoparticles is limited according to their sizes and shapes due to Mie Theory (only applicable nanospheres and nanorods having longitudinal length less than 80 nm (Nehl and Hafner 2008; Mayer and Hafner 2011) (Equation 1). Thus, LSPR response of gold nanoparticle on adsorbed layers is completely dependent on the geometry and this determines the limits of sensitivity for gold nanoparticles. Gold nanoparticles can be synthesized with different geometries including nanospheres, nanorods, nanotriangles, nanocubes, nanobranches, and nanobipyramids between 10 nm to 8 µm. Among all these geometries, gold nanorods (AuNRs) have the best index sensitivity for the same aspect ratios among different shapes (Cao, Sun, and Grattan 2014; Khan et al. 2014).

LSPR response and sensitivity is strongly dependent on the size and the shape of the nanorods. To be able to get the maximum optical response from biomolecule binding, optimizing the EM (matching the thickness upon the nanorods up to detection biomolecule) and maximizing the sensitivity are crucial (Tian et al. 2012). The EM also depends on the configuration of nanostructures as end-to-end or side-by-side and also the gap between the structures. It is known that end-to-end configuration of gold nanorods leads to the maximum coupling (Jain, Eustis, and El-Sayed 2006). Even though increasing the size of the nanoparticles leads to increasing EM, it also results in a decrease in the gap between nanoparticles and a reduction of the near field influence (Huang, Neretina, and El-Sayed 2009). Optimization for the conformation and particulate gap between gold nanoparticles is very important to create the best LSPR response for relevant detection methodology. In biosensor applications, detecting of a relevant antigen (depending upon the application) is possible via incorporation of the monoclonal specific antibody on the surfaces. Thus, antibody conjugation to the surfaces is crucial in biosensor applications.

2.4.1. Preparation of Functional LSPR Surfaces

There are different techniques to create AuNRs patterned surfaces for LSPR. The most common methodology for AuNRs synthesis is based on using cetrimonium bromide (CTAB) as the surfactant as AuNRs are more stable within CTAB solutions over time (Smith and Korgel 2008). However, the high concentration and positive charge of CTAB create sterical hindrance between the surface and AuNRs which leads to non-homogenous and unsuccessful attempts for the gold self-assembly process of LSPR chips. Additionally, using CTAB stabilized AuNRs in biological fluids causes aggregations because of the positive charge of CTAB. Thus, surfactant exchange on CTAB stabilized AuNRs with cysteine, different molecular weights of polyethylene glycol (PEG), and citrate has been studied in literature (Guerrini, Alvarez-Puebla, and Pazos-Perez 2018). Among these surfactants; biocompatible, non-fouling, hydrophilic properties of PEG make it a very good agent for the surfactant exchange with CTAB (Thierry et al. 2009). Molecular weight of PEG molecules affects the stability of AuNRs. Decreasing the molecular weight of PEG (i.e. 356 g/mol) leads to aggregation of AuNRs despite the fact that further surface modification is easier in this case (Joshi et al. 2013). In this work, 1K (Mw: 1000 g/mol), 2K (Mw: 2000 g/mol) and 5K PEG (Mw: 5000 g/mol) were used to investigate the effect of molecular weight on the self-assembly of AuNRs on LSPR chips and small alkane thiol functionalization for further antibody conjugation. It is well-known that the surfactant exchange with 2K PEG creates more brushed-like oriented molecules and high density coverage of PEG molecules and thiolated ligand exchange can be easily achieved with 2K PEG (Hore et al. 2015). In literature, a study on ligand exchange around PEGylated gold nanoparticles showed that lower molecular weight PEG such as 2K PEG exchanged with the incoming thiolated ligand and also created more tethered structures compared to higher molecular weight PEG, i.e. 5000 Da, thus easily allowing the backfilling of the incoming thiolated ligands (Burrows et al. 2016). In this thesis, similar findings were obtained supporting the literature.

It is crucial to create homogeneous AuNRs patterned surfaces to be able to get repeatable LSPR responses. Also, AuNRs patterns need to be stable under further functionalization and utilization. For this purpose, silanization of glass wafers is a well-known methodology in literature to control the assembly of gold particles since Si-Au bond is a strong bond that can keep the stability of AuNRs upon utilization (Yochelis et al. 2012). There are several different methodologies for the silanization procedures including the use of aminopropyltriethoxysilane (APTES) and 3-(Mercaptopropyl) trimethoxysilane (MPTMS) molecules with different surfactant stabilized AuNRs (e.g. CTAB, citrate, cysteamine and PEG) (Haddada et al. 2013; Kyaw et al. 2015; Lin and Chung 2008; Mayer et al. 2008; Scarpettini and Bragas 2010; Weinrib et al. 2012; Yochelis et al. 2012). In this work, the effect of two different silanes (APTES and MPTMS) on creation of AuNRs patterns on glass surfaces were investigated.

Antibody conjugation to gold nanoparticles can be done via numerous methodologies. The most common and easy-to-apply methodology is having carboxylic acid functional groups on the surfaces of the gold nanoparticles and react these groups with amine-groups of antibodies. This can be achieved via incorporation of carboxylic acid functionalized alkane thiol molecules which can self-assemble on gold nanoparticles. However, hydrophobicity of these molecules is known for having secondary interactions with proteins and other molecules in biological fluids (Love et al. 2005). Thus, incorporation of OEG units that creates the protein repellant nature on the surfaces and inhibits the non-specific bindings is required (Chapman et al. 2000). In this work, a new strategy was performed for creating functional and protein-repellent surfaces. PEGylated

AuNRs were self-assembled on glass wafers and then carboxyl/azide and hydroxyl functionalized alkane thiol molecules were assembled on PEGylated AuNRs, leading to hydrophilic surfaces with carboxylic acid or azide functional groups.

Antibody conjugation to the gold patterned LSPR surfaces is mostly studied using carboxylic acid functionalized surfaces that are ready for EDC/NHS chemistry. Alternatively, streptavidin-biotin interactions were used to conjugate antibodies to LSPR surfaces. Using carboxylic acid-functionalized surfaces along with EDC/NHS chemistry is a well-established and easy methodology for conjugating antibodies. However it lacks the ability to control the Fab region orientation of antibodies on the surface, which ultimately reduces the sensitivity of the biosensor surface (Jazayeri et al. 2016). In this work, in parallel to conventional EDC/NHS strategy, a relatively new strategy was used by incorporating a small protein-G fragment to ensure the conjugation of antibodies through their Fc regions.

2.5. Exosome Detection via LSPR

A few studies in literature focuses on the detection of exosomes via plasmonic techniques. While no detection technique is still better than another, plasmonic techniques provide advantages by large throughput and application to low concentrations. To the best of the author's knowledge, first ever study that used the plasmonic properties for the detection of exosomes was performed by Rupert et. al. (Rojalin et al. 2019). In this study, Rupert and coworkers modified commercial gold coated SPR chips with anti-CD63 antibody and used the surfaces for human mast cell (HMC) exosome detection (Rupert et al. 2014). They determined the concentration of exosomes by the calculation of surface bound mass related to SPR response. For this purpose, HMC exosomes firstly isolated by ultracentrifugation method and analyzed with NTA and BCA assay. While NTA results showed an average size of 234 nm for 1.3×10^9 particles/mL, total protein amount found to 4.1µg/mL with BCA assay results. They found a twice larger amount of exosome proteins by comparing the total protein amount on exosomes by two methods (BCA and SPR). However, they assumed that exosome samples did not contain any contaminant proteins and one exosome contains one CD63 protein along with the assumptions of monodisperse distribution of exosomes and same buoyant density. These assumptions alter this comparison of the BCA and SPR methodologies (Rupert et al. 2014). Another early study that was based on a plasmonic technique used SPR method with anti-CD9 antibodies along with anti-CD41b antibodies. The authors knocked down Rab27a gene in liver cancer (MHCC97H) cells and compared the exosome amount before and after knocking down process. This technique allowed to monitor the regulation of exosome secretion which can ultimately lead to observation of a cancer treatment process. In this study, the authors found 4.9×10^7 exosomes/cm^2 based on the assumptions of exosomes composed from DOPC lipids and calculations were performed using physical properties of DOPC lipids (Zhu et al. 2014).

Exosome detection via LSPR methodology was demonstrated by Im and coworkers. In this study, the authors prepared a nano-plasmonic exosome assay (nPLEX) for quantitative analysis of exosomes using anti-CD63 antibodies. For this purpose, they prepared gold nanohole arrays via electron-beam metal evaporation technique firstly with 200 nm thick Au and 2 nm thick Ti deposition on the surface followed by ion-beam milling to create 200 nm diameter gold nanohole patterns and combined the surfaces with PDMS microfluidic channels. They isolated exosomes via ultracentrifugation method from human ovarian carcinoma cell lines (CaOV3, OVCAR3 and SKOV3). Further, they modified the surfaces with functionalized PEG chains (Mw:1 kDa and Mw:0.2 kDa) followed by binding of anti-CD63 antibodies to the surfaces. The detection methodology was the comparison of relative LSPR response of two channels: one modified with anti-CD63 and the other was modified with control antibody based on pre-quantified exosomes via NTA. LoD of 3000 exosomes was reported (Im et al. 2014).

One of the first studies on detection of exosomes using LSPR technique was performed by Thakur et. al. In this study, researchers created gold nano-islands (AuNIs) with a size of 40 nm diameter and 5 nm thickness on LSPR surfaces via thermal annealing Au films. The scope of this work was to distinguish exosomes from other microvesicles (MVs). For this purpose, the surface of the gold left without any further functionalization and the mixture of exosomes and MVs (all EVs) was obtained from human A549 lung cancer cell line and SH-SY5Y neuroblastoma cell line via ultracentrifugation method followed by an isolation by fractionation of exosomes and EVs. These fractions were analyzed via DLS and an average size of 150 nm for A549 and approximately 60 nm for SH-SY5Y was determined for exosomal fractions while MVs showed a wide range of size distribution. Varying concentrations of these exosome fractions were loaded on LSPR surfaces and an LoD of 0.194 µg/mL was obtained with a detection range of 0.194-100 µg/mL. Furthermore, exosomes and MVs showed higher specificity with AuNIs depending on different membrane properties. Exosomes were found to have distinguishable interactions with AuNIs compared to MVs due to their more negative membrane nature (Thakur et al. 2017).

A very recent study by Lv and coworkers is based on creating gold nano-ellipsoid arrays followed by modification with anti-CD63 antibodies and using this microfluidic platform for quantitative detection of exosomes. For this purpose, they used electron-beam deposition of gold films followed by thermal annealing to create ellipsoid patterns. To be able to modify the surfaces with anti-CD63 antibodies, the authors used functionalized alkane thiol molecules and used EDC/NHS chemistry to conjugate the antibodies on the surface. In this study, commercial exosomes were utilized. The concentration of these exosomes was also determined via a commercial protocol. A LoD of 1 ng/mL was found after subtracting the non-specific bindings of BSA to the surface (Lv et al. 2019). This concentration corresponds to approx. $2x10^6$ particles/mL assuming all exosomes have the same diameter of 100 nm with an average density of 1.2 g/mL.

Inspired by all these studies; in this work, it was intended to develop a more practical and sensitive LSPR based method for detection of exosomes.

CHAPTER 3

MATERIALS and METHODS

3.1. Materials

AuNR synthesis: Hexadecyltrimethylammonium bromide (CTAB), sodium borohydride, ascorbic acid were purchased from Sigma. Silver nitrate and hydrogen tetrachloroaurate(III) hydrate were obtained from Alfa Aesar.

Surfactant exchange from CTAB to PEG: Potassium carbonate, mPEG-SH (Mw: 1 kDa, 2 kDa and 5 kDa) were purchased from Sigma as well as mPEG-SH (Mw: 5 kDa) was custom-synthesized by JenKem Tech.

Self-assembly of PEGylated AuNRs on the surface: silanization agents (SA1 and SA2), sulfuric acid and hydrogen peroxide were purchased from Sigma-Aldrich. Glass slides were Superior Marienfeld.

Surface functionalization of PEGylayted AuNRs on the wafers: 11-Mercaptoundecanoic acid, 11-Mercapto-1-undecanol and 11-Azido-1-undecanethiol (bis(11-azidoundecyl) disulfide) were obtained from Assemblon (Seattle, WA) and Sigma-Aldrich. DBCO-ImmuneLink^{TM} procured from AlphaThera. N-(3-Dimethylaminopropyl)-N′-ethylcarbodiimide hydrochloride (EDC), (N-hydroxysulfosuccinimide) (sulfo-NHS) were procured from Sigma. Antibodies were purchased from three different companies: rabbit anti-mouse IgG (Jackson ImmunoResearch, 115–005-008), mouse anti-human CD63 (BD, clone H5C6) and anti-mouse IgG are from Sigma and anti-PLAP antibody was purchased from ABCAM.

Detection: PLAP protein was procured from ABCAM. Human semen and MCF-7 and MDA-MB-231 cell line exosome samples were kind gifts from Dr. Lucia Vojtech's Laboratory (University Washington, Seattle, WA, USA) and Dr. Devrim Pesen Okvur's and Dr. Özden Yalçın's Joint Laboratory (Izmir Institute of Technology, Izmir, TURKEY) .

Solvents: Toluene, ethanol and isopropanol were purchased from Sigma. Ethanol 200 proof was purchased from Thomas Scientific. Distilled water was obtained from a Millipore Milli-Q Plus water purification system fitted with a 0.22 μm filter.

Others: Ethanol amine and bovine serum albumin were obtained from Sigma. 40% Acrylamide/Bis Solution 29:1 (3.3 % C) and ammonium persulfate were obtained from Bio-Rad. Tetramethyl ethylene diamine (TEMED) was from Amresco, Tris-(hydroxymethyl) aminomethane (Tris base) and sodium dodecyl sulphate were from VWR.

3.2. Instruments

3.2.1. UV-Visible Spectrophotometry

UV-visible spectroscopy of the AuNRs was performed using a Thermo Scientific Evolution 201 UV-visible spectrophotometer using quartz cuvettes. Glass wafers were cut with diamond glass pen in either to 1 x 1 cm or 1 x 1.7 cm sizes to fit inside either the sample cell or quartz cuvettes to be able to achieve LSPR measurements. Exosome calibration curve, semen exosomes measurements and PLAP protein detections were performed using an Insplorion X1 LSPR device in NESACBIO, University of Washington (Seattle, WA, USA) and other LSPR measurements completed with Thermo Scientific Evolution 201 in IZTECH (İzmir, Turkey). The cut wafers were fitted into relevant sample cell depending upon the device thus the measurement area was fixed for all samples. All measurements were completed in PBS pH 7.4 if not specified.

3.2.2. Dynamic Light Scattering (DLS) and Zeta Potential

DLS and zeta potential measurements of AuNRs, functionalized AuNRs and antibodies were taken with NanoPlus DLS Nano Particle Size and Zeta Potential Analyzer. Measurements were completed either in solution or on the surface for zeta potential measurements. Range for size measurements: 0.1 nm to 12.30 µm and for zeta measurements: -500 to +500 mV; laser source: diode laser; laser wavelength: 660 nm; laser power: dual laser 30 mW + 70 mW). All measurements were completed in PBS pH 7.4 or ultra-pure (UP) water.

3.2.3. X-ray Photoelectron Spectroscopy (XPS)

Kratos AXIS Ultra DLD instrument using a monochromatic Al Kα X-ray source were used for XPS measurements in Molecular Analysis Faculty (MAF), University of Washington. Measurements took place with 0^o angle if not specified.

3.2.4. Scanning Electron Microscope (SEM)

Thermo Apreo S with Lovac or Quanta 250FEG device in MAF, University of Washington and FEI Quanta 250FEG device in Materials Research Centre (MAM) at IZTECH were used for SEM images.

3.2.5. Fourier-transform Infrared Spectroscopy (FTIR)

Perkin Elmer UATR Two device in Biotechnology and Bioengineering Research and Application Centre (Biomer) at IZTECH was used for FTIR experiments. Measurements took place using either in air or water baseline depending upon the surface or solution measurements.

3.3. Methods

3.3.1. Gold Nanorod (AuNRs) Synthesis

Gold nanorods were synthesized with seed-mediated method according to the procedure reported by Green et. al. (Green et al. 2011). Briefly, cetrimonium bromide (CTAB) (0.1 M), $HAuCl_4$ (0.01 M), $NaBH_4$ (0.01 M), $AgNO_3$ (0.01 M) and ascorbic acid (0.1 M) solutions were mixed at predetermined ratios and stirred for 2 h until use. The growth solution was prepared by mixing seed solution with 20 mL of $HAuCl_4$ solution, 20 mL of CTAB solution, 120 µL of $AgNO_3$ solution and 360 µL of ascorbic acid solution. The color of the solution was yellow or orange at the beginning. Finally, it turned to a dark-purple color. The rod solutions were purified via centrifugation and dissolved in ultrapure (UP) water to be able to remove the excess CTAB. The final rods were characterized via UV-spectroscopy and zeta potential measurements.

3.3.2. Surfactant Exchange from CTAB to PEG Around AuNRs

Surfactant exchange with PEG was completed with the following procedure: CTAB stabilized gold nanorods were centrifuged once and resuspended in 2 mM potassium carbonate, then mixed with 20 µL of 20 mM of mPEG-SH (Mw: 5 kDa) or mPEG-SH (Mw: 2 kDa) or mPEG-SH (Mw: 1 kDa). After the incubation, the solutions were centrifuged at 12000 rpm for 15 min to be able to remove excess surfactant in the solution. The incubation times between 1 h to overnight were studied for PEGylation with 1K, 2K and 5K PEG. PEGylated AuNRs were checked via UV-spectroscopy, DLS and zeta potential measurements.

3.3.3. Wafer Cleaning and Silanization

For cleaning of the glass substrates three methodologies that were tested are as follows: cleaning with piranha, cleaning with isopropanol mixture and cleaning using oxygen plasma. For isopropanol mixture cleaning; 1% (w/v) of sodium dodecyl sulfate detergent was dissolved in isopropanol and the glass substrates were sonicated for 15 min in isopropanol mixture cleaning solution, followed by sonication in DI water for 10 min, in ethanol for 10 min, and two more sonication cycles in DI water for 10 min. The clean substrates were kept in DI water until use. Before the silanization procedure, glass wafers were dried with nitrogen thoroughly. Here it should be noted that the dryness of the substrates is the key parameter for silanization since silane undergoes polymerization by itself in aqueous media and creates multilayers of silanes on the surface (Gamble, Jung, and Campbell 1995). For piranha cleaning: sulfuric acid (H_2SO_4) and hydrogen peroxide (H_2O_2) were mixed with 3:1 ratio and cooled down for 10 min (Caution: Piranha solution is extremely dangerous and should be handled carefully). The substrates were immersed ins piranha solution and kept for 30 min followed by rinsing with water thoroughly. The substrates were used immediately after cleaning. For oxygen plasma cleaning: substrates were exposed to O_2 plasma for 5 mins and substrates were used immediately in order to keep the surface hydrophilicity (Alam, Howlader, and Deen 2014).

Silanization of bare glass surfaces was performed and followed by self-assembly of gold nanorods. Acidic piranha solution, high-power oxygen plasma or methanol/isopropyl alcohol/DI water solution (isopropanol mixture) (1/1/64 by volume) was used as cleaning media for cleaning of the substrates. The substrates were immersed in silane solutions for 2 hours, 8 hours or overnight and rinsed with ethanol. After washing with excess ethanol to remove unbonded APTES, the silanized glass substrates were immersed in PEGylated gold nanorod solutions immediately for specified time incubation. Here, it is known that the orientation of the nanoparticles is another key parameter for the LSPR response and diminishing effect of the interparticle gap (Jain, Eustis, and El-Sayed 2006). PEGylated gold nanorod patterned surfaces were characterized via SEM, XPS, FTIR, zeta potential and LSPR. Here it should be noted that all LSPR data were smoothed according to gaussian smoothing and data points were normalized fitting the maximum absorbance to 1 and minimum absorbance to 0 using ORIGIN 2016 or MATLAB.

The prepared patterned substrates were exposed to oxygen plasma for 10 seconds. Theoretically, plasma etches the PEGs from the AuNRs surface without disrupting the self-assembly of AuNRs leaving bare AuNRs on the surface that are ready for further modifications (Mayer et al., 2008).

3.3.4. Performance Evaluation of AuNRs Patterned Surfaces

The performance of the PEGylated AuNRs patterned surfaces was evaluated measuring the change of maximum wavelength shift upon the change in the refractive index (RI) of the solutions (water: 1.33, ethanol: 1.36, 3:1 (v/v) ethanol/toluene: 1.39, 1:1 (v/v) ethanol/toluene: 1.4, 1:3 (v/v) ethanol/toluene: 1.43, and toluene: 1.45) using a Insplorion X1 LSPR device.

3.3.5. Surface Functionalization of the AuNRs

Self-assembly of 11-Mercaptoundecanoic acid (COOH) and 11-Mercapto-1-undecanol (OH) molecules on AuNRs surfaces was performed in absolute ethanol with a final concentration of each molecule: 10 mM, 5 mM and 1 mM. The ratio between COOH:OH molecules was 1:1 and incubation period was overnight. Calculation for required amounts of self-assembly molecules is shown in Appendix A. At least 10000-fold excess molecules have been used during self-assembly process. PEGylated (2K and 5K) AuNRs patterned surfaces were investigated to determine the optimum functionalization conditions. After determining the optimum concentration for self-assembly process, 1 mM concentration of COOH/OH molecules with a 1:1 ratio was incubated in absolute ethanol during overnight with plasma treated AuNRs surfaces and used for further antibody conjugation along with non-plasma treated 2K PEGylated AuNRs surfaces. To conjugate antibodies through click chemistry, surfaces were functionalized with azide groups. The same procedure was followed to incorporate azide groups onto the surfaces. The conditions for the self-assembly of bis(11-azidoundecyl) disulfide (N3) and 11-Mercapto-1-undecanol (OH) molecules were 1:1 ratio at a final concentration of 1 mM for each molecule.

3.3.6. Antibody Conjugation to Functionalized AuNRs

The specific antibodies (i.e. anti-CD63 and anti-PLAP) were conjugated to the COOH/OH or N3/OH functionalized surfaces. After the self-assembly of COOH/OH molecules, EDC/NHS chemistry was applied on the surfaces for activation of COOH groups to be able to conjugate the antibodies through their amines. Briefly, NHS (33 mM) and EDC (133 mM) were dissolved in PB pH 6 and surfaces were treated for 10-30 min either by immersion or using the flow cell of the Insplorion X1 LSPR device at a flow rate of 5 µL/min. NHS activated surfaces were immediately incubated with relevant antibody solutions either by immersing in or exposing to the flow of antibody solution at concentrations of 10 µg/mL or 1 µg/mL at a flow rate of 5 µL/min, respectively. The calculations to determine the required antibody amount is shown in Appendix A. 20-fold excess antibody amount based on the available COOH groups on the surface was used during conjugation process. The incubation time for antibody conjugation was 1 h. After antibody binding, NHS esters of COOH groups were deactivated by applying 0.1 M ethanolamine to the surfaces and followed by incubation with BSA solution at 0.1 g/mL to minimize the non-specific bindings on the surfaces. The functionalized surfaces were analyzed via XPS, FTIR and zeta potential.

Furthermore, a relatively new strategy for conjugation of antibodies to LSPR surfaces was performed. This strategy includes the incorporation of Fc region specific protein, ImmuneLink™ to the surface in order to conjugate specific antibodies to the surface through their Fc regions, hence to expose the antigen binding region of Abs to the solution away from the surface.

ImmuneLink protein was purchased with a modification of dibenzocyclooctyne (DBCO) and thus ready to click chemistry with azide functionalized surfaces. For this purpose, the LSPR chip surfaces were modified with azide bearing self-assembly molecule, Bis(11-azidoundecyl) disulfide (N3) and OH (using 1:1 mol ratio at 1 mM final concentration). The results were confirmed via XPS. In parallel, DBCO-ImmuneLink protein was conjugated to the specific antibodies to be used on LSPR surfaces using a protein: antibody molar ratio of 1:10 at 0^oC for 4 hours under UV irradiation. After the confirmation of conjugation with SDS-PAGE, the conjugate mixture was purified by preparative HPLC (Agilent) using UP water as running solvent and Jupiter 5 µm C18 300 Å column (Phenomenex) which followed by further purification and concentration with centrifugation. Further, click chemistry between azide functionalized surfaces and DBCO-functionalized protein-Ab conjugates were carried out in PBS pH 7.4 at 4^oC for 16 hours and all surfaces were washed thoroughly after each step. Freshly prepared surfaces were used for LSPR detection experiments.

The comparison of two antibody conjugation methodologies (NHS/EDC chemistry and click chemistry) in terms of antibody orientation is shown schematically in Figure 3.1. The orientation of the antibodies was investigated by incubating anti-IgG antibody solution (1 pM, 1nM and 1 µM) in PBS with antibody modified surfaces (EDC/NHS chemistry and click-chemistry) and measuring the binding of anti-IgG antibodies via LSPR.

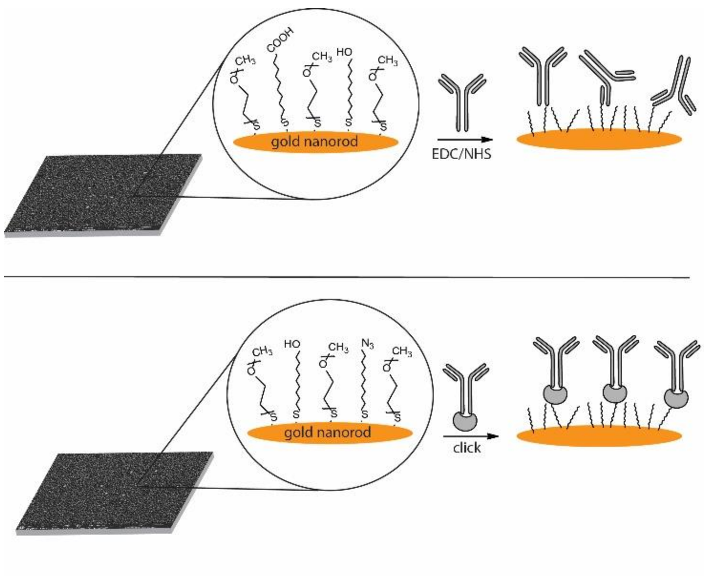

Figure 3.1. Illustrative comparison of antibody orientations with conventional EDC/NHS chemistry (A) and ImmuneLink strategy (click-chemistry) (B)

3.3.7. LSPR Measurements for Detection of Exosomes and Proteins

First of all, as the proof of concept, surfaces were activated via EDC/NHS chemistry and then they were incubated with 10 µg/mL goat anti-human IgG in 1 h and washed with PB thoroughly. This is followed by the incubation of these surfaces with 0-100000 pM human IgG within 1 h in PB.

Human semen exosome samples were obtained from Dr. Lucia N. Vojtech, (University of Washington, UW). These samples contained purified exosomes at known concentration as they were prepared by ultra-centrifugation method followed by size exclusion chromatography (SEC) by Dr. Lucia N. Vojtech at UW. MCF-7 and MDA-MB-231 cell culture supernatants were obtained from the joint laboratory of Dr. Devrim Pesen Okvur and Dr. Özden Yalçın (Izmir Institute of Technology, IzTech). The cell culture supernatants were collected by Dr. Aslı Kısım, from Dr. Pesen Okvur and Dr. Yalçın laboratory at IzTech and contained unknown concentrations of exosomes in serum-free media that were seeded in six well plate as $4x10^5$ cells. Anti-CD63 antibody was used to detect exosomes in both purified human semen exosome samples at known concentrations and in breast cancer cell culture media at unknown concentrations, because of their known high-selectivity comparing to other tetraspanins (Lv et al. 2019; Oliveira-Rodríguez et al. 2016).

Calibration curves for exosome detection were prepared using several different biochip surfaces patterned with 2K PEGylated AuNRs for comparison. These different surfaces included surfaces functionalized with EDC/NHS chemistry (i) with and (ii) without oxygen plasma, and (iii) surfaces functionalized with click chemistry without plasma. In this way, the effect of oxygen plasma treatment (in other words the presence or absence of PEG on the surfaces) and the effect of conjugation strategy (NHS/EDC vs. click) on the exosome detection sensitivity of chip surfaces were investigated. The calibration range was 10^2-10^{10} particles/mL which was within the limits of exosome concentrations in plasma. The stock concentration of semen exosome samples was 5.824 x 10^{12} particles/mL and they were diluted to the necessary concentrations (10^2-10^{10} particles/mL) with PBS. For experiments with exosomes collected from cancer cell culture medium, cell culture medium was diluted at a 100X and 1000X ratio with relevant cell-culture medium. The concentration was unknown for exosomes in cell culture media. Separately, a calibration curve for anti-PLAP antibody conjugated surfaces were established for detection of PLAP protein. The concentration of PLAP protein was in the range between 1.2-1250 ng/mL dissolved in PBS. For measurements, surfaces were incubated with relevant concentrations of antigen solutions (exosome or protein solutions) in either PBS or cell culture medium for 1 h and rinsed thoroughly with the incubation solution before measurements. All measurements were carried out in solution. For exosome detections, three independent experiments were carried out for every data point and for PLAP detection two experiments were carried out for every data point. Statistical analysis was completed with using t-test with a $p<0.05$ value.

Several control experiments were carried out as follows. First, anti-CD63 or anti-PLAP antibody modified surfaces were exposed to BSA solution in PBS pH 7.4 (0.1 g/mL) to determine the non-specific binding to the surfaces applying 0.1 g/mL BSA to the antibody (anti-CD63 or anti-PLAP) modified surfaces. Then 10^4 and 10^{10} particles/mL concentration of exosomes were incubated with anti-IgG modified surfaces to be able to evaluate the specificity of the exosomes to their relevant antibodies (anti-CD63). Also, antibody (anti-CD63 and anti-PLAP) modified surfaces were incubated with IgG (1 µM) to be able to evaluate specificity of the relevant antibody-antigen system. Furthermore, the response of the antibody (anti-CD63) modified surfaces in cell culture medium and cell culture medium with 40% FBS were evaluated to be able to investigate the non-specific bindings.

CHAPTER 4

RESULTS and DISCUSSIONS

In the scope of this thesis, glass wafers were first patterned with plasmonic nanoparticles, i.e. gold nanorods. Specific monoclonal antibodies were then incorporated onto gold nanorod patterns of glass wafers via two different methodologies. These functionalized biosensor chips were finally used to quantitatively detect pregnancy associated PLAP protein and exosomes from different sources via localized surface plasmon resonance (LSPR).

4.1. Synthesis and PEGylation of Gold Nanorods (AuNRs)

Gold nanorods (AuNRs) were first synthesized following a procedure reported in the literature (Mayer et al. 2008; Marinakos, Chen, and Chilkoti 2007). Since the size of exosomes varies between 50 and 200 nm, the AuNRs were aimed to be approx. 40 nm in longitudinal length to be able to detect one exosome per one nanorod. UV-vis spectroscopy and SEM analyses of AuNRs are shown in Figure 4.1 (A) and (B, C and D), respectively. SEM images were taken before purification of CTAB stabilized AuNRs which showed the presence of some gold nanoparticles (some inhomogeneity). The dimension of AuNRs was characterized using ImageJ program (measuring at least 100 nanorods). The sizes were 40±1.3 nm (longitudinal) and 14±0.8 nm (transverse) yielding an aspect ratio (AR) of 2.88. The maximum absorbance wavelength (λ_{max}) was 684 nm which was consistent with the calculated theoretical value ($\lambda_{max\ theo}$= 693 nm) from Equation 2 (Brioude, Jiang, and Pileni 2005; Link, Mohamed, and El-Sayed 1999; Tian et al. 2012). The nanorods were found to keep their colloidal stability in solution for 6 months.

$$\lambda_{max} = 95AR + 420 \tag{2}$$

The next step was to exchange the surfactant (CTAB) with PEG on gold nanorods to have self-assembled gold nanopatterns on LSPR surfaces. The surfactant exchange around AuNRs has been proposed with several different methodologies (Smith et al. 2015). Since CTAB is known to have highly positive charge, the impact of the CTAB on LSPR detection systems are always controversary. For this study, CTAB displays unfavorable properties such as positive charges and hydrophobicity which potentially leads to non-specific binding events during the detection of the biomolecules. To modify the surface with the relevant antibodies, the surface of AuNRs needs to be functionalized with reactive groups such as carboxylic acid or azide. Additionally, while the surfactant exchange is possible from CTAB to small alkane thiol molecules, the non-specific interactions of alkane thiols with biomolecules create a major drawback for LSPR detections (Willets and Van Duyne 2007). For this purpose, the surfactant exchange from CTAB to a protein repellent molecule such as PEG can be a useful approach (Gao, Liu, et al. 2018).

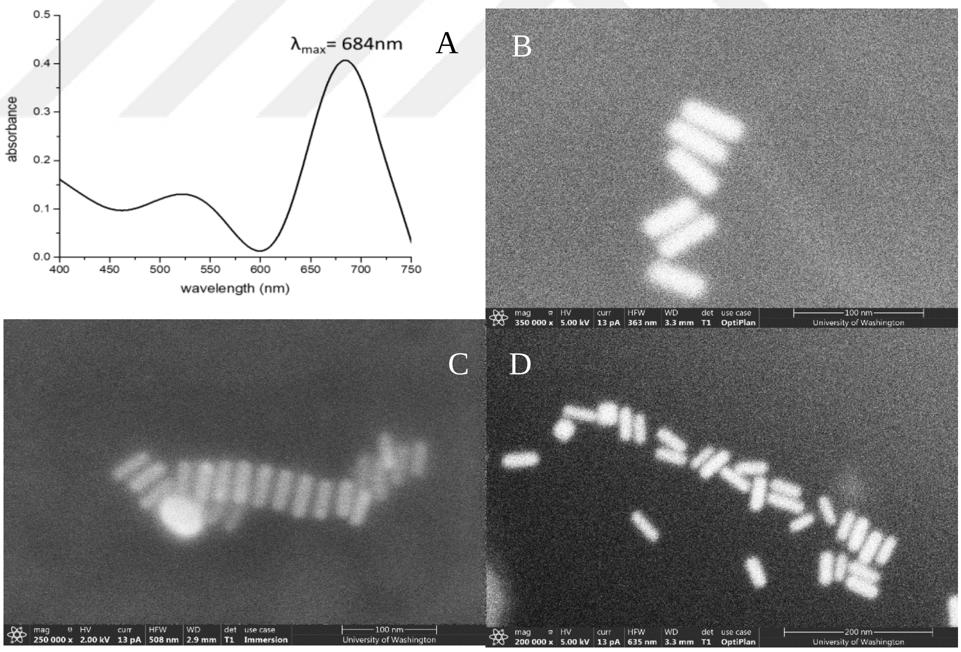

Figure 4.1. UV-vis spectrum of AuNRs in solution (length 40±1.35 nm; λ_{max}=684nm) (A) and SEM images of CTAB stabilized AuNRs (B (scale: 200 nm), C (scale: 100 nm) and D (scale: 200 nm)

In this study, PEGylation of AuNRs was performed by incubating CTAB-stabilized AuNRs with PEG in 2 mM potassium carbonate solution using PEGs with three different molecular weights, 1K, 2K and 5K PEGs. PEGylation was first confirmed via UV-vis spectroscopy (Appendix Figure A1). There was no significant maximum wavelength change before and after PEGylation regardless of the molecular weight of PEG, as expected, and decantation of supernatant which was inevitable during the purification process of PEGylated AuNRs caused some intensity difference in UV-vis absorbance of AuNRs. Insignificant shift in the maximum wavelength was expected as densely packed CTAB molecules are exchanged from the surface of the AuNRs with polymer molecules which leads to only a small change in plasmonic properties of AuNRs (Mayer et al. 2008). Since the irreversible aggregation of the AuNRs is a major problem faced during the long incubation periods of time for PEGylations, the optimum duration for PEGylation experiment was found to be 16 hours for 5K PEG, 4 hours for 2K PEG and 1 hour for 1K PEG without any aggregation and loss of stability. These conditions are consistent with literature since smaller molecular weight thiol-ended PEG can interact with Au easier when compared with larger molecular weight thiol-ended PEGs (Rahme et al. 2013). It should be noted that 5K PEG having thiol bifunctionality was also tried using the same conditions of PEGylation experiment with 5K PEG having thiol monofunctionality for surfactant exchange. This experiment resulted in irreversible agglomeration of AuNRs possibly due to the disulfide formation between different AuNRs. Surfactant exchange from CTAB to PEG was also characterized by zeta-potential measurements and results are shown in Figure 4.2. Zeta potential of cationic CTAB-stabilized AuNRs decreased significantly from +2.6 ± 0.1 to -2.7 ± 0.5 after surfactant exchange with PEG (2K). Although PEG is a neutral compound, its capability to adsorb negatively charged ions from buffer solutions may result in a decrease in zeta-potential (Barany 2015).

The zeta potential results showed that while CTAB stabilized AuNRs have positive charge (+2.6 ± 0.1), after PEGylation the zeta potential decreases significantly as well as it decreases with the increasing molecular weight of PEG (-1.9 ± 0.3 for 1K, -2.6 ± 0.3 for 2K, -9.2 ± 1.1 for 5K). A control experiment was done to determine whether there was excess CTAB or PEG in AuNRs solutions. Zeta potential of CTAB- or PEG-stabilized AuNR solutions was measured after by washing AuNRs with ethanol several times. It should be noted that CTAB and PEG are soluble in ethanol. Results showed that there was no significant zeta potential difference before or after ethanol wash, indicating the success of PEGylation process (Figure 4.2).

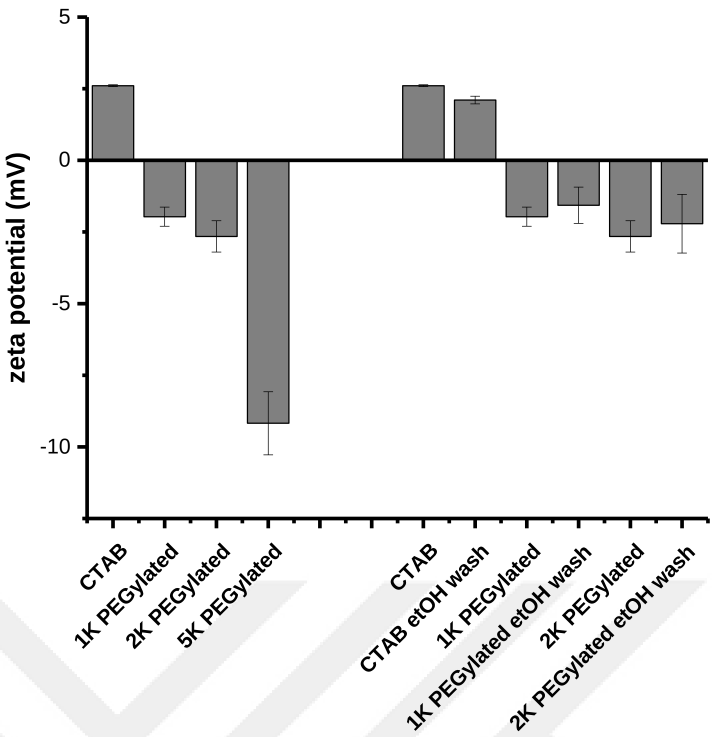

Figure 4.2. Zeta potential results of CTAB stabilized AuNRs, 1K PEG stabilized AuNRs, 2K PEG stabilized AuNRs, CTAB stabilized AuNRs after ethanol wash, 1K stabilized AuNRs after ethanol wash, 2K PEG stabilized AuNRs after ethanol wash. Measurements were performed in UP water. Results are the average of 3 independent measurements. Bars represent the standard deviation of 3 measurements.

Furthermore, the hydrodynamic size of CTAB stabilized, 2K and 5K PEGylated AuNRs were determined via DLS to be 42.2 ± 1.2 nm, 46.6 ± 2.1 nm and 65.9 ± 9.1 nm, respectively (Figure 4.3). The hydrodynamic sizes are expected to increase after PEGylation due to the larger hydrodynamic size of PEG molecules when compared with that of CTAB molecules. It is well-known that PEG is highly hydrophilic polymer and strongly interacts with water molecules and therefore adopts an expanded chain configuration. When the molecular weight of PEG increases, the hydrodynamic volume of the polymeric chain becomes larger which leads to increased size observed by DLS. The hydrodynamic size of AuNRs determined by DLS may be misleading (Khlebtsov et al. 2006), however, increase in the hydrodynamic size of AuNRs with the increase in PEG molecular weight may be indicative of successful PEGylation. The concentration of synthesized AuNRs were calculated from Beer-Lambert's law with assuming an extinction coefficient of $20x10^8$ L/mol.cm (Near et al. 2013) as 5000 pM.

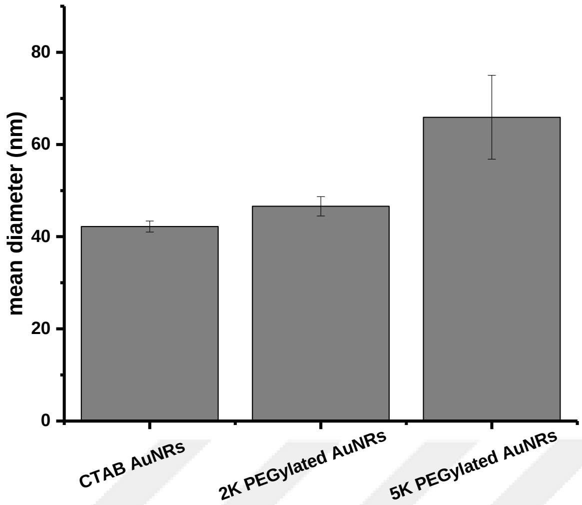

Figure 4.3. Number based mean diameter of CTAB, 2K PEG and 5K PEG stabilized AuNRS determined by DLS. Measurements were performed in UP water where AuNRs concentration were calculated as 5000 pM. Results are the average of 3 independent measurements. Bars represent the standard deviation of 3 measurements.

4.2. Wafer Cleaning Procedures

After obtaining the AuNRs, the self-assembly of AuNRs on glass wafers was investigated in detail. In literature, there are various methodologies for the self-assembly process of AuNRs on glass wafers (Alaqad and Saleh 2016; Chen et al. 2008; Khan et al. 2014; Love et al. 2005). Silanization of glass is one of the most used methods since the Si-Au bond is known to have a high binding energy of 304.6 ± 6.0 kJ/mol (Luo, 2002). It should be noted that this energy is even higher than S-Au bond (253.6 ± 14.6 kJ/mol) which is known as a strong bonding energy for self-assembly process (Xue et al. 2014). For self-assembly of AuNRs, silanization of glass with amine or thiol bearing silanes have been reported in literature (Yochelis et al. 2012). Silane interaction with glass wafers is a very delicate experimental procedure and requires very clean surface area to have uniform silanization. Presence of any residual organic compound on the surface leads to inhomogeneity and lack of reproducibility (Cras et al. 1999). There are several methodologies for cleaning of the wafers using piranha solution, isopropanol solution or plasma treatment. In this work, all three of these cleaning methods were investigated on microscope slides followed by silanization with amino or thiol functionalized silanes. First, piranha solution treated surfaces were analyzed via contact angle measurements. The results showed an increase in surface hydrophilicity after treatment with piranha solution, which also indicated the removal of residual compounds from the surface (Appendix Figure A7). The surfaces cleaned via three different methods were silanized followed by interaction with PEGylated AuNRs. The silanization procedures have been discussed in detail in the next section. The self-assembly of PEGylated AuNRs on glass wafers cleaned via three different methods were compared by means of LSPR responses using UV-vis spectroscopy. The results showed that there was not any difference between the surfaces cleaned with piranha or isopropanol solution while surfaces cleaned via plasma treatment showed no self-assembly (no LSPR shift) of AuNRs (Figure 4.4). Thus, isopropanol solution cleaning procedure was chosen as the cleaning procedure as it was less dangerous because there was no handling of sulfuric acid. Furthermore, treatment with piranha solution leads to polyamorphous SiO_2 structures and thus inhomogeneity in the self-assembly of particles (Sarangan 2016).

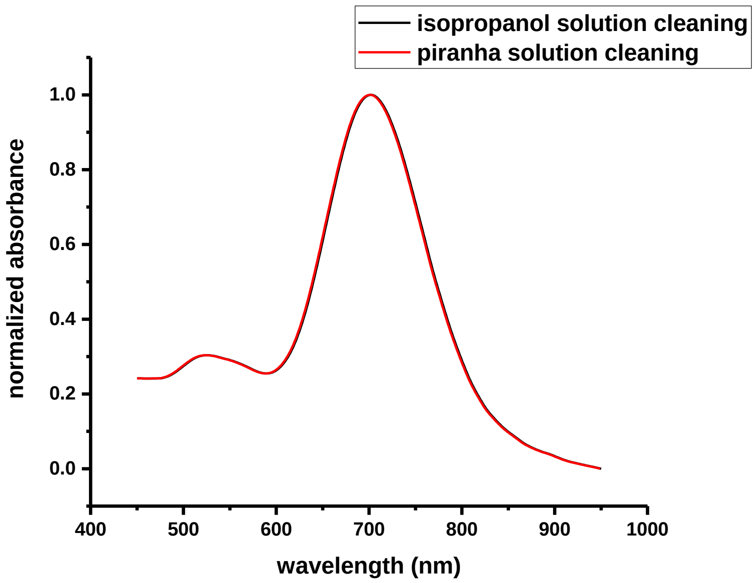

Figure 4.4. LSPR spectra of 2K PEGylated AuNRs patterned surfaces silanized after isopropanol or piranha solution cleaning.

4.3. Silanization of Different Glass Wafer Types

As explained in the methods section, the prepared surfaces yield a reliable LSPR response only in a region with a diameter of 2 mm at the middle of the glass wafers. Any inhomogeneity in this region may cause false response (higher exact value of λ_{max}) or broadening of the LSPR peak. To overcome this problem, silanization procedures were investigated in detail for patterning of surfaces with 5K or 2K PEGylated AuNRs via UV-vis spectroscopy (Figure 4.5) and SEM (Figure 4.6). 2K PEGylated AuNRs on silanized surfaces showed the best distribution on the surface along with the best intensity and peak broadening LSPR response. SEM images revealed that red shift in the case of 5K PEGylated AuNRs on MPTMS was caused by aggregation of AuNRs on the surface which can be explained by gold aggregates tending to have the properties of large gold particles (Chegel et al. 2012). It should be noted that when PEGylated AuNRs were applied on the bare surfaces (without any silane modification), the gold assembly could not be observed by eye due to lack of interaction between the surface oxygen atoms and PEG molecules around AuNRs.

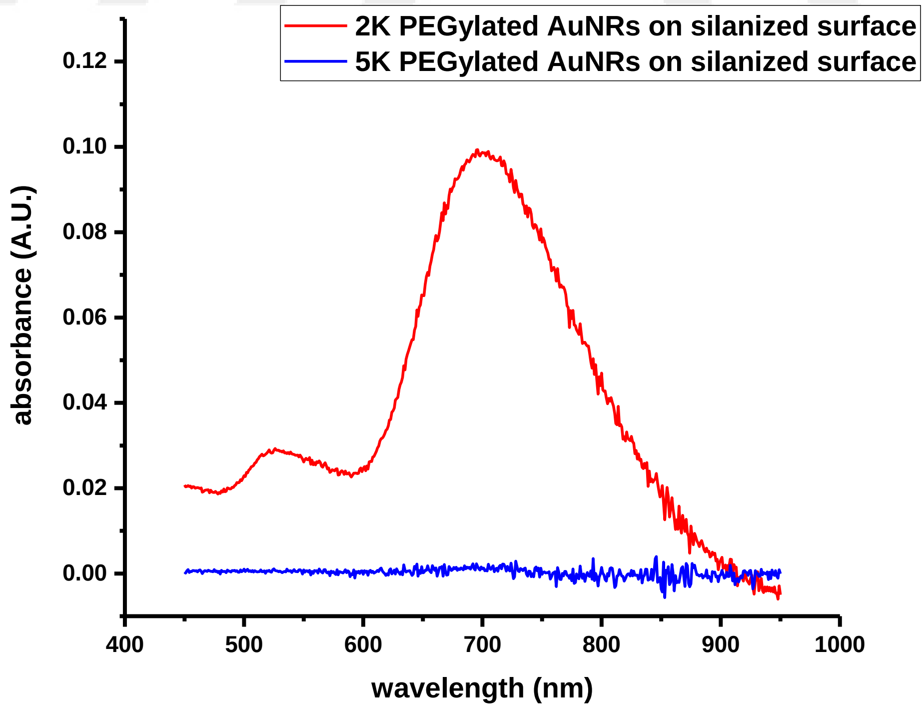

Figure 4.5. LSPR results for 2K PEGylated and 5K PEGylated AuNRs on silanized surfaces.

As mentioned above, silanization is a very delicate process. Silanes undergo polymerization very easily when exposed to water, creating cross-linked multilayers of silanes which changes the hydrophilic properties of the surface and ultimately alters the surface properties for further modifications (Krasnoslobodtsev and Smirnov 2002). In literature, silanization can even be completed within 5 min and self-assembly of gold nanoparticles has been achieved afterwards (Fujiwara et al. 2006). Even though the surface is clean enough from residual organic molecules and dry enough to prevent the polymerization of silanes, they can undergo different kinds of binding types with surface oxygens changing the surface compound to be Si, NH_2 or CH_3 for APTES (Acres et al. 2012; Kyaw et al. 2015). For gold nanorod self-assembly on MPTMS modified glass wafers, it is known that AuNRs tend to agglomerate faster due to the ionic strength of the solution and silanization can alter the orientation of gold nanorods (Wang and Tang 2013). Since the silanization parameters were kept constant for this study, APTES modified surfaces showed less agglomeration of AuNRs compared to MPTMS. As mentioned in the introduction, there are several studies about self-assembly of gold nanoparticles on glass wafers using APTES or MPTMS via different methodologies. In this work, 2K PEGylated AuNRs on APTES modified surfaces were found to have the best LSPR response and this was proved via SEM by means of particulate gap between the nanoparticles (Figure 4.6).

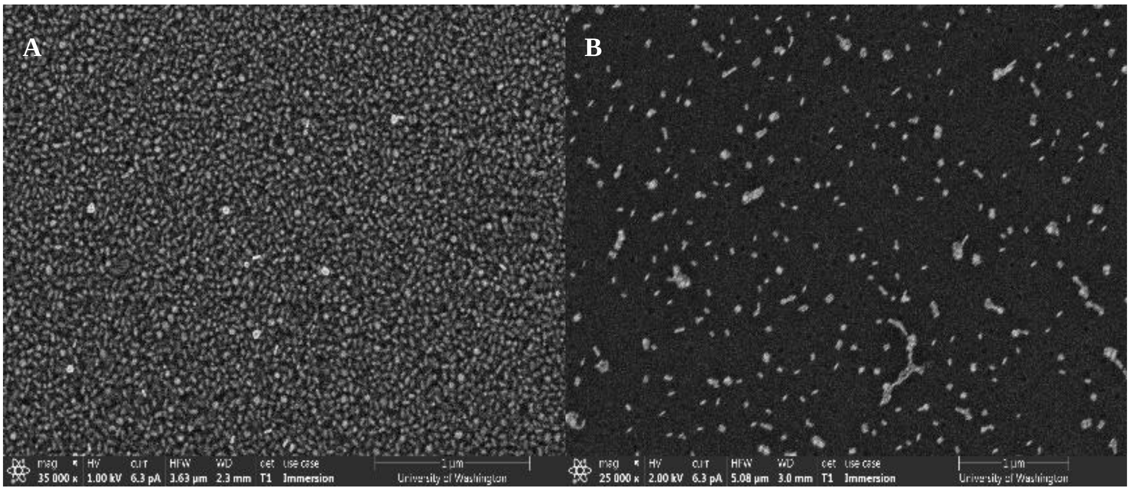

Figure 4.6. SEM images of silanized surfaces after the self-assembly of: (A) 2K PEGylated AuNRs and (B) 5K PEGylated AuNRs.

4.4. Performance Evaluation of the AuNRs Patterned Surfaces

The UV-vis response performance of 1K, 2K and 5K PEGylated AuNRs patterned surfaces were first evaluated by measuring the LSPR response of the surfaces in solution having different refractive index values (water: 1.33, ethanol: 1.36, 3:1 ethanol/toluene: 1.39, 1:1 ethanol/toluene: 1.4, 1:3 ethanol/toluene: 1.43, and toluene: 1.45) (Figure 4.7 and Figure 4.8). The measurements were repeated with 5 different surfaces for each solution. The slope of wavelength shift vs. RI graphs (Figure 4.7) of the wafers constructed with 5K, 2K and 1K PEGylated AuNRs patterned surfaces are 224 nm/RIU, 271 nm/RIU and 257 nm/RIU, respectively. The statistically significant difference between the slopes of the curves was investigated by comparing the slopes of every dataset (n=1, n=2, n=3, n=4 and n=5). 2K PEGylated AuNRs patterned surfaces showed higher slope for every dataset comparing to 1K and 5K while 1K PEGylated AuNRs patterned surfaces showed higher slope compared to 5K (Figure 4.7). In addition, AuNRs patterned surfaces prepared in this study were more sensitive to RI changes of the surrounding than the similar glass surfaces reported in the literature that have 5K PEGylated AuNRs patterned surfaces (198 nm/RIU) (Mayer et al. 2008; Chen et al. 2008). In this study, 2K PEGylated AuNRs patterned surfaces found to have the optimum sensitivity.

Similar results were obtained by the comparison of 2K PEGylated AuNRs before and after plasma treatment (Figure 4.8). Surfaces before plasma treatment showed higher sensitivity (i.e. slope of wavelength shift vs. RI) compared to plasma treated surfaces for each of the dataset. When the average of the slopes was taken for every measurement, slope of the 2K PEGylated AuNRs patterned surfaces showed the highest response to the refractive index change in the surrounding. Plasma treated surfaces showed a 256 nm/RIU sensitivity which was lower than the non-plasma treated surfaces (271nm/RIU). Overall, it can be concluded that both surfaces have good sensitivity values. However, considering that the presence of PEG on untreated surfaces potentially minimizes the non-specific bindings, further steps towards biofunctionalization of PEGylated AuNRs assembled glass wafers were performed without performing plasma-etching.

Plasma untreated AuNRs patterned surfaces were further analyzed via SEM (Figure 4.9), it was seen that 2K PEGylated AuNRs patterned surfaces have AuNRs more homogenously distributed when compared to 1K and 5K PEGylated AuNRs patterned surfaces. Also, the interparticle gap between AuNRs when comparing 2K and 5K PEGylated AuNRs surfaces can also be observed (in comparison with Figure 4.6). The surfaces patterned with 5K PEGylated AuNRs displayed larger unoccupied spaces. As the raw data (Appendix Figure A8) showed clearly, 1K and 2K PEGylated AuNRs patterned surfaces showed higher intensities (0.25 a.u.) compared to 5K PEGylated AuNRs patterned surfaces (0.05 a.u.). However, 1K and 2K PEGylated AuNRs tended to agglomerate faster in solution during the self-assembly process. This can be explained by the lower hydrodynamic volume of PEGs around AuNRs as the molecular weight decreases. Close pack self-assembly for 1K and 2K PEGylated AuNRs as shown via SEM led to high LSPR signal intensity. Considering LSPR theory, when the interparticle gap is increased, consequently plasmon shift decreases (Jain, Huang, and El-Sayed 2007). In fact, the shift disappears if the interparticle gap between two particles is greater than 2.5 times of the particle's dimensions (transverse or longitudinal) (Su et al. 2003). Accordingly, 1K and 2K PEGylated AuNRs on the surfaces are expected to have smaller gaps between each other when compared with 5K PEGylated AuNRs. On the other hand, lower molecular weight PEG (i.e. 1K PEG) may not provide sufficient colloidal stability to AuNRs when compared with 2K PEG. This may result in agglomeration of 1K PEGylated AuNRs on the surfaces compared to 2K PEGylated AuNRs patterned surfaces. All these parameters affect the sensitivity of the surfaces and accordingly the detection limits. In conclusion, 2K PEGylated AuNRs patterned surfaces yielded the best LSPR response with the highest sensitivity as well as the most homogeneous particle distribution.

LSPR response strongly depends on the size and the orientation of the AuNRS. For 40 nm AuNRs, the response increases with elongation until AR>3.4. This phenomenon is explained by the Gans theory (Huang, Neretina, and El-Sayed 2009). When the size of exosomes is considered (50-200 nm), 40 nm longitudinal length for AuNRs was chosen to be able to detect one exosome per gold nanorod and the AR was kept lower than 3.4.

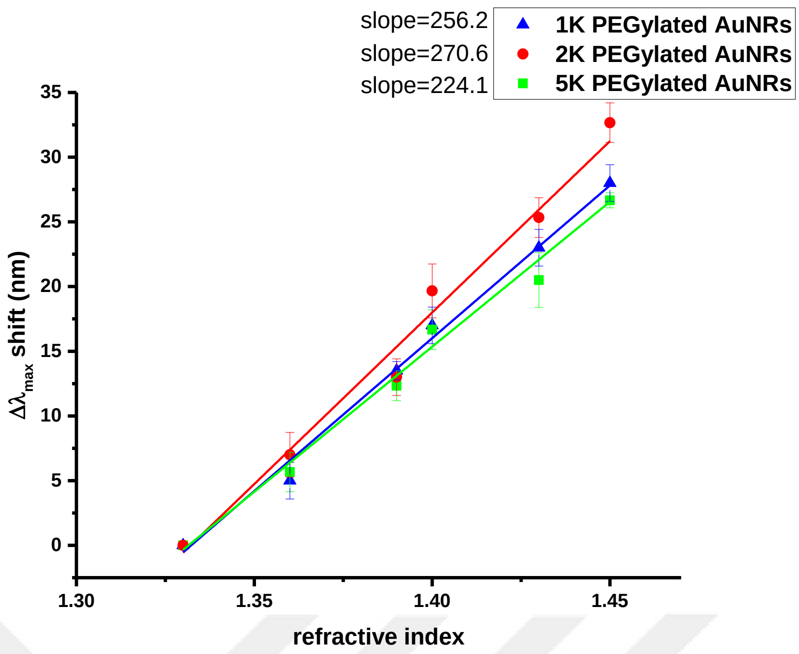

Figure 4.7. λ_{max} shift of 1K, 2K and 5K PEGylated AuNRs patterned surfaces without any plasma treatment (n=5).

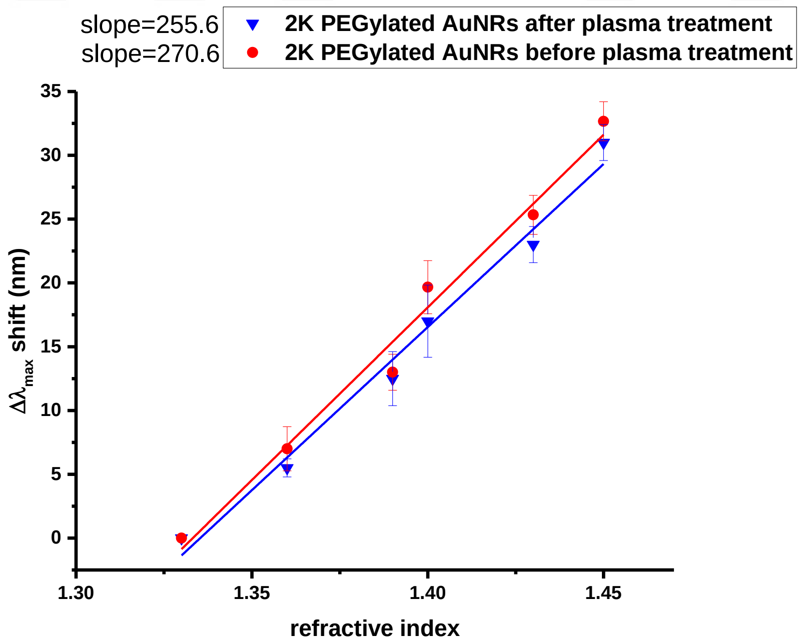

Figure 4.8. λ_{max} shift of 2K PEGylated AuNRs patterned surfaces before and after plasma treatment (n=5)

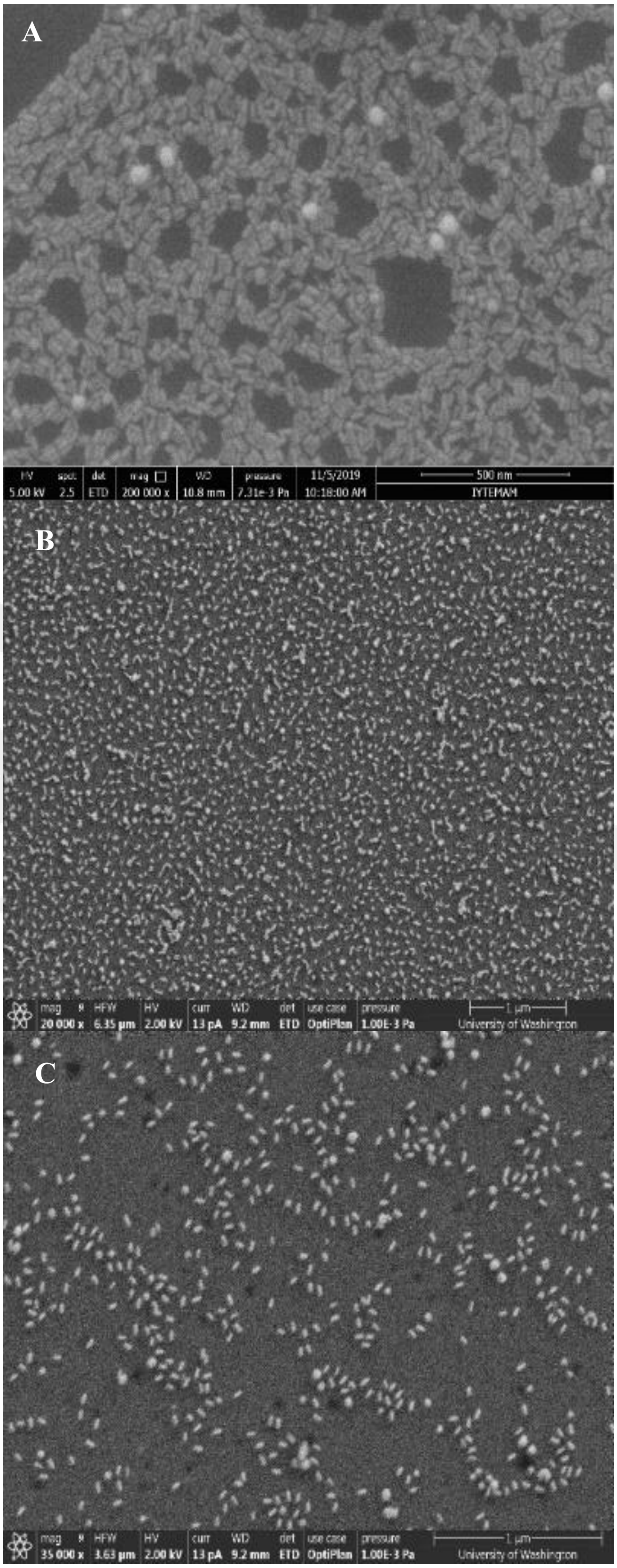

Figure 4.9. SEM images of 1K (A), 2K (B) and 5K (C) PEGylated AuNRs on silanized microscope slides without any plasma treatment.

In literature, the magnitude of response (red-shifting) is significantly higher for 2 kDa PEGylated AuNRs patterned surfaces compared to 6 kDa PEGylated AuNRs patterned surfaces that is explained by the interparticle gap (Mahmoud 2014). The orientation along interparticle axis results in significant red shift while the perpendicular orientation along nanorods results in a small blue-shift (back-shifting). This is explained by the effect on the electromagnetic field of the particles influenced with a nonbonding type of interaction in perpendicular orientation. On the other hand, influence on electromagnetic field is couple for side by side orientation which leads to a red-shifting (Funston et al. 2009). While AuNRs patterned surfaces that have interparticle gap higher than 2.5 times of the nanoparticle size (as in the case of 5K PEGylated AuNRs (Figure 4.9 (C)) showed very broad and less intense peak, AuNRs that are oriented along interparticle axis (as in the case of 2K PEGylated AuNRs (Figure 4.9 (B)) showed narrow and intense LSPR peaks. 1K PEGylated AuNRs patterned surfaces showed similar LSPR response profile as 2K PEGylated AuNRs patterned surfaces. Overall, considering the protein repellent nature of longer PEG chain and higher sensitivity, 2K PEGylated AuNRs patterned surfaces were chosen over 1K PEGylated AuNRs.

4.5. Antibody Functionalization of the Surfaces

The methodology for biofunctionalization of AuNRs on glass wafers involves plasma etching of the self-assembled AuNRs on glass wafers removing all PEG molecules around AuNRs and leaving the bare gold surface. Upon plasma etching and removal of PEG molecules from the surface, bare gold particles remaining on the surface are usually modified with functional alkane thiol or oligoethylene glycol bearing alkane thiol molecules followed by conjugation of biomolecules (Harder et al. 1998; Prime and Whitesides 1993). The most common methodology for conjugation of specific antibodies on surfaces is the usage of small alkane thiol self-assembly molecules that have carboxylic acid and hydroxyl groups. Carboxylic acids can be used with EDC/NHS chemistry to bind the antibodies through their amine groups. Hydroxy groups create hydrophilicity on the surface and accordingly they make the surface protein repellant (Love et al. 2005). In this study, surface modification of PEGylated AuNRs assembled glass wafers was performed using functionalized alkane thiol molecules without treating the surfaces with plasma.

In literature, ligand exchange on PEGylated gold nanoparticles has been commonly investigated in solution (Wijaya and Hamad-Schifferli 2008) and two mechanisms have been proposed for surfactant exchange (Burrows et al. 2016) from PEG to alkane thiols: either by direct exchange of PEGs on the surface with small alkane thiol molecules or backfilling of small molecules while PEG molecules remain on the surface of AuNRs (Smith et al. 2015). According to Rahme et. al. high molecular weight PEG molecules such as 5K PEGs creates more folded structures and higher hydrodynamic size around AuNRs while smaller molecular weight PEG molecules create more tethered structures with less hydrodynamic size around AuNRs (Rahme et al. 2013). Smith et. al. further showed that the smaller molecular weight PEG modified AuNRs tend to have more backfilling profile which is caused by the more tethered structures (Smith et al. 2015). While the molecular weight and thus hydrodynamic size of PEG around AuNRs increase, the interaction of thiol groups on alkane thiol molecules with gold gets harder which might create secondary non-specific interactions between alkane thiols and PEG molecules, preventing functionalization of AuNRs. It is known that 5K PEG creates a radius of gyration more than 5 nm and 5K PEG chains create a shield around AuNRss (Hore et al. 2015). However, with the smaller molecular weight PEG molecules, alkane thiols find enough room to backfill the AuNRs surfaces without any non-specific interactions depending on the concentration. In the light of literature given above, the self-assembly of 11-mercaptoundecanoic acid (COOH) (10 mM, 5 mM and 1 mM) and 11-mercapto-1-undecanol (OH) (10 mM, 5 mM and 1 mM) were used in this study to modify 5K and 2K PEGylated AuNRs patterned surfaces. The results are shown in Figure 4.10 and 4.12, respectively.

After the self-assembly procedure with 11-mercaptoundecanoic acid (COOH) (10 mM, 5 mM and 1 mM) and 11-mercapto-1-undecanol (OH) (10 mM, 5 mM and 1 mM) at three different concentrations onto 5K PEGylated AuNRs patterned surfaces, an LSPR shift of 10 nm was observed for 10 mM and 5 mM concentrations while no shift was observed at 1 mM concentration (Figure 4.10). All these surfaces further immersed into EDC/NHS solution and then immersed into antibody solution followed by ethanolamine deactivation. At none of the concentrations tested, there was no LSPR shift after antibody conjugation procedure. This result indicated that the functionalization of the surface with COOH molecules was unsuccessful. While the long chain 5K PEG molecules around AuNRs may cause secondary interactions with alkane thiols' functional groups (COOH and OH), this may lead to accumulation of the alkane thiol molecules at high concentrations around AuNRs and results in an LSPR shift after the self-assembly process, but COOH groups may be involving with secondary interactions with PEGs and hence not be displayed on the surface to antibody molecules.

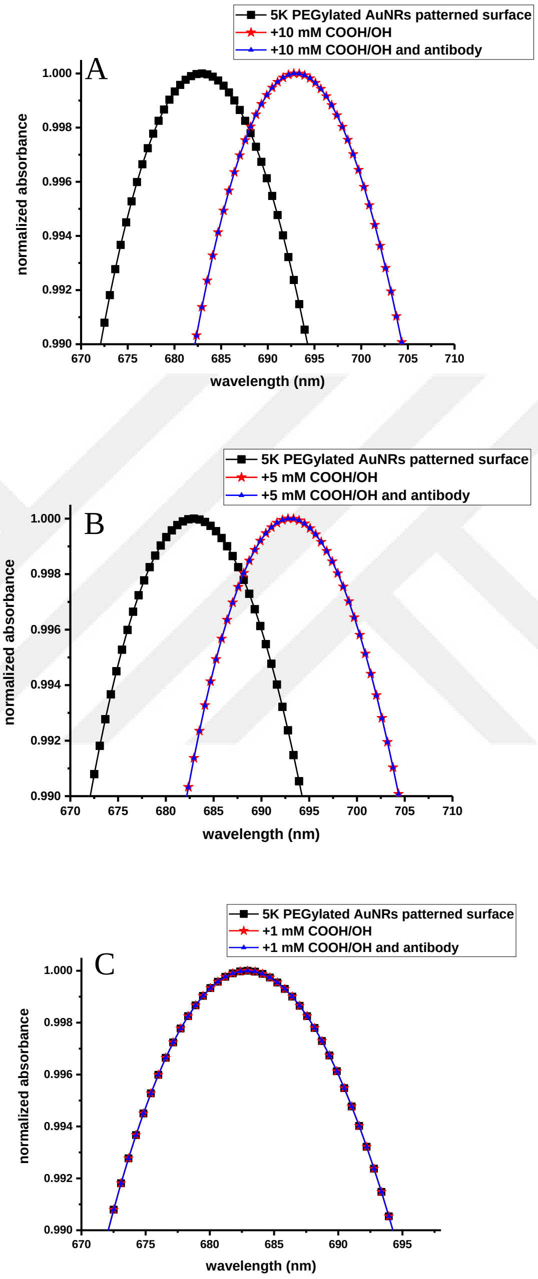

Figure 4.10. LSPR spectra of 5K PEGylated AuNRs patterned surfaces after interaction with 10 mM (A) 5 mM (B) and 1 mM (C) alkane thiol molecules with COOH and OH groups and followed by antibody incubation with EDC/NHS chemistry.

The same procedure was applied onto 2K PEGylated AuNRs patterned surfaces and results are given in Figure 4.11 and Figure 4.12. As it can be seen in the figures, an LSPR shift of 9 nm was observed after incubation of the surfaces with 10 mM and 5 mM concentrations of self-assembly molecules, but no shift was observed after the subsequent antibody conjugation in the presence of EDC/NHS. This result was almost identical with that 5K PEGylated AuNRs patterned surfaces. Interestingly, when 2K PEGylated AuNRs patterned surfaces were incubated with 1 mM of alkane thiol with COOH and OH groups there was no LSPR shift, similar to modification at higher concentrations of alkane thiols. However, after the activation with EDC/NHS and incubation with antibody, an average shift of 6 nm was observed, suggesting the successful functionalization of the surface. In the case where functionalization with alkane thiols before incubation with antibody was absent, 2K PEG AuNRs patterned surfaces did not display any non-specific binding of the antibodies (Figure 4.11), indicating the necessity of COOH functionalization for specific conjugation and the success of 2K PEG in inhibiting non-specific binding.

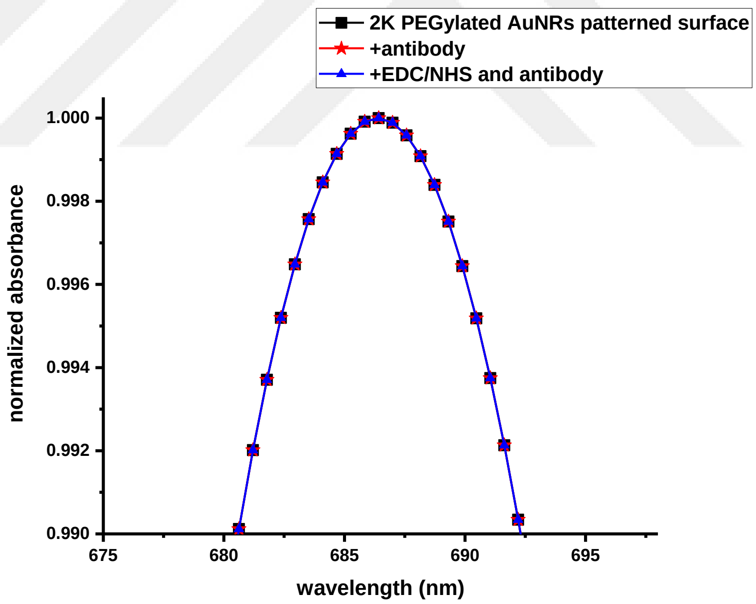

Figure 4.11. LSPR results of the control experiments performed with 2K PEGylated AuNRs patterned surfaces. Surfaces that were not functionalized with alkane thiol molecules were analyzed before and after antibody incubation with or without EDC/NHS activation.

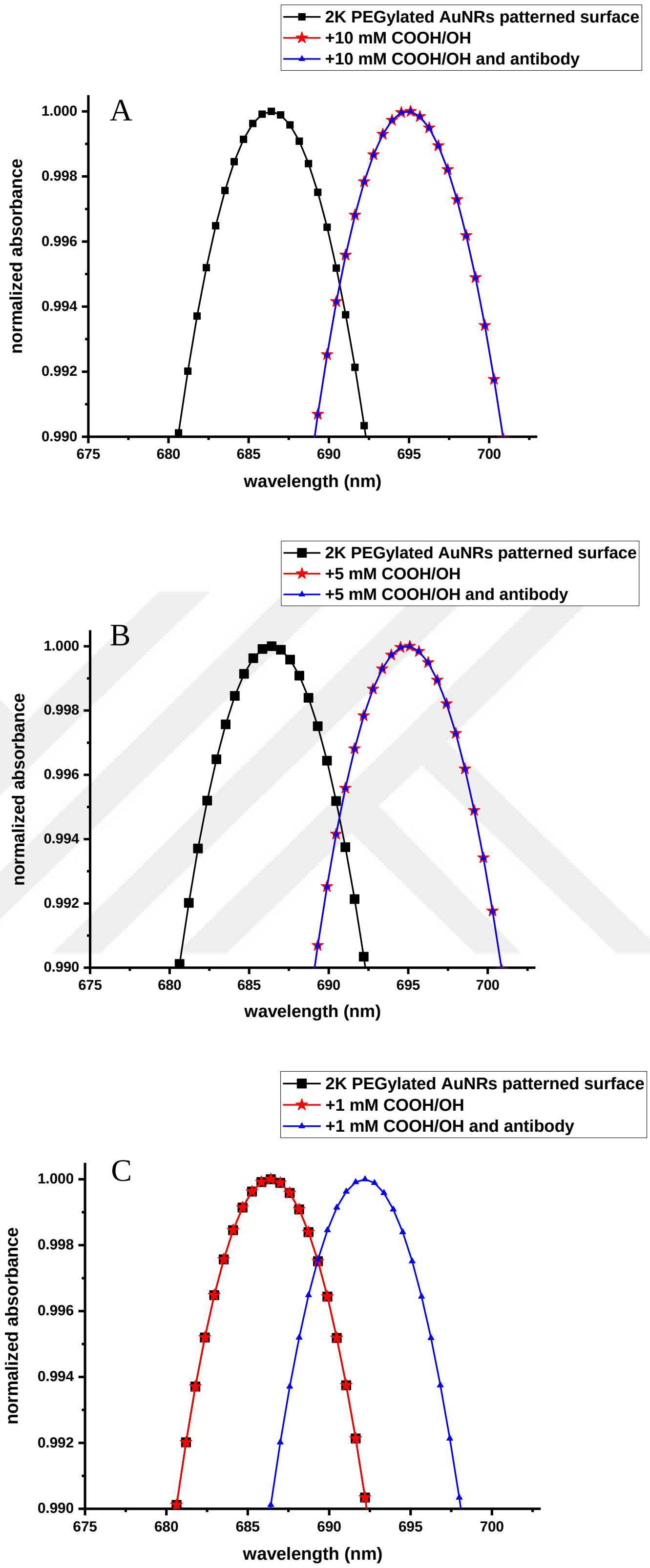

Figure 4.12. LSPR spectra of 2K PEGylated AuNRs patterned surfaces after interaction with 10 mM (A) 5 mM (B) and 1 mM (C) alkane thiol molecules with COOH and OH groups and followed by antibody incubation with EDC/NHS chemistry.

The modification of the surfaces was further analyzed via zeta potential, FTIR spectroscopy and XPS experiments. Figure 4.13 shows the XPS results of 2K and 5K PEGylated AuNRs patterned surfaces before and after the modification with alkane thiol molecules at 1 mM concentration. The percentage of Au atoms (normalized according to Si) on the 2K PEGylated AuNRs patterned surfaces was significantly higher when compared to 5K PEGylated AuNRs patterned surfaces. This was attributed to the smaller hydrodynamic size of 2K PEGs with respect to 5K PEG around AuNRs (Figure 4.3). After modification with functionalized alkane thiols, the percentage of Au atoms on 2K PEGylated AuNRs patterned surfaces significantly decreased while it remained almost the same on 5K PEGylated AuNRs patterned surfaces. It can be speculated that the 2K PEGylated surface was successfully modified with alkanethiol molecules through back-filling mechanism, while the amount of gold remained almost constant for 5K which indicates the unsuccessful attempt for alkane thiol functionalization. In literature, the hydrodynamic size of PEG around gold nanoparticles was investigated and it was found that higher molecular weight PEG showed higher hydrodynamic size (Rahme et al. 2013) which led to a harder surface modification around PEGylated AuNRs (Burrows et al. 2016).

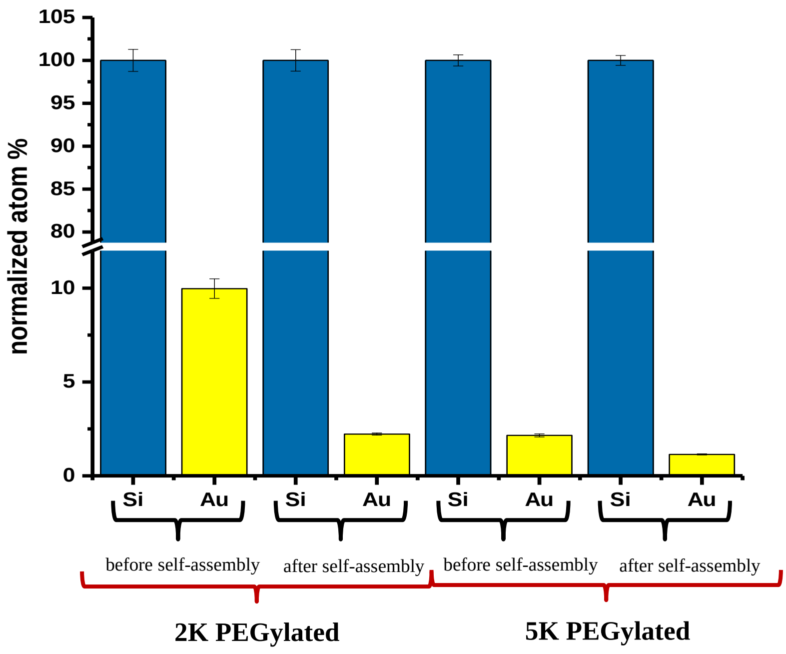

Figure 4.13. XPS comparison for 2K and 5K PEGylated AuNRs surfaces before and after COOH/OH self-assembly (data normalized according to Si atom)

2K PEGylated AuNRs surfaces were further analyzed via zeta potential measurements since these surfaces showed better results in terms of surface functionalization. The zeta potential values of 2K PEGylated AuNRs patterned surfaces before and after plasma-treatment, after modification with alkane thiols and antibodies along with CTAB-stabilized, PEG-stabilized AuNR solutions (in PBS at pH 7.4), antibody solutions in PB or PBS at pH 7.4 are shown in Table 4.1. While oxygen plasma treated surfaces showed a slightly positive charge, in accord with the charge of bare gold, indicating that the plasma etches successfully PEG layer on AuNRs, without plasma-treatment, the surfaces displayed slightly negative zeta potential. Adsorption of negatively charged ions from buffer solutions may result in a decrease in zeta-potential (Burrows et al. 2016). Modification with alkane thiols (1 mM) having COOH and OH groups did not change the zeta potential of the PEGylated AuNRs patterned surface significantly which was expected due to the exchange of PEG molecules with slightly negatively charged COOH group bearing alkane thiols. After the conjugation of the relevant antibody, which is negatively charged at the relevant concentration, the surface zeta potential lowered significantly. The zeta potential of the antibodies also investigated thoroughly, and results are shown in Appendix Figure A6. Zeta potential of the antibodies increases to positive values as the concentration increases in ultra-pure water. The zeta potential of the antibodies is influenced from factors such as pH, temperature, concentration, excipients, etc. All these factors affect the self-association behavior of the antibodies and ultimately effects the zeta potential (Le Basle et al. 2020). Antibodies are conjugated to the functionalized surfaces with a concentration of 10 µg/mL and they are negatively charged within working conditions.

The modified surfaces were further analyzed with FTIR and results are shown in Figure 4.14. Before modification of the surface with alkane thiols, theoretically only PEG molecules are expected to exist around the AuNRs. Accordingly, C-H bonding along with C-O bonding was observed in FTIR spectrum of 2K PEGylated AuNRs patterned surface. After modification with carboxylic acid and hydroxy bearing small alkane thiol molecules, C=O bond band appeared and C-C bending and C-O bending was observed to increase in the 1500-750 cm^{-1} region compared to 2K PEGylated AuNRs patterned surface. After the surfaces were further modified with relevant antibody using EDC/NHS chemistry, a band attributed to C=O amide bond appeared in 1800-1600 cm^{-1} region. Additionally, the same surfaces were analyzed via RAMAN spectroscopy (Figure 4.15). A band showing C=O dominant amide bonding at around 1780 cm^{-1} could be seen clearly.

Overall zeta potential, FTIR, XPS and RAMAN results show the successful biofunctionalization of the surfaces.

Table 4.1. Zeta potential measurements of 2K PEGylated AuNRs patterned surfaces in solution and on surface

AuNRs sample*	zeta potential	measurement type
Sample*	**Zeta potential**	**Measurement medium**
Plasma treated	+4.8 ± 1.0	surface
No plasma treated (PEGylated surface)	-3.26 ± 0.9	surface
PEGylated surface COOH/OH modified	-1.25 ± 0.9	Surface
PEGylated surface COOH/OH + antibody modified	-6.31 ± 0.2	surface
CTAB-stabilized AuNRs	+2.6 ± 0.1	solution
PEGylated AuNRs	-2.7 ± 0.5	solution
Antibody in PB	-9.8 ± 0.4	Solution
Antibody in PBS	-4.9 ± 0.3	solution

*n=3 repeats in PB or PBS at pH 7.4

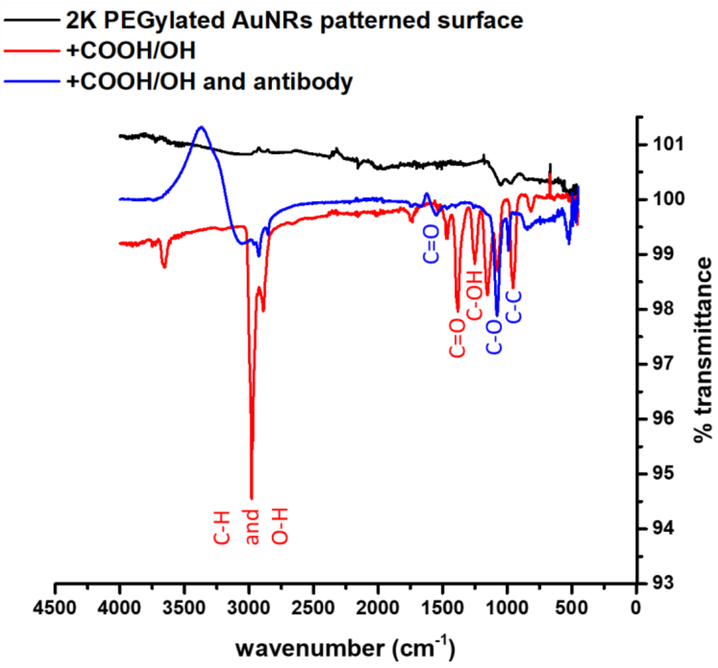

Figure 4.14. FTIR spectrum of 2K PEGylated AuNRs patterned surfaces before and after self-assembly of alkane thiols having COOH and OH groups.

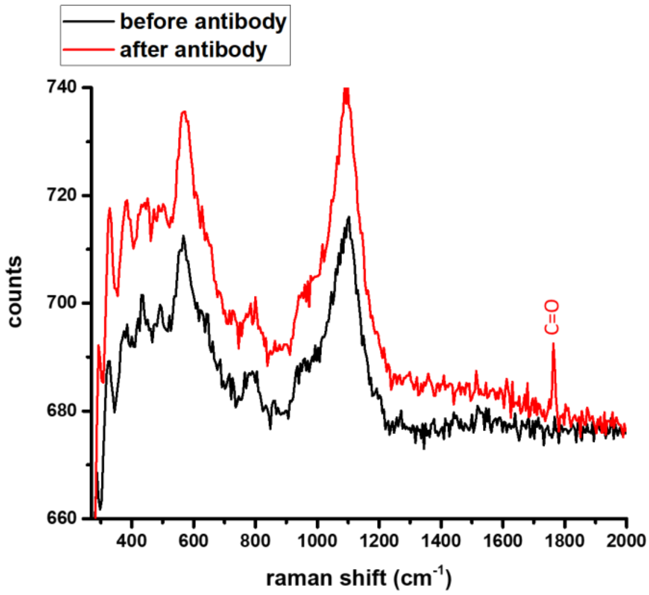

Figure 4.15. RAMAN spectrum of 2K PEGylated AuNRs patterned surface after modification with alkane thiols before (black line) and after (red line) antibody conjugation.

The antibody conjugated surfaces were first validated for their specific recognition ability using 2K PEGylated AuNRs patterned surfaces functionalized with anti-IgG antibody via NHS/EDC chemistry. Goat anti-human IgG antibody was used to detect human IgG as a representative antibody-antigen system for validating the biosensor surfaces. The concentration range for IgG detection was between 0 and100000 pM. The system showed a shift of 0.4 nm after incubation with 100 pM IgG and the wavelength shift increased when the analyte concentration increased. A shift of 4 nm was observed when the analyte IgG concentration was 6700 pM (Figure 4.16) and a final shift of 8.2 nm was observed at 100000 pM concentration. Importantly, the surface was washed with PB for 24 hours and then checked for LSPR response to evaluate any back shifting due to loss of interactions. No back shifting was recorded, indicating that all binding events were through specific bio affinity interactions. These results are consistent with literature results that apply similar gold nanoparticle systems for the detection of IgG (Mun'delanji et al. 2015).

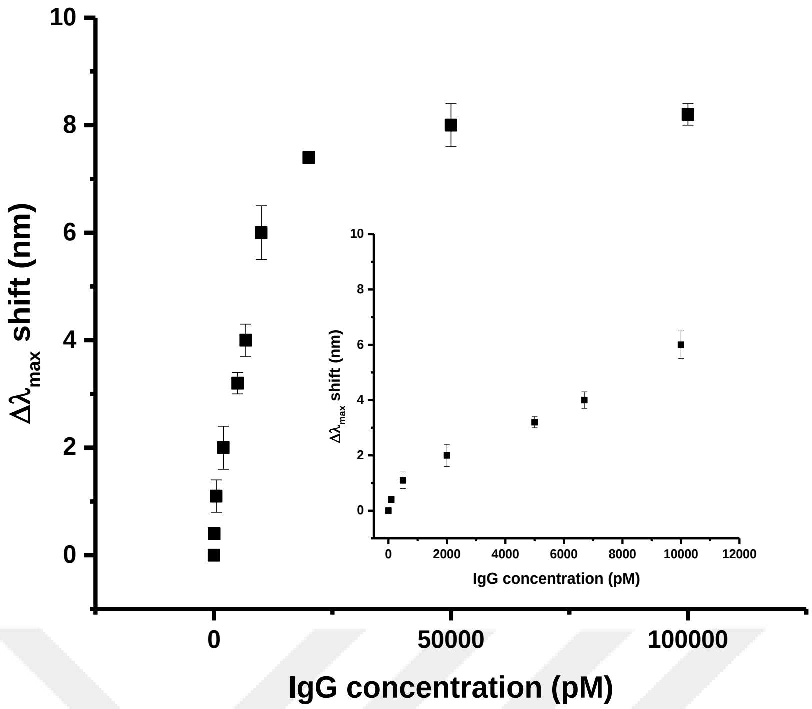

Figure 4.16. LSPR detection of human IgG standard solutions at varying concentrations using 2K PEGylated AuNRs patterned surfaces functionalized with goat anti-human IgG antibody via EDC/NHS chemistry. Inset shows the range between 0 and 10000 pM concentration.

In literature, the most common methodology for antibody conjugation onto gold nanoparticles is conventional EDC/NHS chemistry (Jazayeri et al. 2016). This chemistry may have drawbacks on the antibody orientation since the EDC/NHS chemistry occurs between carboxylic acids on the surface and amine groups of the antibodies yielding amide covalent bonding. Since there are lysine residues in Fab as well as Fc regions of the antibodies, it is possible that antibodies are conjugated to the surface through their Fab region when EDC/HNS chemistry is used for conjugation, causing a decrease in the sensitivity of the biosensor surface. . An Fc region specific protein, protein G (Björck and Kronvall 1984), has been widely used to conjugate antibodies to the surface through their Fc region for SPR/LSPR systems (Oh et al. 2019; Makaraviciute, Ramanavicius, and Ramanaviciene 2015).

Derived from the Fc binding specific region of protein G, a commercial product, dibenzylcyclooctyne (DBCO)-modified-ImmuneLink^{TM} (IL) (Jung et al. 2009; Hui et al. 2015) was utilized in this study to conjugate antibodies to the surface through their Fc region. Conjugation of DBCO-ImmuneLink^{TM} (IL) with relevant antibodies (Ab) was carried out via UV-irradiation followed by the purification of DBCO-IL-Ab conjugates via HPLC. The proposed strategy and advantages over conventional EDC/NHS system in terms of antibody orientation are shown in Figure 3.1.

First of all, azide functionalization on the surface of AuNRs was necessary to conjugate DBCO-IL protein via click-chemistry. For this purpose, bis(11-azidoundecyl) disulfide (N3) and 11-Mercapto-1-undecanol (OH) were used as functional alkyl thiol molecules for functionalization of 2K PEGylated AuNRs patterned surfaces. Optimized conditions for COOH/OH were used for the self-assembly of N3 bearing alkylthiols as given in the method section. In literature it is known that R-SH and R-SS-R have the similar interaction with gold and the rate of formation of self-assembly monolayers for these two molecules are the same (Dilimon et al. 2013). Incorporation of azide groups onto the surface was analyzed by XPS experiments (Figure 4.17). A high resolution carbon scan revealed that before modification, the surface had C-C (285 eV) and C-O bonding (~286 eV) (Figure 4.17 (A)) which showed the presence of PEG molecules on the surface, and after modification, the shift to higher energies demonstrated C-N and more C-O bonding (Figure 4.17 (B)). Furthermore, the decrease of Au atom percentage and increase for C and O can be seen when the data were normalized to Si percentage. , When the detailed nitrogen scan was evaluated (right-bottom) a shift to higher binding energies from $-NH_2$ (BN3) (the presence of organic matrix for nitrogen before azide modification) to $N=N^+=N^-$ (AN3) was which proved the successful azide functionalization on the surfaces (Figure 4.17 (D) black line).

In parallel, Ab conjugation to DBCO-IL was performed followed by HPLC purification and SDS-PAGE characterization (Figure 4.18). First DBCO-IL-Ab conjugation was completed in solution (PBS) and purified via preparative HPLC. During HPLC experiment, the sample was collected at 8 mins which was indeed the elution time of pure Ab. It should be noted that Abs that were not modified with DBCO-IL were not expected to bind onto LSPR surfaces, as suggested by the results of control experiments showing no detectable non-specific binding events onto the prepared surfaces, (Figure Figure 4.11 and Appendix Figure A3). The presence of PEG molecules that create a repellent nature for proteins is expected to minimize the non-specific binding. In SDS-PAGE results, since the molecular weight of IL is too small, free IL appears at the end of the gel. After the conjugation reaction (AR), No free IL band was not observed for the conjugate thus DBCO-IL-Ab conjugate was successfully obtained.

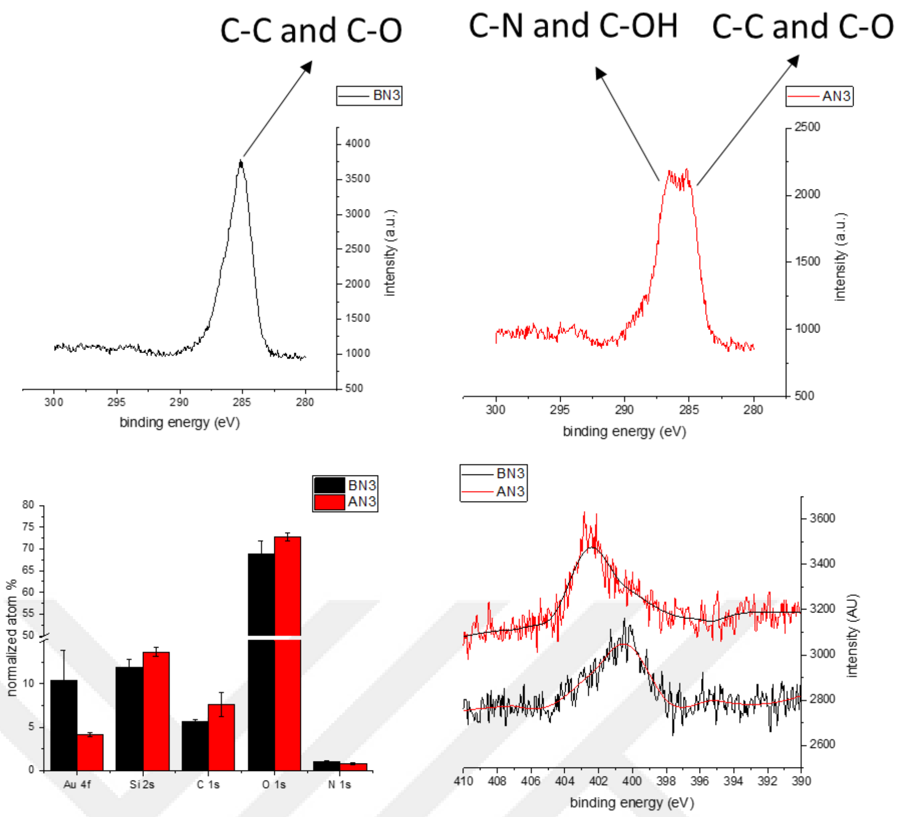

Figure 4.17**.** XPS analyses of LSPR surfaces before (BN3) and after (AN3) azide/hydroxy (OH) functionalization.

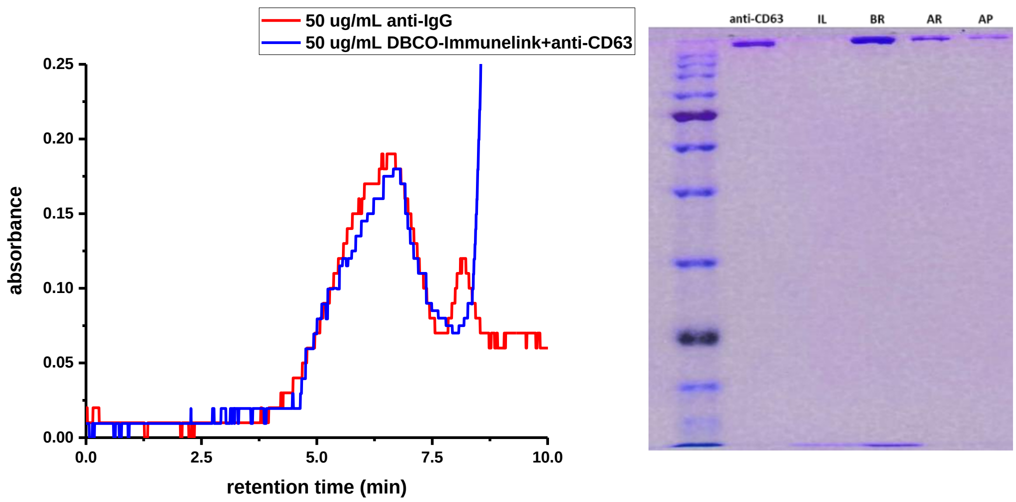

Figure 4.18. HPLC chromatograms of DBCO-IL-Ab conjugate (blue line) and free Ab (red line) (A) and SDS-PAGE gel image of anti-cd63 antibody, ImmuneLink Protein (IL), before reaction (BR), after UV reaction (AR) and after purification (AP) (B).

DBCO-IL-Ab was conjugated to the azide functionalized surfaces via click chemistry. For this purpose, the conjugates and azide bearing surfaces were incubated overnight at 4^{o}C in PBS and LSPR response was checked after conjugation (Figure 4.19). The concentration of the antibody was the same with the concentration used with EDC/NHS chemistry. λ_{max} shift of 6 nm was found after antibody conjugation to the surfaces.

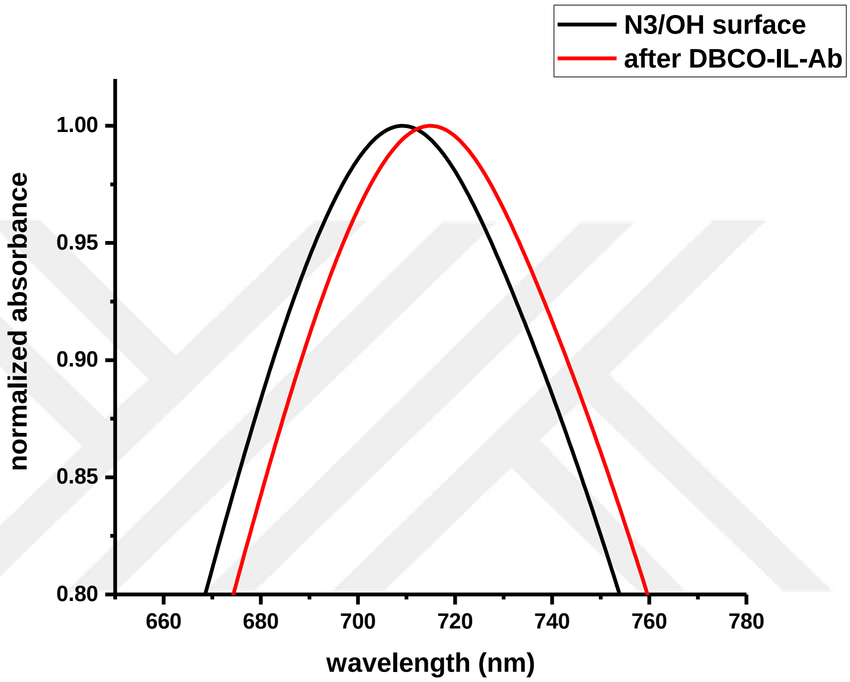

Figure 4.19. 2K PEGylated AuNRs patterned surface after functionalization with azide and hydroxyl (N3/OH) groups (by incubation with 1 mM alkylthiols for 24 h) followed by antibody conjugation using Immune-Link strategy (10 µg/mL DBCO-IL-Ab) ($\Delta\lambda_{antibody}$: 6 nm and $\lambda_{max\ N3/OH\ surface}$: 710 nm)

Placental exosomes are responsible for cell-cell communications between placental and maternal body and along with preparation of maternal organs for metabolic changes. Since they carry the cell specificities, placental exosomes are expected to provide unique information about and during pregnancy (Pillay et al. 2016). Furthermore, during pregnancy related disfunctions, it is known that the amount of placental exosomes increases (Krishna and Bhalerao 2011). In this part of the thesis, the 2K PEGylated AuNRs patterned surfaces were functionalized with anti-PLAP antibodies via ImmuneLink strategy and used for quantitative detection of PLAP for validation of these surfaces. LoD for PLAP protein was found to be 5 ng/mL (0.3 pM) (Figure 4.20). The LoD value was 100 pM for EDC/NHS chemistry for IgG detection while LoD was found to be 86 pM for PLAP detection via click-chemistry methodology. When the EDC/NHS chemistry and click-chemistry is compared: the click-chemistry strategy is expected to provide higher number of Fab regions available for antigen detection. Thus, the surface of the AuNRs can have more binding events which ultimately leads to lower LoD.

A control experiment was performed to investigate the specificity of anti-PLAP functionalized biosensor surface. These surfaces were incubated with an IgG solution (5 nM) instead of PLAP solution. The results showed no red-shifting indicating the PLAP-specific detection ability of the prepared surfaces (Appendix Figure A5).

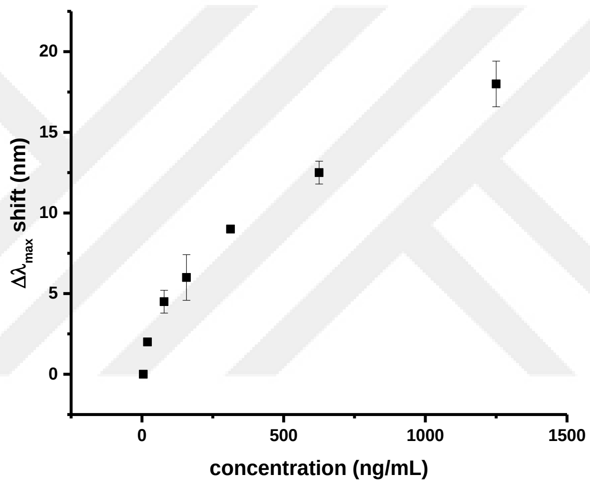

Figure 4.20. LSPR detection of PLAP standard solutions at varying concentrations using 2K PEGylated AuNRs patterned surfaces functionalized with anti-PLAP antibody via ImmuneLink strategy (n=2).

Immunelink strategy was used to enhance the sensitivity of biosensor surfaces by conjugating antibodies through their Fc regions. Orientation of the antibodies on the surface to expose their Fab regions towards solution is crucial to detect the antigens in a sensitive manner. To determine whether ImmuneLink strategy displayed an advantage over the conventional EDC/NHS chemistry in terms of antibody orientation on the surface, a control experiment was carried out. In this experiment, anti-IgG antibodies, used as analyte, were incubated with 2K PEGylated AuNRs patterned surfaces functionalized with IgG antibodies via NHS/EDC or click (ImmuneLink) chemistry. Anti-IgG antibodies have affinity to the Fc region of the IgG antibodies. Thus, it was expected that anti-IgG antibodies used as analyte could not bind to specific IgG antibodies conjugated onto the surface via ImmuneLink strategy since the Fc regions of specific IgG antibodies were occupied by the ImmuneLink reagent. (Figure 4.21). Surfaces functionalized with EDC/NHS chemistry showed a small LSPR shift upon incubation with anti-IgG antibody at 1 pM concentration. Moreover, these surfaces showed an increase in the LSPR shift with the increase in anti-IgG antibody concentration. On the other hand, the LSPR shift was zero for all surfaces functionalized via click chemistry (ImmuneLink strategy) at all anti-IgG concentrations tested. This data suggested strongly that the Fc regions of IgG antibodies conjugated onto the surface via NHS/EDC chemistry were exposed more to the analyte solution when compared with the surfaces prepared via ImmuneLink strategy. Accordingly, this result implied that the Fab regions of IgG antibodies on the surface functionalized via ImmuneLink strategy were more available to the analyte solution with respect to the surfaces prepared via NHS/EDC chemistry. According to LSPR theory, dielectric layer thickness (analyte layer thickness and receptor) is also crucial and consequently increases the response (Tian et al. 2012). Incorporation of a protein linker (ImmuneLink) onto the surface was also expected to increase the receptor thickness and thus the response.

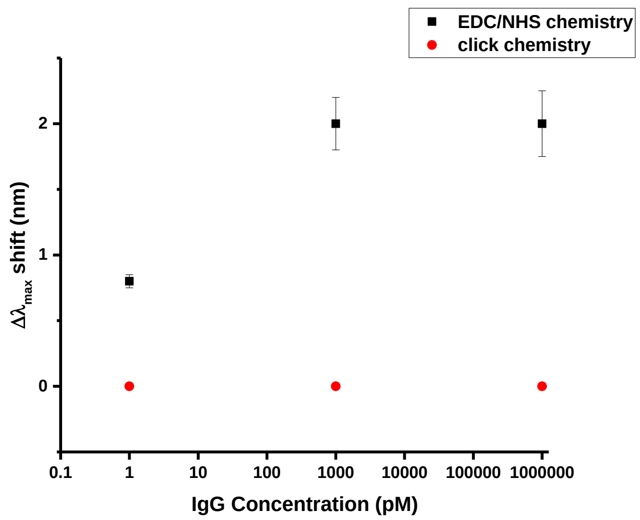

Figure 4.21. Comparison of LSPR shifts of 2K PEGylated AuNRs patterned surfaces functionalized with IgG antibodies via EDC/NHS or click (ImmuneLink) chemistries upon incubation with anti-IgG antibodies at varying concentrations. Surfaces functionalized via click-chemistry showed no LSPR shift at any concentration investigated (n=3)

4.6. Exosome Detection

2K PEGylated AuNRs patterned surfaces functionalized with anti-CD63 IgG antibodies via EDC/NHS chemistry were first utilized to investigate the effect of plasma treatment on LSPR responses to human semen exosomes at varying concentrations (10^2-10^{10} particles/mL) (Figure 4.22). In parallel, control experiments investigating non-specific bindings were performed using the same surfaces without antibody functionalization. All data points for LSPR responses of plasma treated and without plasma treatment surfaces were found to be statistically significant when t-test was applied assuming equal variances, $t<0.05$. The LoD was found to be between 10^3-10^4 exosomes/mL for both type of surfaces. However, without plasma treatment, surfaces showed higher LSPR red-shift values when compared with plasma-treated surfaces. In the control experiments, plasma treated surfaces after alkylthiol modification without any antibody conjugation showed approx. 10 nm red-shift when exposed to 10^{10} particles/mL exosomes, evidencing the non-specific interaction of exosomes with small alkane thiols (COOH and OH) as well as bare Au. Plasma treated surfaces modified with anti-CD63 antibodies showed a 15 nm shift at 10^9 exosome/mL concentration. At 10^4 exosomes/mL concentration; the interaction of plasma treated AuNRs surfaces that were functionalized with COOH/OH groups only showed a higher shift compared to the same surfaces that were functionalized with anti-CD63 antibody following the alkyl thiol modification. This suggests the low specificity of the surface towards exosomes. On the other hand, the surfaces modified with alkyl thiols without plasma treatment did not have any non-specific interaction with exosomes, showing the advantage of maintaining the PEG layer on AuNRs. The surfaces without plasma treatment after functionalization with anti-CD63 antibodies showed a shift of 23 nm and 3 nm at 10^9 exosomes/mL and 10^4 exosomes/mL concentrations, respectively.

Furthermore, in another control experiments, all of the surfaces were treated with %1 (w/v) BSA after antibody conjugation to reduce the non-specific bindings of exosomes. While plasma treated surfaces showed 5 nm red shift after BSA treatment, the surfaces that have not been treated with plasma showed no red shifting showing the favorable effect of PEG around AuNR patterns on the non-specific bindings. In addition, 2K PEGylated AuNRs patterned surfaces functionalized with anti-IgG antibodies and passivized with BSA did not show any detectable binding of exosomes (showing the anti-

CD63 antibody specificity against exosomes and no secondary interactions between the PEGylated AuNRs surface and exosomes). PEG is a well-known protein repellent polymer due to their strong hydrogen bonding with water. The higher the molecular weight of the PEG better the protein repellent properties (Leng et al. 2015). The observed non-specific interactions between exosomes and alkyl thiol modified AuNRs patterned surfaces that were not functionalized with antibodies after plasma treatment can be attributed to the hydrophobic interactions between hydrophobic small alkane thiol molecules and lipid bilayer structure of exosomes.

A series of additional control experiments were performed with 2K PEGylated AuNRs patterned surfaces functionalized via EDC/NHS chemistry and the results are shown in Appendix. In one of the control experiments, it was intended to check whether the surfaces (without plasma treatment) non-specifically interacted with BSA after the self-assembly of functional alkyl thiols or conjugation of antibodies (Appendix Figure A2). Results showed that BSA did not bind to COOH/OH functionalized surfaces as well as antibody modified surfaces. In another control experiment, antibody functionalized surfaces (without plasma treatment) were incubated with PBS, cell culture medium or cell culture medium with 40% FBS (Appendix Figure A3). Results showed that surfaces had no detectable interaction with none of the medium of interest which also indicated the protein repellent nature of the surfaces provided by the PEG molecules. Additionally, when the anti-CD63 antibody functionalized surfaces (without plasma treatment) were interacted with an IgG antibody solution at 5 nM concentration, the surfaces showed no red shifting (Appendix Figure A4 (B)) showing that there was no interaction of anti-CD63 antibody functionalized surface with another protein-based analyte. When the surfaces were functionalized with anti-IgG antibody (instead of anti-CD63 antibody) and checked for their interaction with exosomes at 10^4 and 10^{10} exosomes/mL concentrations, no forward shifting was observed (Appendix Figure A4 (A)). Overall, these results proved that the anti-CD63 antibody functionalized biosensor surfaces prepared in this study greatly minimized the non-specific binding events (attributable to the absence of plasma treatment) and furthermore highly sensitive towards exosomes.

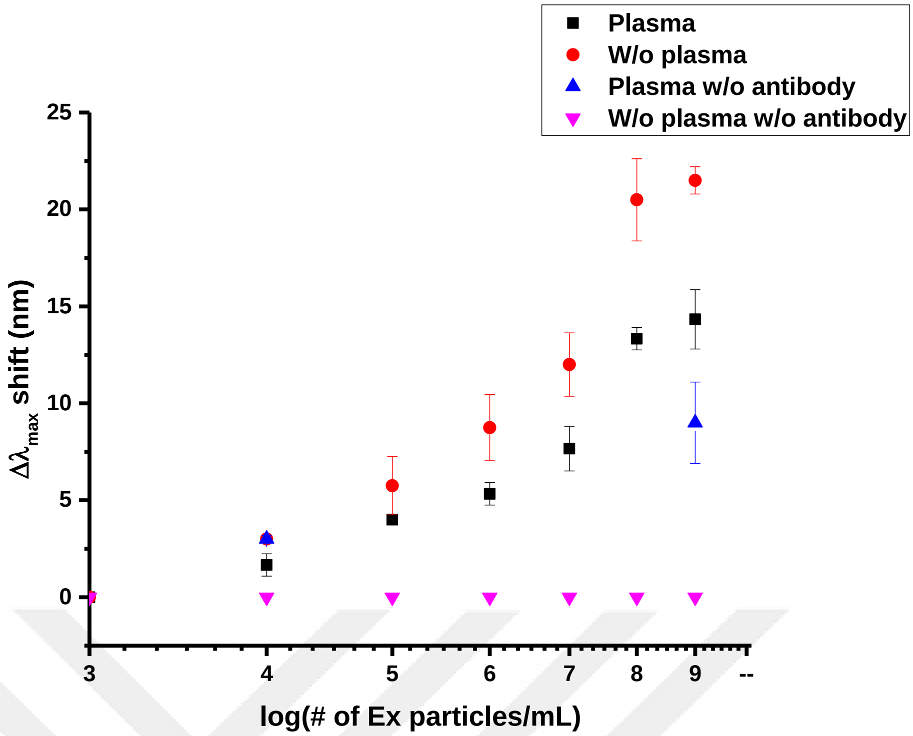

Figure 4.22. The effect of plasma treatment on LSPR responses of 2K PEGylated AuNRs patterned surfaces functionalized with anti-CD63 IgG antibodies via EDC/NHS chemistry. Human semen exosomes at varying concentrations (10^2-10^{10} particles/mL) were detected. Control experiments showing non-specific binding utilized the same surfaces without antibodies conjugated. The plasma-treated surfaces without antibody functionalization showed significantly high non-specific binding. (n=3)

In the next step, the effect of functionalization chemistry on LSPR responses of 2K PEGylated AuNRs patterned surfaces functionalized with anti-CD63 IgG antibodies was investigated. Human semen exosomes at varying concentrations (10^2-10^{10} particles/mL) were detected by the surfaces functionalized with antibodies via Immunlink (click chemistry) approach or conventional EDC/NHS chemistry. The results are shown in Figure 4.23. Click chemistry (ImmuneLink) methodology showed higher LSPR responses, which was attributed to the antibody orientation exposing the Fab regions to the analyte solution. The LSPR responses were similar after antibody conjugation to the surfaces functionalized via both type of chemistries while the surface functionalized via click chemistry displayed higher LSPR shifts upon incubation with exosomes. This indirectly showed the higher number of well-oriented antibodies on the surfaces prepared with click-chemistry compared to those prepared via EDC/NHS chemistry. Here it should be noted that the difference between two types of surfaces at every concentration point between 10^4-10^7 particles/mL was statistically significant. For the two high concentration points (10^8 and 10^9 particles/mL), these differences (both the difference between two approaches and between two concentrations for each approach) were found to become insignificant. This was attributed to the saturation of the surfaces at high exosome concentrations. Click-chemistry approach proved to be advantageous for the detection of low exosome concentrations. These results suggest that the developed surfaces present a potent candidate for the detection of specific types of exosomes that might have lower concentrations of target proteins on their membranes, such as cancer-related exosomes.

Here it should be noted that the surfaces without plasma treatment and functionalized with azide and hydroxyl groups were also exposed to 0.1 g/mL BSA solution to detect non-specific bindings if there was any. There was no shift in LSPR response, indicating that there were no detectable non-specific binding events.

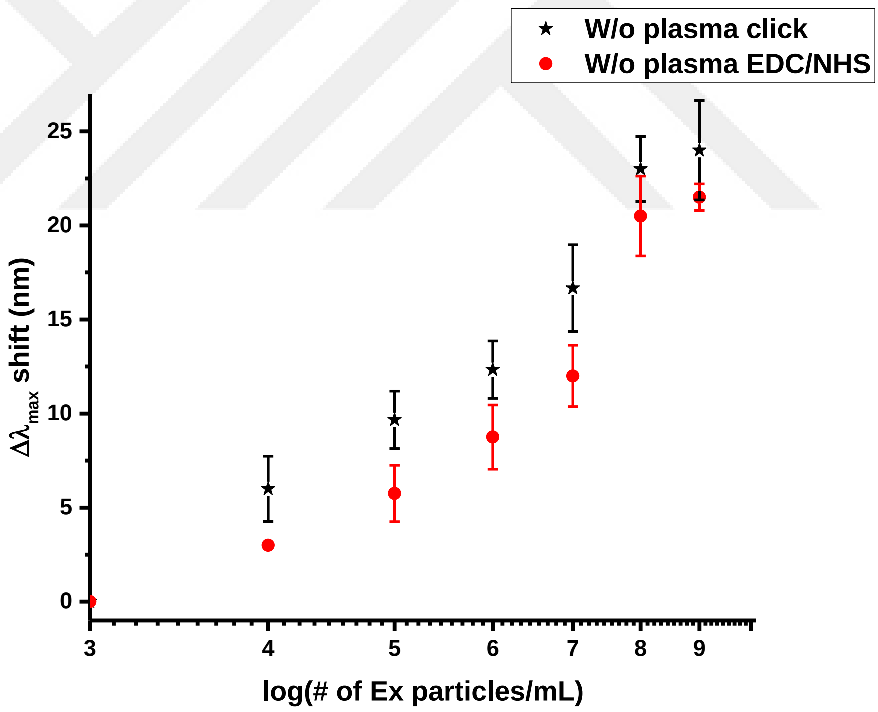

Figure 4.23. The effect of functionalization chemistry on LSPR responses of 2K PEGylated AuNRs patterned surfaces functionalized with anti-CD63 IgG antibodies. Human semen exosomes at varying concentrations (10^2-10^{10} particles/mL) were detected (n=3)

To summarize the exosome detection results, three different methodologies were applied for the detection of exosomes as (i) plasma treated EDC/NHS chemistry (ii) without plasma treatment EDC/NHS chemistry (iii) without plasma treatment click chemistry and these results compared with each other by means of detection sensitivity. The LoD for (i), (ii) and (iii) was found to be between 10^3-10^4 exosomes/mL for each of the methodologies while the LSPR response was highest for without plasma treatment click chemistry methodology. The linear detection range was 10^3 to 10^7 exosomes/mL. Without plasma treated surfaces that were prepared via click chemistry proved to offer highly sensitive and quantitative detection of exosomes in the linear region with higher LSPR responses (higher slope) compared to other methodologies. Without plasma treatment methodologies (EDC/NHS chemistry and click chemistry) showed a complete inhibition of non-specific bindings. In literature, there are few works that focus on detection of exosomes via LSPR technique and all the techniques are based on expensive and time-consuming top-down gold nanopatterning methodologies. Im et al studied the quantification of exosomes with LSPR technique and reached a LoD of $3x10^3$ particles/mL. Here their samples were human ovarian carcinoma cell lines and exosomes samples were pre-quantified with NTA (Im et al. 2014). Thakur et al studied the detection of exosomes with creating gold nano island via top-down methodology and their LoD was found to be 0.194 µg/mL with a detection range of 0.194-100 µg/mL. In this work, exosomes samples were obtained from human lung cancer cell lines and samples were not quantified (Thakur et al. 2017). Lv et al studied-on detection of human colon carcinoma cell lines with a LoD of 1 ng/mL with a detection range of 1 ng/mL to 10 µg/mL with having some non-specific bindings on the surfaces (Lv et al. 2019). This thesis has advantages by means of LoD, dynamic detection range, application of LSPR technique to pre-quantified human samples and complete inhibition of non-specific bindings comparing the other studies. Finally, Raghu et al achieved to detect single exosome via LSPR technique by constructing a novel optical detection system and creating nano-pillar via top-down methodology using human breast cancer cell line (Raghu et al. 2018). This thesis used easy and cheap application of LSPR via bottom-up methodology with using UV-vis spectrophotometer on detection of pre-quantified human exosome samples.

The 2K PEGylated AuNRs patterned surfaces having alkylthiol modification and functionalization without or with antiCD63 antibodies (via EDC/NHS chemistry) were also analyzed using SEM (Figure 4.24). The surfaces without antibodies were not able to bind exosomes as there were only a very small number of exosome visible in the SEM image (Figure 4.24 A and B). Interestingly, a large number of exosomes were clearly observed in the SEM images of antiCD63-functonalized surfaces. The SEM results were a direct visual proof of the success of the prepared biosensor surfaces in specific recognition of exosomes. Furthermore, SEM investigations showed a very interesting behavior of exosomes on the antiCD-63 functionalized surfaces (Figure 4.24). Exosomes showed a migration tendency throughout the anti-CD63 modified surfaces while their spherical shape remained on the surfaces without antiCD63 antibodies. The affinity between numerous anti-CD63 antibodies spread throughout the surface and CD63 proteins on an exosome membrane might be leading to the elongation of a single exosome on antibody distributed surface. This was also proven experimentally by taking snapshots of anti-CD63 modified surfaces after incubation with exosomes by Yang et. al (Yang et al. 2018).

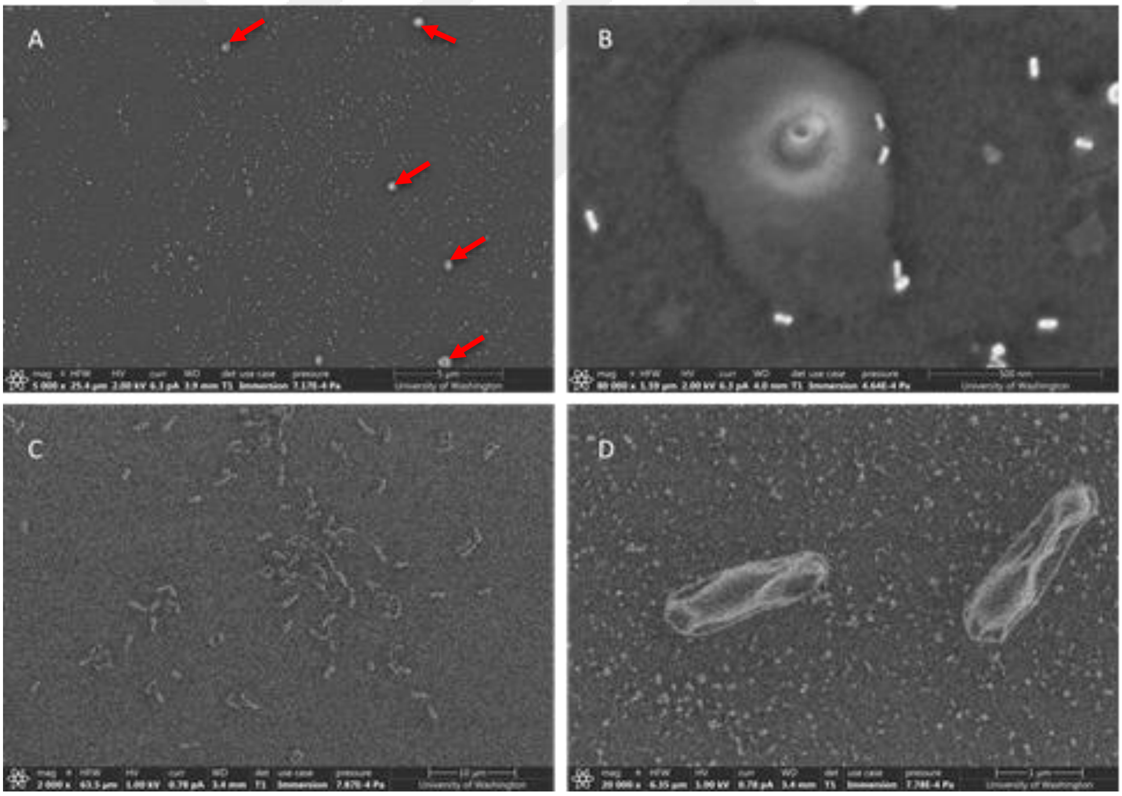

Figure 4.24. SEM images of alkane thiol modified 2K PEGylated AuNRs patterned surfaces without (A and B) or with anti-CD63 antibodies (via EDC/NHS chemistry) (C and D) after incubation with human semen exosome solution. (A: scale 1µm and B: scale 500 nm; C: scale 1µm and D: scale 1µm). (Exosomes in A are shown by arrows)

4.6.1. Detection of Exosomes Derived from Cancer Cell Cultures

In this part of the thesis, the ability of the developed biosensor surfaces (2K PEGylated and functionalized with antiCD63 antibodies via ImmuneLink strategy) to quantitatively detect exosomes from cancer cell cultures was investigated using MDA-MB-231 and MCF-7 cell lines. The exosomes were obtained directly from cell culture starvation medium via centrifugation and diluted 10, 100, 1000, 10000 or 100000 times directly from obtained supernatants with cell culture medium. The concentration of exosomes in these samples was unknown, the dilution ratio was therefore given in the results instead of concentration values. The results are shown in Figure 4.25.

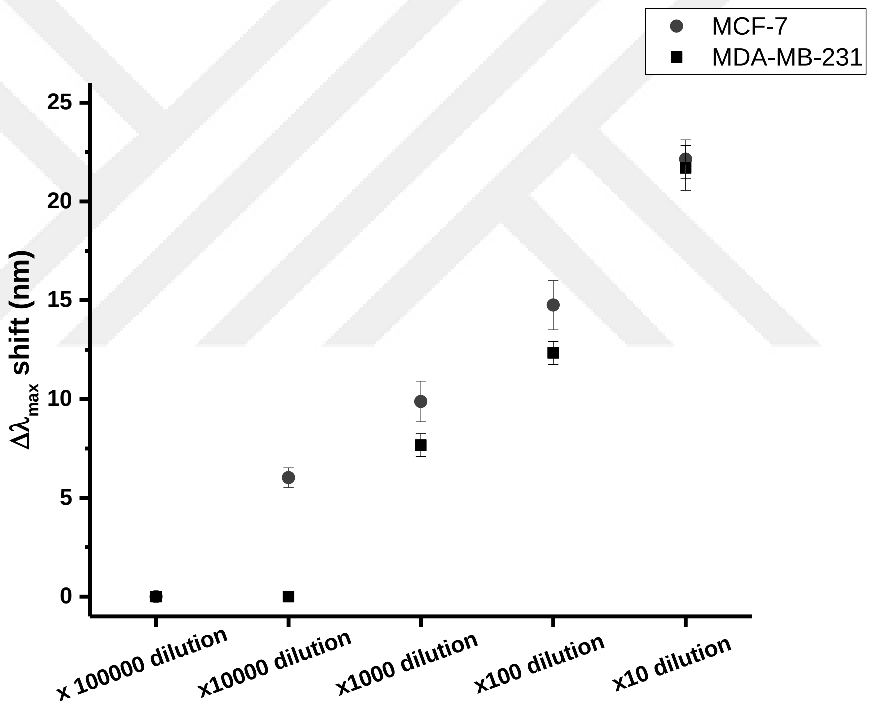

Figure 4.25. Detection of exosomes in MDA-MB-231 and MCF-7 cell culture (n=3)

The samples were in cell culture medium. A control experiment showed no interaction of the antibody modified surface with cell culture medium only (Appendix Figure A3). Since the size of AuNRs on the biosensor surface was around 40 nm in length and the size of an exosome is between 50-200 nm, it can be estimated that one AuNR was capable of capturing one exosome. Accordingly, the calibration curve (Figure 4.23) prepared with human semen exosomes can be used to estimate the unknown concentration of any exosome sample regardless of its source. It is important to indicate that above the saturation concentration for the prepared wafers, it is not possible to measure the concentration of the unknown exosome sample, the concentration of the solution of interest therefore needed to be diluted to obtain the right results. According to calibration curve, the concentration of exosomes in the unknown cell culture samples was found as 10^7 exosomes/mL for MDA-MB-231 cell culture and 10^8 exosomes/mL for MCF-7 cell culture. When these results are compared with literature studies, the amount of exosomes are correlated precisely in a work reported by Hannafon et al. (Hannafon et al. 2016). The researchers studied on human breast cancer cell lines used in this study (MCF-7 and MDA-MB-231) and quantitatively analyzed the number of exosomes via nanoparticle tracking analysis (NTA). They found the exosome amount as $2x10^9$ particles/mL for MCF-7 cell culture and $5x10^8$ particles/mL for MDA-MB-231 cell culture with initial seeded cell amount of $5x10^6$ cells (Hannafon et al. 2016). Even though MDA-MB-231 breast cancer cells is more invasive compared to MCF-7 breast cancer cells, the amount of secreted exosomes was reported to be less while the amount of metastatic proteins to be more (Kruger et al. 2014).

CHAPTER 5

CONCLUSION

This thesis aimed to develop an LSPR based biosensing platform for quantitative and sensitive detection of exosomes. For this purpose, AuNRs with a mean diameter of 40 nm and an AR of 2.9 were synthesized and characterized. In parallel, for preparation of surfaces, the microscope slides cleaned with isopropanol solution along with piranha solutions yielded the optimum surfaces for homogenous immobilization of AuNRs. Separately, PEGylation of CTAB stabilized AuNRs was carried out using three different molecular weight PEGs (1K, 2K and 5K). The optimum time for PEGylation procedure was determined to be 1 h for 1K PEG, 4 h for 2K PEG and 16 h for 5K PEG. PEG stabilized AuNRs were characterized via zeta potential and XPS measurements. Zeta potential measurements showed a significant decrease in surface potential of CTAB stabilized AuNRs, from $+2.6 \pm 0.1$ to -2.7 ± 0.5 after surfactant exchange with PEG (2K) at neutral pH. Although PEG is a neutral compound, its capability to adsorb negatively charged ions resulted as a negative increase in zeta-potential. The surfactant exchange was also proven via XPS and FTIR spectroscopy showing the presence of PEG molecules on the surface.

The PEGylated AuNRs were successfully self-assembled on silane modified glass wafers as evidenced by SEM images. After obtaining AuNRs modified glass wafers, the surface functionalization was investigated in detail in order to functionalize the surface with specific antibodies. First of all, conventional EDC/NHS chemistry was chosen for antibody conjugation onto the surfaces. Small alkane thiol molecules, 11-mercapto undecanoicacid (COOH) and 11-mercapto undecanol (OH) were used to modify the surfaces before and after plasma treatment. To the best of author’s knowledge, modification of PEGylated AuNRs patterned surfaces with alkane thiols without any plasma treatment was studied for the first time in literature. Through several control experiments, this strategy was proven to minimize the non-specific binding events to the surface while allowing efficient functionalization with antibodies. After optimizing the surface functionalization conditions for PEGylated AuNRs patterned surfaces, the surfaces were conjugated with specific IgG antibodies using EDC/NHS chemistry. The surfaces functionalized with anti-IgG antibodies displayed an LoD of 100 pM and a linear detection range between 100 pM and 10000 pM against IgG analyte. While the EDC/NHS chemistry has been perhaps the most widely used approach for functionalization of biosensor surfaces, it does not offer Fc region-specific conjugation of antibodies to the surface, as shown through a control experiment in which the surface functionalized with IgG antibodies via EDC/NHS chemistry displayed an LSPR response upon incubation with anti-IgG antibodies.

To increase the sensitivity of biosensor surfaces and thus decrease the LoD thereof, it is necessary to bind antibodies to the sensor surface from their Fc region so that the antigen binding sites remain available for detection of target analyte. To do this, a commercial small fragment of protein-G (ImmuneLink) with DBCO modification (IL) was utilized. This reagent enables the conjugation of antibodies through their Fc region to azide-bearing (N3) surfaces via copper-free click chemistry. The conjugation of IL to relevant antibodies was confirmed via HPLC and SDS-PAGE experiments. In parallel, surface functionalization of PEGylated AuNRs patterned surfaces were modified with alkane thiol molecules to have N3/OH groups using the same protocol established for COOH/OH groups for EDC/EDC chemistry. The XPS experiments revealed the success in modification of PEGylated AuNRs patterned surfaces with azide bearing alkane thiol molecules. The conjugation of antibodies to the surface via click chemistry was evidenced by FTIR, zeta potential and LSPR results. Appearance of amide bond along with disappearance of C=O bond observed within 2000-1500 cm^{-1} region in FTIR as well as negative increase in zeta potential results along with a red shift of LSPR response indicated the successful conjugation of antibodies. A control experiment in which the surfaces functionalized with IgG antibodies via click chemistry did not display any LSPR response upon incubation with anti-IgG antibodies, suggested that the Fc region-specific conjugation of antibodies to the surface took place. The surfaces functionalized with anti-PLAP antibodies displayed an LoD of 0.3 pM and a linear detection range between 0.3 pM and 3 pM against PLAP analyte. To the best of the author's knowledge, this has been the first study reporting the LSPR-based quantitative detection of PLAP protein which is a pregnancy related protein.

Finally, the developed surfaces were used for sensitive detection of exosomes. First, pre-quantified exosome samples derived from human semen were used as analyte solutions to build LSPR response vs. exosome concentration curves for surfaces prepared via three different methodologies: (i) plasma treated EDC/NHS chemistry (ii) without plasma treatment EDC/NHS chemistry (iii) without plasma treatment click chemistry. Plasma treated surfaces showed high non-specific binding shifts to exosome samples that ultimately increased the LoD. The LoD for (ii) and (iii) was found to be between 10^3-10^4 exosomes/mL while the LSPR response was higher for without plasma treatment click chemistry methodology. The linear detection range was between 10^3 and 10^7 exosomes/mL for (ii) and (iii). Without plasma treated surfaces that were prepared via click chemistry or EDC/NHS chemistry proved to offer highly sensitive and quantitative detection of exosomes. Although LoD was in between 10^3-10^4 exosomes/mL for without plasma treated surfaces that were prepared via EDC/NHS chemistry and click chemistry, click chemistry methodology provided Fc-selective conjugation of antibodies and ultimately yielded higher LSPR responses. The results contribute to the literature by providing lower LoD, wider dynamic detection range as well as by applying LSPR technique to pre-quantified human samples and presenting a methodology inhibiting non-specific bindings when compared to the other studies in the literature.

At the last step, breast cancer cell cultures having unknown concentration of exosomes were analyzed for their exosome content using the biosensor surfaces that were prepared via click chemistry. The concentration of exosomes in MCF-7 and MDA-MB-231 cell cultures was measured to be 10^8 exosome/mL and 10^7 exosome/mL, respectively. These results were consistent with literature findings. Overall results showed successful preparation and application of LSPR sensors via using a bottom-up methodology with having well-oriented antibody structures on the surfaces for detection of exosomes from different sources.

This research can be further extended by the following suggestions:

1. Healthy breast cells (MCF-10A) can be used for the determination of exosome concentrations to be able to distinguish the differences between healthy and cancer cell lines.

2. To enhance the signal, antibody modified AuNRs can be incorporated on the exosome attached surfaces.

3. The size effect of AuNRs can be also checked to evaluate the LSPR responses on exosomes detection since this study used one exosome per one rod methodology. The bigger rods in size can influence the LSPR response because they might have the ability to bind more than one exosome to their surfaces.

4. Detection of PLAP bearing exosomes was not possible during this work but the system can be used to check the placental related exosomes since the amount of placenta related exosomes are suspected to give insights on pregnancy related diseases.

REFERENCES

Acres, Robert G, Amanda V Ellis, Jason Alvino, Claire E Lenahan, Dmitriy A Khodakov, Gregory F Metha, and Gunther G Andersson. 2012. 'Molecular structure of 3-aminopropyltriethoxysilane layers formed on silanol-terminated silicon surfaces', *The Journal of Physical Chemistry C*, 116: 6289-97.

Ahmadi Badi, Sara, Arfa Moshiri, Abolfazl Fateh, Fatemeh Rahimi Jamnani, Meysam Sarshar, Farzam Vaziri, and Seyed Davar Siadat. 2017. 'Microbiota-derived extracellular vesicles as new systemic regulators', *Frontiers in microbiology*, 8: 1610.

Alam, AU, MMR Howlader, and MJ Deen. 2014. 'The effects of oxygen plasma and humidity on surface roughness, water contact angle and hardness of silicon, silicon dioxide and glass', *Journal of Micromechanics and Microengineering*, 24: 035010.

Alaqad, Khalid, and Tawfik A Saleh. 2016. 'Gold and silver nanoparticles: synthesis methods, characterization routes and applications towards drugs', *J. Environ. Anal. Toxicol*, 6: 525-2161.

Altan-Bonnet, Nihal. 2016. 'Extracellular vesicles are the Trojan horses of viral infection', *Current opinion in microbiology*, 32: 77-81.

Alvarez, M Lucrecia, Mahdieh Khosroheidari, Rupesh Kanchi Ravi, and Johanna K DiStefano. 2012. 'Comparison of protein, microRNA, and mRNA yields using different methods of urinary exosome isolation for the discovery of kidney disease biomarkers', *Kidney international*, 82: 1024-32.

Arslan, Fatih, Ruenn Chai Lai, Mirjam B Smeets, Lars Akeroyd, Andre Choo, Eissa NE Aguor, Leo Timmers, Harold V van Rijen, Pieter A Doevendans, and Gerard Pasterkamp. 2013. 'Mesenchymal stem cell-derived exosomes increase ATP levels, decrease oxidative stress and activate PI3K/Akt pathway to enhance myocardial viability and prevent adverse remodeling after myocardial ischemia/reperfusion injury', *Stem cell research*, 10: 301-12.

Ayers, Lisa, Malcolm Kohler, Paul Harrison, Ian Sargent, Rebecca Dragovic, Marianne Schaap, Rienk Nieuwland, Susan A Brooks, and Berne Ferry. 2011. 'Measurement of circulating cell-derived microparticles by flow cytometry: sources of variability within the assay', *Thrombosis research*, 127: 370-77.

Baietti, Maria Francesca, Zhe Zhang, Eva Mortier, Aurélie Melchior, Gisèle Degeest, Annelies Geeraerts, Ylva Ivarsson, Fabienne Depoortere, Christien Coomans, and Elke Vermeiren. 2012. 'Syndecan–syntenin–ALIX regulates the biogenesis of exosomes', *Nature cell biology*, 14: 677-85.

Barany, Sandor. 2015. 'Polymer adsorption and electrokinetic potential of dispersed particles in weak and strong electric fields', *Advances in Colloid and Interface Science*, 222: 58-69.

Barile, Lucio, Vincenzo Lionetti, Elisabetta Cervio, Marco Matteucci, Mihaela Gherghiceanu, Laurentiu M Popescu, Tiziano Torre, Francesco Siclari, Tiziano Moccetti, and Giuseppe Vassalli. 2014. 'Extracellular vesicles from human cardiac progenitor cells inhibit cardiomyocyte apoptosis and improve cardiac function after myocardial infarction', *Cardiovascular research*, 103: 530-41.

Björck, L, and G Kronvall. 1984. 'Purification and some properties of streptococcal protein G, a novel IgG-binding reagent', *The Journal of Immunology*, 133: 969-74.

Bobrie, Angélique, Marina Colombo, Graça Raposo, and Clotilde Théry. 2011. 'Exosome secretion: molecular mechanisms and roles in immune responses', *Traffic*, 12: 1659-68.

Brioude, A, XC Jiang, and MP Pileni. 2005. 'Optical properties of gold nanorods: DDA simulations supported by experiments', *The Journal of Physical Chemistry B*, 109: 13138-42.

Budnik, Vivian, Catalina Ruiz-Cañada, and Franz Wendler. 2016. 'Extracellular vesicles round off communication in the nervous system', *Nature Reviews Neuroscience*, 17: 160-72.

Burnett, Lindsey A, and Romana A Nowak. 2016. 'Exosomes mediate embryo and maternal interactions at implantation and during pregnancy', *Front. Biosci.(Schol. Ed.)*, 8: 79-96.

Burrows, Nathan D, Wayne Lin, Joshua G Hinman, Jordan M Dennison, Ariane M Vartanian, Nardine S Abadeer, Elissa M Grzincic, Lisa M Jacob, Ji Li, and Catherine J Murphy. 2016. 'Surface chemistry of gold nanorods', *Langmuir*, 32: 9905-21.

Cao, Jie, Tong Sun, and Kenneth TV Grattan. 2014. 'Gold nanorod-based localized surface plasmon resonance biosensors: A review', *Sensors and actuators B: Chemical*, 195: 332-51.

Carnell-Morris, Pauline, Dionne Tannetta, Agnieszka Siupa, Patrick Hole, and Rebecca Dragovic. 2017. 'Analysis of extracellular vesicles using fluorescence nanoparticle tracking analysis.' in, *Extracellular Vesicles* (Springer).

Castaño, Carlos, Susana Kalko, Anna Novials, and Marcelina Párrizas. 2018. 'Obesity-associated exosomal miRNAs modulate glucose and lipid metabolism in mice', *Proceedings of the National Academy of Sciences*, 115: 12158-63.

Chang, Guojing, Jean-François Mouillet, Takuya Mishima, Tianjiao Chu, Elena Sadovsky, Carolyn B Coyne, W Tony Parks, Urvashi Surti, and Yoel Sadovsky. 2017. 'Expression and trafficking of placental microRNAs at the feto-maternal interface', *The FASEB Journal*, 31: 2760-70.

Chapman, Robert G, Emanuele Ostuni, Lin Yan, and George M Whitesides. 2000. 'Preparation of mixed self-assembled monolayers (SAMs) that resist adsorption of proteins using the reaction of amines with a SAM that presents interchain carboxylic anhydride groups', *Langmuir*, 16: 6927-36.

Chegel, Volodymyr, Oleksandre Rachkov, Andrii Lopatynskyi, Shinsuke Ishihara, Igor Yanchuk, Yoshihiro Nemoto, Jonathan P Hill, and Katsuhiko Ariga. 2012. 'Gold nanoparticles aggregation: drastic effect of cooperative functionalities in a single molecular conjugate', *The Journal of Physical Chemistry C*, 116: 2683-90.

Chen, Huanjun, Xiaoshan Kou, Zhi Yang, Weihai Ni, and Jianfang Wang. 2008. 'Shape- and size-dependent refractive index sensitivity of gold nanoparticles', *Langmuir*, 24: 5233-37.

Chen, Lechuang, Zhimin Feng, Hong Yue, Douglas Bazdar, Uri Mbonye, Chad Zender, Clifford V Harding, Leslie Bruggeman, Jonathan Karn, and Scott F Sieg. 2018. 'Exosomes derived from HIV-1-infected cells promote growth and progression of cancer via HIV TAR RNA', *Nature communications*, 9: 1-12.

Chitti, Sai V, Pamali Fonseka, and Suresh Mathivanan. 2018. 'Emerging role of extracellular vesicles in mediating cancer cachexia', *Biochemical Society Transactions*, 46: 1129-36.

Cras, JJ, CA Rowe-Taitt, DA Nivens, and FS Ligler. 1999. 'Comparison of chemical cleaning methods of glass in preparation for silanization', *Biosensors and Bioelectronics*, 14: 683-88.

Crenshaw, Brennetta J, Linlin Gu, Brian Sims, and Qiana L Matthews. 2018. 'Exosome biogenesis and biological function in response to viral infections', *The open virology journal*, 12: 134.

de Hoog, Vince C, Leo Timmers, Arjan H Schoneveld, Jiong-Wei Wang, Sander M van de Weg, Siu Kwan Sze, J Karlijn van Keulen, Arno W Hoes, Hester M den Ruijter, and Dominique PV de Kleijn. 2013. 'Serum extracellular vesicle protein levels are associated with acute coronary syndrome', *European Heart Journal: Acute Cardiovascular Care*, 2: 53-60.

Dilimon, VS, Sundar Rajalingam, J Delhalle, and Z Mekhalif. 2013. 'Self-assembly mechanism of thiol, dithiol, dithiocarboxylic acid, disulfide and diselenide on gold: An electrochemical impedance study', *Physical Chemistry Chemical Physics*, 15: 16648-56.

Dragovic, Rebecca A, Christopher Gardiner, Alexandra S Brooks, Dionne S Tannetta, David JP Ferguson, Patrick Hole, Bob Carr, Christopher WG Redman, Adrian L Harris, and Peter J Dobson. 2011. 'Sizing and phenotyping of cellular vesicles using Nanoparticle Tracking Analysis', *Nanomedicine: Nanotechnology, Biology and Medicine*, 7: 780-88.

Duque, JS, JS Blandón, and H Riascos. 2017. "Localized Plasmon resonance in metal nanoparticles using Mie theory." In *Journal of Physics: Conference Series*, 012017. IOP Publishing.

Edgar, James R. 2016. 'Q&A: What are exosomes, exactly?', *BMC biology*, 14: 46.

Escrevente, Cristina, Sascha Keller, Peter Altevogt, and Júlia Costa. 2011. 'Interaction and uptake of exosomes by ovarian cancer cells', *BMC cancer*, 11: 108.

Fernando, M Rohan, Chao Jiang, Gary D Krzyzanowski, and Wayne L Ryan. 2017. 'New evidence that a large proportion of human blood plasma cell-free DNA is localized in exosomes', *PloS one*, 12: e0183915.

Fujiwara, Kazuhiko, Hitoshi Watarai, Hideaki Itoh, Erika Nakahama, and Nobuaki Ogawa. 2006. 'Measurement of antibody binding to protein immobilized on gold nanoparticles by localized surface plasmon spectroscopy', *Analytical and bioanalytical chemistry*, 386: 639-44.

Funston, Alison M, Carolina Novo, Tim J Davis, and Paul Mulvaney. 2009. 'Plasmon coupling of gold nanorods at short distances and in different geometries', *Nano letters*, 9: 1651-58.

Gamble, Lara, Linda S Jung, and CT Campbell. 1995. 'Interaction of silane coupling agents with the TiO2 (110) surface', *Langmuir*, 11: 4505-14.

Gangadaran, Prakash, Chae Moon Hong, and Byeong-Cheol Ahn. 2017. 'Current perspectives on in vivo noninvasive tracking of extracellular vesicles with molecular imaging', *BioMed research international*, 2017.

Gao, Hui-Min, Hong Liu, Hu-Jun Qian, Gui-Sheng Jiao, and Zhong-Yuan Lu. 2018. 'Multiscale simulations of ligand adsorption and exchange on gold nanoparticles', *Physical Chemistry Chemical Physics*, 20: 1381-94.

Gao, Liang, Lin Wang, Tong Dai, Ke Jin, Zhengkui Zhang, Shuai Wang, Feng Xie, Pengfei Fang, Bing Yang, and Huizhe Huang. 2018. 'Tumor-derived exosomes antagonize innate antiviral immunity', *Nature immunology*, 19: 233-45.

Gercel-Taylor, Cicek, Siobhan M O'Connor, Garrett K Lam, and Douglas D Taylor. 2002. 'Shed membrane fragment modulation of CD3-zeta during pregnancy: link with induction of apoptosis', *Journal of reproductive immunology*, 56: 29-44.

Grasso, Luigino, Romain Wyss, Lorenz Weidenauer, Ashwin Thampi, Davide Demurtas, Michel Prudent, Niels Lion, and Horst Vogel. 2015. 'Molecular screening of cancer-derived exosomes by surface plasmon resonance spectroscopy', *Analytical and bioanalytical chemistry*, 407: 5425-32.

Green, Hadiyah N, Dmitry V Martyshkin, Cynthia M Rodenburg, Eben L Rosenthal, and Sergey B Mirov. 2011. 'Gold nanorod bioconjugates for active tumor targeting and photothermal therapy', *Journal of Nanotechnology*, 2011.

Guerrini, Luca, Ramon Alvarez-Puebla, and Nicolas Pazos-Perez. 2018. 'Surface modifications of nanoparticles for stability in biological fluids', *Materials*, 11: 1154.

Gurunathan, Sangiliyandi, Min-Hee Kang, Muniyandi Jeyaraj, Muhammad Qasim, and Jin-Hoi Kim. 2019. 'Review of the isolation, characterization, biological function, and multifarious therapeutic approaches of exosomes', *Cells*, 8: 307.

Habel, Joachim, Anayo Ogbonna, Nanna Larsen, Solène Cherré, Søren Kynde, Søren Roi Midtgaard, Koji Kinoshita, Simon Krabbe, Grethe Vestergaard Jensen, and Jesper Søndergaard Hansen. 2015. 'Selecting analytical tools for characterization of polymersomes in aqueous solution', *RSC Advances*, 5: 79924-46.

Haddada, Maroua Ben, Juliette Blanchard, Sandra Casale, Jean-Marc Krafft, Anne Vallée, Christophe Méthivier, and Souhir Boujday. 2013. 'Optimizing the immobilization of gold nanoparticles on functionalized silicon surfaces: amine- vs thiol-terminated silane', *Gold Bulletin*, 46: 335-41.

Hanahan, Douglas, and Robert A Weinberg. 2011. 'Hallmarks of cancer: the next generation', *cell*, 144: 646-74.

Hannafon, Bethany N, Yvonne D Trigoso, Cameron L Calloway, Y Daniel Zhao, David H Lum, Alana L Welm, Zhizhuang J Zhao, Kenneth E Blick, William C Dooley, and WQ Ding. 2016. 'Plasma exosome microRNAs are indicative of breast cancer', *Breast Cancer Research*, 18: 90.

Harder, P, M Grunze, R Dahint, GM Whitesides, and PE Laibinis. 1998. 'Molecular conformation in oligo (ethylene glycol)-terminated self-assembled monolayers on gold and silver surfaces determines their ability to resist protein adsorption', *The Journal of Physical Chemistry B*, 102: 426-36.

Harding, Clifford, John Heuser, and Philip Stahl. 1983. 'Receptor-mediated endocytosis of transferrin and recycling of the transferrin receptor in rat reticulocytes', *The Journal of cell biology*, 97: 329-39.

Hartjes, Thomas A, Serhii Mytnyk, Guido W Jenster, Volkert van Steijn, and Martin E van Royen. 2019. 'Extracellular vesicle quantification and characterization: common methods and emerging approaches', *Bioengineering*, 6: 7.

Haynes, Christy L, Adam D McFarland, and Richard P Van Duyne. 2005. "Surface-enhanced Raman spectroscopy." In.: ACS Publications.

Hore, Michael JA, Xingchen Ye, Jamie Ford, Yuzhi Gao, Jiayang Fei, Qiong Wu, Stuart J Rowan, Russell J Composto, Christopher B Murray, and Boualem Hammouda. 2015. 'Probing the structure, composition, and spatial distribution of ligands on gold nanorods', *Nano letters*, 15: 5730-38.

Hoshino, Ayuko, Bruno Costa-Silva, Tang-Long Shen, Goncalo Rodrigues, Ayako Hashimoto, Milica Tesic Mark, Henrik Molina, Shinji Kohsaka, Angela Di Giannatale, and Sophia Ceder. 2015. 'Tumour exosome integrins determine organotropic metastasis', *Nature*, 527: 329-35.

Huang, Xiaohua, Svetlana Neretina, and Mostafa A El-Sayed. 2009. 'Gold nanorods: from synthesis and properties to biological and biomedical applications', *Advanced Materials*, 21: 4880-910.

Hui, James Z, Shereen Tamsen, Yang Song, and Andrew Tsourkas. 2015. 'LASIC: Light activated site-specific conjugation of native IgGs', *Bioconjugate chemistry*, 26: 1456-60.

Im, Hyungsoon, Huilin Shao, Yong Il Park, Vanessa M Peterson, Cesar M Castro, Ralph Weissleder, and Hakho Lee. 2014. 'Label-free detection and molecular profiling of exosomes with a nano-plasmonic sensor', *Nature biotechnology*, 32: 490.

Jain, Prashant K, Susie Eustis, and Mostafa A El-Sayed. 2006. 'Plasmon coupling in nanorod assemblies: optical absorption, discrete dipole approximation simulation, and exciton-coupling model', *The Journal of Physical Chemistry B*, 110: 18243-53.

Jain, Prashant K, Wenyu Huang, and Mostafa A El-Sayed. 2007. 'On the universal scaling behavior of the distance decay of plasmon coupling in metal nanoparticle pairs: a plasmon ruler equation', *Nano letters*, 7: 2080-88.

Jatschka, Jacqueline, André Dathe, Andrea Csáki, Wolfgang Fritzsche, and Ondrej Stranik. 2016. 'Propagating and localized surface plasmon resonance sensing—A critical comparison based on measurements and theory', *Sensing and bio-sensing research*, 7: 62-70.

Javeed, Naureen, Gunisha Sagar, Shamit K Dutta, Thomas C Smyrk, Julie S Lau, Santanu Bhattacharya, Mark Truty, Gloria M Petersen, Randal J Kaufman, and Suresh T Chari. 2015. 'Pancreatic cancer–derived exosomes cause paraneoplastic β-cell dysfunction', *Clinical Cancer Research*, 21: 1722-33.

Jazayeri, Mir Hadi, Hamed Amani, Ali Akbar Pourfatollah, Hamidreza Pazoki-Toroudi, and Bijan Sedighimoghaddam. 2016. 'Various methods of gold nanoparticles (GNPs) conjugation to antibodies', *Sensing and bio-sensing research*, 9: 17-22.

Jeppesen, Dennis K, Michael L Hvam, Bjarke Primdahl-Bengtson, Anders T Boysen, Bradley Whitehead, Lars Dyrskjøt, Torben F Ørntoft, Kenneth A Howard, and Marie S Ostenfeld. 2014. 'Comparative analysis of discrete exosome fractions obtained by differential centrifugation', *Journal of extracellular vesicles*, 3: 25011.

Jin, Jin, and Ramkumar Menon. 2018. 'Placental exosomes: a proxy to understand pregnancy complications', *American Journal of Reproductive Immunology*, 79: e12788.

Johnstone, Rose M, Mohammed Adam, JR Hammond, L Orr, and Claire Turbide. 1987. 'Vesicle formation during reticulocyte maturation. Association of plasma membrane activities with released vesicles (exosomes)', *Journal of Biological Chemistry*, 262: 9412-20.

Jørgensen, Malene Møller, Rikke Bæk, and Kim Varming. 2015. 'Potentials and capabilities of the Extracellular Vesicle (EV) Array', *Journal of extracellular vesicles*, 4: 26048.

Joshi, Gayatri K, Samantha Deitz-McElyea, Thakshila Liyanage, Katie Lawrence, Sonali Mali, Rajesh Sardar, and Murray Korc. 2015. 'Label-free nanoplasmonic-based short noncoding RNA sensing at attomolar concentrations allows for quantitative and highly specific assay of microRNA-10b in biological fluids and circulating exosomes', *ACS nano*, 9: 11075-89.

Joshi, Pratixa P, Soon Joon Yoon, William G Hardin, Stanislav Emelianov, and Konstantin V Sokolov. 2013. 'Conjugation of antibodies to gold nanorods through Fc portion: synthesis and molecular specific imaging', *Bioconjugate chemistry*, 24: 878-88.

Jung, Yongwon, Jeong Min Lee, Jung-won Kim, Jeongwon Yoon, Hyunmin Cho, and Bong Hyun Chung. 2009. 'Photoactivable antibody binding protein: site-selective and covalent coupling of antibody', *Analytical chemistry*, 81: 936-42.

Kalluri, Raghu, and Valerie S LeBleu. 2020. 'The biology, function, and biomedical applications of exosomes', *Science*, 367.

Kamerkar, Sushrut, Valerie S LeBleu, Hikaru Sugimoto, Sujuan Yang, Carolina F Ruivo, Sonia A Melo, J Jack Lee, and Raghu Kalluri. 2017. 'Exosomes facilitate therapeutic targeting of oncogenic KRAS in pancreatic cancer', *Nature*, 546: 498-503.

Kanwar, Shailender Singh, Christopher James Dunlay, Diane M Simeone, and Sunitha Nagrath. 2014. 'Microfluidic device (ExoChip) for on-chip isolation, quantification and characterization of circulating exosomes', *Lab on a Chip*, 14: 1891-900.

Kassem, Moustapha, Malthe Kristiansen, and Basem M Abdallah. 2004. 'Mesenchymal stem cells: cell biology and potential use in therapy', *Basic & clinical pharmacology & toxicology*, 95: 209-14.

Khan, AK, R Rashid, G Murtaza, and A Zahra. 2014. 'Gold nanoparticles: synthesis and applications in drug delivery', *Tropical Journal of Pharmaceutical Research*, 13: 1169-77.

Khlebtsov, NG, AG Mel'Nikov, VA Bogatyrev, AV Alekseeva, and BN Khlebtsov. 2006. 'Depolarization of light scattered by gold nanospheres and nanorods', *Optics and spectroscopy*, 100: 448-55.

Konadu, Kateena Addae, Ming Bo Huang, William Roth, Wendy Armstrong, Michael Powell, Francois Villinger, and Vincent Bond. 2016. 'Isolation of exosomes from the plasma of HIV-1 positive individuals', *JoVE (Journal of Visualized Experiments)*: e53495.

Konoshenko, Maria Yu, Evgeniy A Lekchnov, Alexander V Vlassov, and Pavel P Laktionov. 2018. 'Isolation of extracellular vesicles: general methodologies and latest trends', *BioMed research international*, 2018.

Koritzinsky, Erik H, Jonathan M Street, Robert A Star, and Peter ST Yuen. 2017. 'Quantification of exosomes', *Journal of cellular physiology*, 232: 1587-90.

Krasnoslobodtsev, Alexey V, and Sergei N Smirnov. 2002. 'Effect of water on silanization of silica by trimethoxysilanes', *Langmuir*, 18: 3181-84.

Krishna, Usha, and Sarita Bhalerao. 2011. 'Placental insufficiency and fetal growth restriction', *The Journal of Obstetrics and Gynecology of India*, 61: 505-11.

Kruger, Stefan, Zakaria Y Abd Elmageed, David H Hawke, Philipp M Wörner, David A Jansen, Asim B Abdel-Mageed, Eckhard U Alt, and Reza Izadpanah. 2014. 'Molecular characterization of exosome-like vesicles from breast cancer cells', *BMC cancer*, 14: 1-10.

Kurywchak, Paul, Jena Tavormina, and Raghu Kalluri. 2018. 'The emerging roles of exosomes in the modulation of immune responses in cancer', *Genome medicine*, 10: 23.

Kyaw, Htet H, Salim H Al-Harthi, Azzouz Sellai, and Joydeep Dutta. 2015. 'Self-organization of gold nanoparticles on silanated surfaces', *Beilstein journal of nanotechnology*, 6: 2345.

Latifkar, Arash, Yun Ha Hur, Julio C Sanchez, Richard A Cerione, and Marc A Antonyak. 2019. 'New insights into extracellular vesicle biogenesis and function', *Journal of cell science*, 132: jcs222406.

Le Basle, Yoann, Philip Chennell, Nicolas Tokhadze, Alain Astier, and Valérie Sautou. 2020. 'Physicochemical Stability of Monoclonal Antibodies: A Review', *Journal of Pharmaceutical Sciences*, 109: 169-90.

Leitner, Karl, Roman Szlauer, Isabella Ellinger, Adolf Ellinger, Klaus-Peter Zimmer, and Renate Fuchs. 2001. 'Placental alkaline phosphatase expression at the apical and basal plasma membrane in term villous trophoblasts', *Journal of Histochemistry & Cytochemistry*, 49: 1155-64.

Leng, Chuan, Hsiang-Chieh Hung, Shuwen Sun, Dayang Wang, Yuting Li, Shaoyi Jiang, and Zhan Chen. 2015. 'Probing the surface hydration of nonfouling zwitterionic and PEG materials in contact with proteins', *ACS applied materials & interfaces*, 7: 16881-88.

Levy, Efrat. 2017. 'Exosomes in the diseased brain: first insights from in vivo studies', *Frontiers in neuroscience*, 11: 142.

Li, Pin, Melisa Kaslan, Sze Han Lee, Justin Yao, and Zhiqiang Gao. 2017. 'Progress in exosome isolation techniques', *Theranostics*, 7: 789.

Liang, Kai, Fei Liu, Jia Fan, Dali Sun, Chang Liu, Christopher J Lyon, David W Bernard, Yan Li, Kenji Yokoi, and Matthew H Katz. 2017. 'Nanoplasmonic quantification of tumour-derived extracellular vesicles in plasma microsamples for diagnosis and treatment monitoring', *Nature biomedical engineering*, 1: 0021.

Liga, A, ADB Vliegenthart, W Oosthuyzen, JW Dear, and M Kersaudy-Kerhoas. 2015. 'Exosome isolation: a microfluidic road-map', *Lab on a Chip*, 15: 2388-94.

Lin, Tsao-Jen, and Mon-Fu Chung. 2008. 'Using monoclonal antibody to determine lead ions with a localized surface plasmon resonance fiber-optic biosensor', *Sensors*, 8: 582-93.

Link, Stephan, MB Mohamed, and MA El-Sayed. 1999. 'Simulation of the optical absorption spectra of gold nanorods as a function of their aspect ratio and the effect of the medium dielectric constant', *The Journal of Physical Chemistry B*, 103: 3073-77.

Linzer, Daniel IH, and Susan J Fisher. 1999. 'The placenta and the prolactin family of hormones: regulation of the physiology of pregnancy', *Molecular Endocrinology*, 13: 837-40.

Love, J Christopher, Lara A Estroff, Jennah K Kriebel, Ralph G Nuzzo, and George M Whitesides. 2005. 'Self-assembled monolayers of thiolates on metals as a form of nanotechnology', *Chemical reviews*, 105: 1103-70.

Lv, Xiaoqing, Zhaoxin Geng, Yue Su, Zhiyuan Fan, Shicai Wang, Weihao Fang, and Hongda Chen. 2019. 'Label-Free Exosome Detection Based on a Low-Cost Plasmonic Biosensor Array Integrated with Microfluidics', *Langmuir*, 35: 9816-24.

Madison, Marisa N, Philip H Jones, and Chioma M Okeoma. 2015. 'Exosomes in human semen restrict HIV-1 transmission by vaginal cells and block intravaginal replication of LP-BM5 murine AIDS virus complex', *Virology*, 482: 189-201.

Madison, Marisa N, Richard J Roller, and Chioma M Okeoma. 2014. 'Human semen contains exosomes with potent anti-HIV-1 activity', *Retrovirology*, 11: 102.

Mahmoud, Mahmoud A. 2014. 'Controlling the orientations of gold nanorods inside highly packed 2D arrays', *Physical Chemistry Chemical Physics*, 16: 26153-62.

Makaraviciute, A, A Ramanavicius, and A Ramanaviciene. 2015. 'Development of a reusable protein G based SPR immunosensor for direct human growth hormone detection in real samples', *Analytical Methods*, 7: 9875-84.

Margolis, Leonid, and Yoel Sadovsky. 2019. 'The biology of extracellular vesicles: The known unknowns', *PLoS biology*, 17: e3000363.

Marinakos, Stella M, Sihai Chen, and Ashutosh Chilkoti. 2007. 'Plasmonic detection of a model analyte in serum by a gold nanorod sensor', *Analytical chemistry*, 79: 5278-83.

Mastoridis, Sotiris, Giuliana Minani Bertolino, Gavin Whitehouse, Francesco Dazzi, Alberto Sanchez-Fueyo, and Marc Martinez-Llordella. 2018. 'Multiparametric analysis of circulating exosomes and other small extracellular vesicles by advanced imaging flow cytometry', *Frontiers in immunology*, 9: 1583.

Mayer, Kathryn M, and Jason H Hafner. 2011. 'Localized surface plasmon resonance sensors', *Chemical reviews*, 111: 3828-57.

Mayer, Kathryn M, Seunghyun Lee, Hongwei Liao, Betty C Rostro, Amaris Fuentes, Peter T Scully, Colleen L Nehl, and Jason H Hafner. 2008. 'A label-free immunoassay based upon localized surface plasmon resonance of gold nanorods', *ACS nano*, 2: 687-92.

McNanley, T, and J Woods. 2008. 'Placental physiology', *Global Library of Women's Medicine*: 659-69.

Mincheva-Nilsson, Lucia, and Vladimir Baranov. 2014. 'Placenta-derived exosomes and syncytiotrophoblast microparticles and their role in human reproduction: immune modulation for pregnancy success', *American Journal of Reproductive Immunology*, 72: 440-57.

Mitchell, Murray D, Hassendrini N Peiris, Miharu Kobayashi, Yong Q Koh, Gregory Duncombe, Sebastian E Illanes, Gregory E Rice, and Carlos Salomon. 2015. 'Placental exosomes in normal and complicated pregnancy', *American journal of obstetrics and gynecology*, 213: S173-S81.

Montecalvo, Angela, Adriana T Larregina, William J Shufesky, Donna Beer Stolz, Mara LG Sullivan, Jenny M Karlsson, Catherine J Baty, Gregory A Gibson, Geza Erdos, and Zhiliang Wang. 2012. 'Mechanism of transfer of functional microRNAs between mouse dendritic cells via exosomes', *Blood, The Journal of the American Society of Hematology*, 119: 756-66.

Mulcahy, Laura Ann, Ryan Charles Pink, and David Raul Francisco Carter. 2014. 'Routes and mechanisms of extracellular vesicle uptake', *Journal of extracellular vesicles*, 3: 24641.

Mun'delanji, C Vestergaard, Kagan Kerman, I-Ming Hsing, and Eiichi Tamiya. 2015. *Nanobiosensors and Nanobioanalyses* (Springer).

Munson, Phillip, and Arti Shukla. 2015. 'Exosomes: potential in cancer diagnosis and therapy', *Medicines*, 2: 310-27.

Nabet, Barzin Y, Yu Qiu, Jacob E Shabason, Tony J Wu, Taewon Yoon, Brian C Kim, Joseph L Benci, Angela M DeMichele, Julia Tchou, and Joseph Marcotrigiano. 2017. 'Exosome RNA unshielding couples stromal activation to pattern recognition receptor signaling in cancer', *cell*, 170: 352-66. e13.

Near, Rachel D, Steven C Hayden, Ronald E Hunter Jr, Daniel Thackston, and Mostafa A El-Sayed. 2013. 'Rapid and efficient prediction of optical extinction coefficients for gold nanospheres and gold nanorods', *The Journal of Physical Chemistry C*, 117: 23950-55.

Nehl, Colleen L, and Jason H Hafner. 2008. 'Shape-dependent plasmon resonances of gold nanoparticles', *Journal of Materials Chemistry*, 18: 2415-19.

Nolan, John P, and Jennifer C Jones. 2017. 'Detection of platelet vesicles by flow cytometry', *Platelets*, 28: 256-62.

Oh, Seo Yeong, Nam Su Heo, Sung-Chan Jang, Gyeongsik Ok, Youngjin Cho, and Yun Suk Huh. 2019. 'Development of a Cuvette-Based LSPR Sensor Chip Using a Plasmonically Active Transparent Strip', *Frontiers in bioengineering and biotechnology*, 7: 299.

Oksvold, Morten P, Anette Kullmann, Lise Forfang, Bente Kierulf, Mu Li, Andreas Brech, Alexander V Vlassov, Erlend B Smeland, Axl Neurauter, and Ketil W Pedersen. 2014. 'Expression of B-cell surface antigens in subpopulations of exosomes released from B-cell lymphoma cells', *Clinical therapeutics*, 36: 847-62. e1.

Oksvold, Morten P, Axl Neurauter, and Ketil W Pedersen. 2015. 'Magnetic bead-based isolation of exosomes.' in, *RNA Interference* (Springer).

Oliveira-Rodríguez, Myriam, Sheila López-Cobo, Hugh T Reyburn, Agustín Costa-García, Soraya López-Martín, María Yáñez-Mó, Eva Cernuda-Morollón, Annette Paschen, Mar Valés-Gómez, and Maria Carmen Blanco-López. 2016. 'Development of a rapid lateral flow immunoassay test for detection of exosomes previously enriched from cell culture medium and body fluids', *Journal of extracellular vesicles*, 5: 31803.

Osaki, Mitsuhiko, and Futoshi Okada. 2019. 'Exosomes and their role in cancer progression', *Yonago Acta Medica*, 62: 182-90.

Ostrowski, Matias, Nuno B Carmo, Sophie Krumeich, Isabelle Fanget, Graça Raposo, Ariel Savina, Catarina F Moita, Kristine Schauer, Alistair N Hume, and Rui P Freitas. 2010. 'Rab27a and Rab27b control different steps of the exosome secretion pathway', *Nature cell biology*, 12: 19-30.

Palmieri, Valentina, Donatella Lucchetti, Ilaria Gatto, Alessandro Maiorana, Margherita Marcantoni, Giuseppe Maulucci, Massimiliano Papi, Roberto Pola, Marco De Spirito, and Alessandro Sgambato. 2014. 'Dynamic light scattering for the characterization and counting of extracellular vesicles: a powerful noninvasive tool', *Journal of nanoparticle research*, 16: 2583.

Parolini, Isabella, Cristina Federici, Carla Raggi, Luana Lugini, Simonetta Palleschi, Angelo De Milito, Carolina Coscia, Elisabetta Iessi, Mariantonia Logozzi, and Agnese Molinari. 2009. 'Microenvironmental pH is a key factor for exosome traffic in tumor cells', *Journal of Biological Chemistry*, 284: 34211-22.

Patel, Girijesh Kumar, Mohammad Aslam Khan, Haseeb Zubair, Sanjeev Kumar Srivastava, Seema Singh, and Ajay Pratap Singh. 2019. 'Comparative analysis of exosome isolation methods using culture supernatant for optimum yield, purity and downstream applications', *Scientific reports*, 9: 1-10.

Pedersen, Ketil W, Bente Kierulf, Morten P Oksvold, Mu Li, Alexander V Vlassov, Norbert Roos, Anette Kullmann, and Axl Neurauter. 2013. 'Isolation and characterization of exosomes using magnetic beads', *markers*, 13: 14.

Pegtel, D Michiel, and Stephen J Gould. 2019. 'Exosomes', *Annual review of biochemistry*, 88: 487-514.

Pillay, Preenan, Niren Maharaj, Jagidesa Moodley, and Irene Mackraj. 2016. 'Placental exosomes and pre-eclampsia: maternal circulating levels in normal pregnancies and, early and late onset pre-eclamptic pregnancies', *Placenta*, 46: 18-25.

Pospichalova, Vendula, Jan Svoboda, Zankruti Dave, Anna Kotrbova, Karol Kaiser, Dobromila Klemova, Ladislav Ilkovics, Ales Hampl, Igor Crha, and Eva Jandakova. 2015. 'Simplified protocol for flow cytometry analysis of fluorescently labeled exosomes and microvesicles using dedicated flow cytometer', *Journal of extracellular vesicles*, 4: 25530.

Prime, Kevin L, and George M Whitesides. 1993. 'Adsorption of proteins onto surfaces containing end-attached oligo (ethylene oxide): a model system using self-assembled monolayers', *Journal of the American Chemical Society*, 115: 10714-21.

Quek, Camelia, and Andrew F Hill. 2017. 'The role of extracellular vesicles in neurodegenerative diseases', *Biochemical and biophysical research communications*, 483: 1178-86.

Raghu, Deepa, Joseph A Christodoulides, Marc Christophersen, Jinny L Liu, George P Anderson, Michael Robitaille, Jeff M Byers, and Marc P Raphael. 2018. 'Nanoplasmonic pillars engineered for single exosome detection', *PloS one*, 13: e0202773.

Rahmati, Shima, Fereshteh Shojaei, Ali Shojaeian, Leila Rezakhani, and Mehdi Banitalebi Dehkordi. 2019. 'An overview of current knowledge in biological functions and potential theragnostic applications of exosomes', *Chemistry and physics of lipids*: 104836.

Rahme, Kamil, Lan Chen, Richard G Hobbs, Michael A Morris, Caitriona O'Driscoll, and Justin D Holmes. 2013. 'PEGylated gold nanoparticles: polymer quantification as a function of PEG lengths and nanoparticle dimensions', *RSC Advances*, 3: 6085-94.

Rajendran, Lawrence, Masanori Honsho, Tobias R Zahn, Patrick Keller, Kathrin D Geiger, Paul Verkade, and Kai Simons. 2006. 'Alzheimer's disease β-amyloid peptides are released in association with exosomes', *Proceedings of the National Academy of Sciences*, 103: 11172-77.

Raposo, Graça, and Willem Stoorvogel. 2013. 'Extracellular vesicles: exosomes, microvesicles, and friends', *J Cell Biol*, 200: 373-83.

Rojalin, Tatu, Brian Phong, Hanna J Koster, and Randy P Carney. 2019. 'Nanoplasmonic approaches for sensitive detection and molecular characterization of extracellular vesicles', *Frontiers in chemistry*, 7.

Rupert, Déborah LM, Cecilia Lässer, Maria Eldh, Stephan Block, Vladimir P Zhdanov, Jan O Lotvall, Marta Bally, and Fredrik Höök. 2014. 'Determination of exosome concentration in solution using surface plasmon resonance spectroscopy', *Analytical chemistry*, 86: 5929-36.

Sabapatha, Anuradha, Cicek Gercel-Taylor, and Douglas D Taylor. 2006. 'Specific Isolation of Placenta-Derived Exosomes from the Circulation of Pregnant Women and Their Immunoregulatory Consequences 1', *American Journal of Reproductive Immunology*, 56: 345-55.

Salih, Mahdi, Robert A Fenton, Jeroen Knipscheer, Joost W Janssen, Mirella S Vredenbregt-van den Berg, Guido Jenster, Robert Zietse, and Ewout J Hoorn. 2016. 'An immunoassay for urinary extracellular vesicles', *American Journal of Physiology-Renal Physiology*, 310: F796-F801.

Salomon, Carlos, Miharu Kobayashi, Keith Ashman, Luis Sobrevia, Murray D Mitchell, and Gregory E Rice. 2013. 'Hypoxia-induced changes in the bioactivity of cytotrophoblast-derived exosomes', *PloS one*, 8.

Salomon, Carlos, Maria Jose Torres, Miharu Kobayashi, Katherin Scholz-Romero, Luis Sobrevia, Aneta Dobierzewska, Sebastian E Illanes, Murray D Mitchell, and Gregory E Rice. 2014. 'A gestational profile of placental exosomes in maternal plasma and their effects on endothelial cell migration', *PloS one*, 9: e98667.

Sarangan, Andrew. 2016. *Nanofabrication: Principles to Laboratory Practice* (CRC Press).

Scarpettini, Alberto F, and Andrea V Bragas. 2010. 'Coverage and aggregation of gold nanoparticles on silanized glasses', *Langmuir*, 26: 15948-53.

Shao, Huilin, Jaehoon Chung, Kyungheon Lee, Leonora Balaj, Changwook Min, Bob S Carter, Fred H Hochberg, Xandra O Breakefield, Hakho Lee, and Ralph Weissleder. 2015. 'Chip-based analysis of exosomal mRNA mediating drug resistance in glioblastoma', *Nature communications*, 6: 6999.

Sherry, Leif J, Shih-Hui Chang, George C Schatz, Richard P Van Duyne, Benjamin J Wiley, and Younan Xia. 2005. 'Localized surface plasmon resonance spectroscopy of single silver nanocubes', *Nano letters*, 5: 2034-38.

Sisquella, Xavier, Yifat Ofir-Birin, Matthew A Pimentel, Lesley Cheng, Paula Abou Karam, Natália G Sampaio, Jocelyn Sietsma Penington, Dympna Connolly, Tal Giladi, and Benjamin J Scicluna. 2017. 'Malaria parasite DNA-harbouring vesicles activate cytosolic immune sensors', *Nature communications*, 8: 1-15.

Smith, Ashley M, Lauren E Marbella, Kathryn A Johnston, Michael J Hartmann, Scott E Crawford, Lisa M Kozycz, Dwight S Seferos, and Jill E Millstone. 2015.

'Quantitative analysis of thiolated ligand exchange on gold nanoparticles monitored by 1H NMR spectroscopy', *Analytical chemistry*, 87: 2771-78.

Smith, Danielle K, and Brian A Korgel. 2008. 'The importance of the CTAB surfactant on the colloidal seed-mediated synthesis of gold nanorods', *Langmuir*, 24: 644-49.

Su, K-H, Q-H Wei, X Zhang, JJ Mock, David R Smith, and S Schultz. 2003. 'Interparticle coupling effects on plasmon resonances of nanogold particles', *Nano letters*, 3: 1087-90.

Sullivan, Robert, Fabrice Saez, Julie Girouard, and Gilles Frenette. 2005. 'Role of exosomes in sperm maturation during the transit along the male reproductive tract', *Blood Cells, Molecules, and Diseases*, 35: 1-10.

Sun, Li, Rongman Xu, Xiaoxian Sun, Yuping Duan, Yiwen Han, Yuanyuan Zhao, Hui Qian, Wei Zhu, and Wenrong Xu. 2016. 'Safety evaluation of exosomes derived from human umbilical cord mesenchymal stromal cell', *Cytotherapy*, 18: 413-22.

Tai, Yu-Ling, Ko-Chien Chen, Jer-Tsong Hsieh, and Tang-Long Shen. 2018. 'Exosomes in cancer development and clinical applications', *Cancer science*, 109: 2364-74.

Tauro, Bow J, David W Greening, Rommel A Mathias, Hong Ji, Suresh Mathivanan, Andrew M Scott, and Richard J Simpson. 2012. 'Comparison of ultracentrifugation, density gradient separation, and immunoaffinity capture methods for isolating human colon cancer cell line LIM1863-derived exosomes', *Methods*, 56: 293-304.

Teng, Xiaomei, Lei Chen, Weiqian Chen, Junjie Yang, Ziying Yang, and Zhenya Shen. 2015. 'Mesenchymal stem cell-derived exosomes improve the microenvironment of infarcted myocardium contributing to angiogenesis and anti-inflammation', *Cellular Physiology and Biochemistry*, 37: 2415-24.

Teow, Sin-Yeang, Alif Che Nordin, Syed A Ali, and Alan Soo-Beng Khoo. 2016. 'Exosomes in human immunodeficiency virus type I pathogenesis: threat or opportunity?', *Advances in virology*, 2016.

Thakur, Abhimanyu, Guangyu Qiu, NG Siu-Pang, Jintao Guan, Jianbo Yue, Youngjin Lee, and Chi-Man Lawrence Wu. 2017. 'Direct detection of two different tumor-derived extracellular vesicles by SAM-AuNIs LSPR biosensor', *Biosensors and Bioelectronics*, 94: 400-07.

Théry, Clotilde, Sebastian Amigorena, Graça Raposo, and Aled Clayton. 2006. 'Isolation and characterization of exosomes from cell culture supernatants and biological fluids', *Current protocols in cell biology*, 30: 3.22. 1-3.22. 29.

Thierry, Benjamin, Jane Ng, Tina Krieg, and Hans J Griesser. 2009. 'A robust procedure for the functionalization of gold nanorods and noble metal nanoparticles', *Chemical Communications*: 1724-26.

Tian, Limei, Enze Chen, Naveen Gandra, Abdennour Abbas, and Srikanth Singamaneni. 2012. 'Gold nanorods as plasmonic nanotransducers: distance-dependent refractive index sensitivity', *Langmuir*, 28: 17435-42.

Tian, Tian, Yan-Liang Zhu, Yue-Yuan Zhou, Gao-Feng Liang, Yuan-Yuan Wang, Fei-Hu Hu, and Zhong-Dang Xiao. 2014. 'Exosome uptake through clathrin-mediated endocytosis and macropinocytosis and mediating miR-21 delivery', *Journal of Biological Chemistry*, 289: 22258-67.

Timmers, Leo, Sai Kiang Lim, Imo E Hoefer, Fatih Arslan, Ruenn Chai Lai, Angelique AM van Oorschot, Marie Jose Goumans, Chaylendra Strijder, Sui Kwan Sze, and Andree Choo. 2011. 'Human mesenchymal stem cell-conditioned medium improves cardiac function following myocardial infarction', *Stem cell research*, 6: 206-14.

Vaidyanathan, Ramanathan, Maedeh Naghibosadat, Sakandar Rauf, Darren Korbie, Laura G Carrascosa, Muhammad JA Shiddiky, and Matt Trau. 2014. 'Detecting exosomes specifically: a multiplexed device based on alternating current electrohydrodynamic induced nanoshearing', *Analytical chemistry*, 86: 11125-32.

van der Post, Joris AM, Christianne AR Lok, Kees Boer, Auguste Sturk, Ian L Sargent, and Rienk Nieuwland. 2011. "The functions of microparticles in pre-eclampsia." In *Seminars in thrombosis and hemostasis*, 146-52. © Thieme Medical Publishers.

Vlassov, Alexander V, Susan Magdaleno, Robert Setterquist, and Rick Conrad. 2012. 'Exosomes: current knowledge of their composition, biological functions, and diagnostic and therapeutic potentials', *Biochimica et Biophysica Acta (BBA)-General Subjects*, 1820: 940-48.

Vojtech, Lucia, Sangsoon Woo, Sean Hughes, Claire Levy, Lamar Ballweber, Renan P Sauteraud, Johanna Strobl, Katharine Westerberg, Raphael Gottardo, and Muneesh Tewari. 2014. 'Exosomes in human semen carry a distinctive repertoire of small non-coding RNAs with potential regulatory functions', *Nucleic acids research*, 42: 7290-304.

Wang, Yanyan, and Liang Tang. 2013. 'Chemisorption assembly of Au nanorods on mercaptosilanized glass substrate for label-free nanoplasmon biochip', *Analytica chimica acta*, 796: 122-29.

Watson, Dionysios C, Defne Bayik, Avinash Srivatsan, Cristina Bergamaschi, Antonio Valentin, Gang Niu, Jenifer Bear, Mitchell Monninger, Mei Sun, and Aizea

Morales-Kastresana. 2016. 'Efficient production and enhanced tumor delivery of engineered extracellular vesicles', *Biomaterials*, 105: 195-205.

Weinrib, Hadas, Amihai Meiri, Hamootal Duadi, and Dror Fixler. 2012. 'Uniformly immobilizing gold nanorods on a glass substrate', *Journal of Atomic, Molecular, and Optical Physics*, 2012.

Welch, Jennifer L, Hussein Kaddour, Patrick M Schlievert, Jack T Stapleton, and Chioma M Okeoma. 2018. 'Semen exosomes promote transcriptional silencing of HIV-1 by disrupting NF-κB/Sp1/Tat circuitry', *Journal of virology*, 92: e00731-18.

Welch, Jennifer L, Jack T Stapleton, and Chioma M Okeoma. 2019. 'Vehicles of intercellular communication: exosomes and HIV-1', *Journal of General Virology*, 100: 350-66.

Wijaya, Andy, and Kimberly Hamad-Schifferli. 2008. 'Ligand customization and DNA functionalization of gold nanorods via round-trip phase transfer ligand exchange', *Langmuir*, 24: 9966-69.

Willets, Katherine A, and Richard P Van Duyne. 2007. 'Localized surface plasmon resonance spectroscopy and sensing', *Annu. Rev. Phys. Chem.*, 58: 267-97.

Wu, Miaowei, Guosheng Wang, Weilei Hu, Yihan Yao, and Xiao-Fang Yu. 2019. 'Emerging roles and therapeutic value of exosomes in cancer metastasis', *Molecular cancer*, 18: 53.

Xue, Yurui, Xun Li, Hongbin Li, and Wenke Zhang. 2014. 'Quantifying thiol–gold interactions towards the efficient strength control', *Nature communications*, 5: 1-9.

Yamashita, Takuma, Yuki Takahashi, and Yoshinobu Takakura. 2018. 'Possibility of exosome-based therapeutics and challenges in production of exosomes eligible for therapeutic application', *Biological and Pharmaceutical Bulletin*, 41: 835-42.

Yang, Yuting, Guangxia Shen, Hui Wang, Hongxia Li, Ting Zhang, Nongjian Tao, Xianting Ding, and Hui Yu. 2018. 'Interferometric plasmonic imaging and detection of single exosomes', *Proceedings of the National Academy of Sciences*, 115: 10275-80.

Yochelis, Shira, Eran Katzir, Yoav Kalcheim, Vitaly Gutkin, Oded Millo, and Yossi Paltiel. 2012. 'Formation of Au-Silane Bonds', *Journal of Nanotechnology*, 2012.

Yong, QIU, MA Jing, and ZENG Yi. 2018. 'Therapeutic Potential of Anti-HIV RNA-loaded Exosomes', *Biomedical and environmental sciences*, 31: 215-26.

Yu, Li-Li, Jing Zhu, Jin-Xia Liu, Feng Jiang, Wen-Kai Ni, Li-Shuai Qu, Run-Zhou Ni, Cui-Hua Lu, and Ming-Bing Xiao. 2018. 'A comparison of traditional and novel methods for the separation of exosomes from human samples', *BioMed research international*, 2018.

Yuan, Lin, and Jia-Yi Li. 2019. 'Exosomes in Parkinson's disease: current perspectives and future challenges', *ACS chemical neuroscience*, 10: 964-72.

Yuana, Yuana, Auguste Sturk, and Rienk Nieuwland. 2013. 'Extracellular vesicles in physiological and pathological conditions', *Blood reviews*, 27: 31-39.

Zakharova, Liudmila, Maria Svetlova, and Alla F Fomina. 2007. 'T cell exosomes induce cholesterol accumulation in human monocytes via phosphatidylserine receptor', *Journal of cellular physiology*, 212: 174-81.

Zhang, Guohua, Zhelong Liu, Hui Ding, Yong Zhou, Hoang Anh Doan, Ka Wai Thomas Sin, Zhiren J Zhu, Rene Flores, Yefei Wen, and Xing Gong. 2017. 'Tumor induces muscle wasting in mice through releasing extracellular Hsp70 and Hsp90', *Nature communications*, 8: 1-16.

Zhang, Peng, Mei He, and Yong Zeng. 2016. 'Ultrasensitive microfluidic analysis of circulating exosomes using a nanostructured graphene oxide/polydopamine coating', *Lab on a Chip*, 16: 3033-42.

Zhang, Wei, Zi-Li Yu, Min Wu, Jian-Gang Ren, Hou-Fu Xia, Guo-Liang Sa, Jun-Yi Zhu, Dai-Wen Pang, Yi-Fang Zhao, and Gang Chen. 2017. 'Magnetic and folate functionalization enables rapid isolation and enhanced tumor-targeting of cell-derived microvesicles', *ACS nano*, 11: 277-90.

Zhang, Yuan, Yunfeng Liu, Haiying Liu, and Wai Ho Tang. 2019. 'Exosomes: biogenesis, biologic function and clinical potential', *Cell & bioscience*, 9: 19.

Zhu, Ling, Kun Wang, Jian Cui, Huan Liu, Xiangli Bu, Huailei Ma, Weizhi Wang, He Gong, Christopher Lausted, and Leroy Hood. 2014. 'Label-free quantitative detection of tumor-derived exosomes through surface plasmon resonance imaging', *Analytical chemistry*, 86: 8857-64.

APPENDIX I. CALCULATIONS

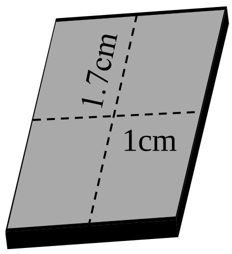

$Surface\ Area\ of\ the\ Wafer\ (\boldsymbol{A_w})$: $1.7\ cm\ x\ 1\ cm = \mathbf{1.7\ cm^2}$

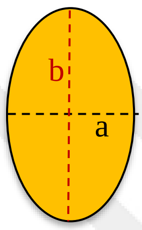

$Surface\ Area\ of\ the\ AuNR\ (\boldsymbol{A_{AuNR}})$: πab

$\boldsymbol{A_{AuNR}} = \pi\ x\ 40\ nm\ x\ 17\ nm = \mathbf{1758\ nm^2}$

(assuming ellipse shape)

Antibody Amount Calculations:

$Surface\ Area\ of\ an\ Antibody\ (\boldsymbol{A_{Ab}})$: $\pi r^2 = \pi\ x\ 5^2\ nm^2 = \mathbf{78.5\ nm^2}$

(assuming an average size of 10 nm for an antibody and uniform circular shape)

$$Max\ number\ of\ AuNRs\ on\ the\ surface: \frac{\boldsymbol{A_w}}{\boldsymbol{A_{AuNR}}} = 1.7\ x\ 10^{14}\ nm^2/1758\ nm^2$$

$$= \#\ \boldsymbol{of\ AuNRs} = \mathbf{9.7\ x\ 10^{10}}\ \boldsymbol{AuNRs}$$

(assuming all the surface covered with AuNRs without any gap)

$$Max\ number\ of\ Antibody\ on\ the\ AuNR: \frac{\boldsymbol{A_{AuNR}}}{\boldsymbol{A_{Ab}}} = 1758\ nm^2/\ 78.5\ nm^2 = \mathbf{22}\ \boldsymbol{Ab}$$

$$Max\ number\ of\ Antibody\ on\ the\ wafer: \#\ \boldsymbol{of\ AuNRs\ x}\ \#\ \boldsymbol{of\ Ab}$$

$$= \mathbf{2.1\ x\ 10^{12}}\ \boldsymbol{Ab}$$

$$Max\ required\ Ab\ amount: \frac{\boldsymbol{max\ number\ of\ Ab}}{\boldsymbol{N_{Avogadro}}} \boldsymbol{x\ M_w\ of\ an\ Ab}$$

$$= \frac{2.1\ x\ 10^{12}\ Ab}{6.02\ x\ 10^{23}\ molecule/mol} x\ 150000\ x\ 10^{6}\ \mu g/mol = \mathbf{0.5}\ \mu\boldsymbol{g\ Ab}$$

(assuming an average molecular weight for an Antibody is 150000 g/mol)

$Surface\ Area\ of\ an\ small\ alkane\ thiol\ (\boldsymbol{A_{COOH}}): \pi r^2 = \pi\ x\ 0.5^2\ nm^2 =$ $\mathbf{0.78}\ \boldsymbol{nm^2}$ (assuming an average size of 1 nm for an antibody and uniform circular shape)

Self-assembly molecule amount calculations:

$$Max\ required\ COOH\ amount: \frac{\boldsymbol{max\ number\ of\ COOH}}{\boldsymbol{N_{Avogadro}}} \boldsymbol{x\ M_w\ of\ COOH}$$

$$= \frac{2250\ x\ 10^{12}\ COOH}{6.02\ x\ 10^{23}\ molecule/mol} x\ 218\ x\ 10^{6}\ \mu g/mol = \mathbf{0.08}\ \mu\boldsymbol{g\ COOH}$$

APPENDIX II. FIGURES

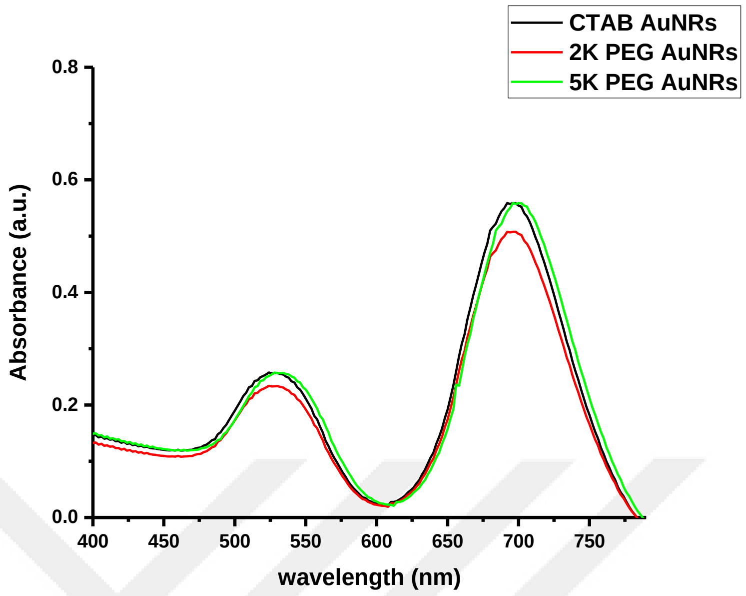

Figure A1. UV-vis spectra for CTAB, 2 kDa and 5 kDa PEG stabilized AuNRs in solution

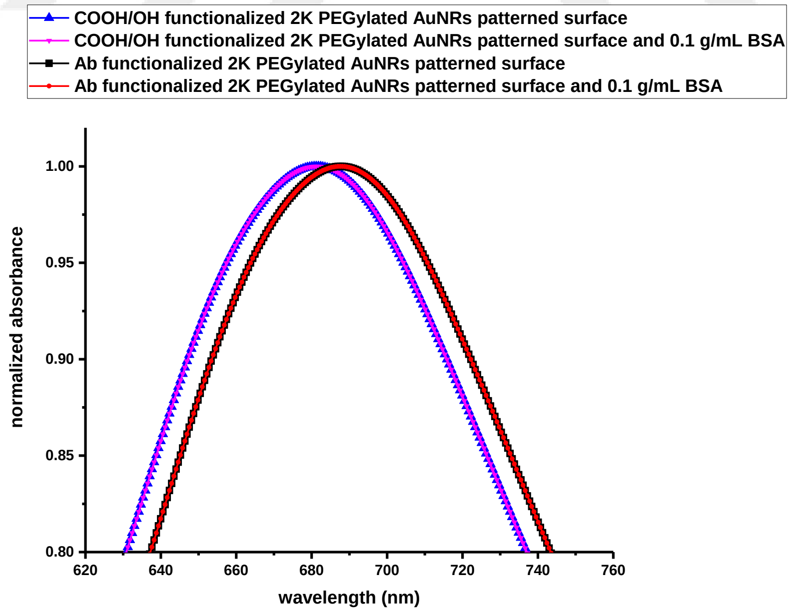

Figure A2. Control experiments for 2K PEGylated AuNRs patterned surfaces after surface functionalization with COOH/OH and treatment with BSA. COOH/OH surfaces further modified with relevant antibodies (Ab) via EDC/NHS chemistry and followed by BSA incubation

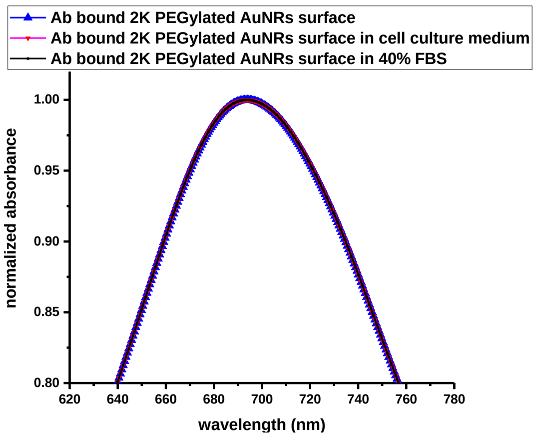

Figure A3. Control experiments: antibody (Ab) functionalized 2K PEGylated AuNRs patterned surfaces in PBS, in cell culture medium and cell culture medium having 40% v/v FBS. The result shows that the Ab bound surfaces did not have any detectable non-specific binding in cell culture media with or without FBS.

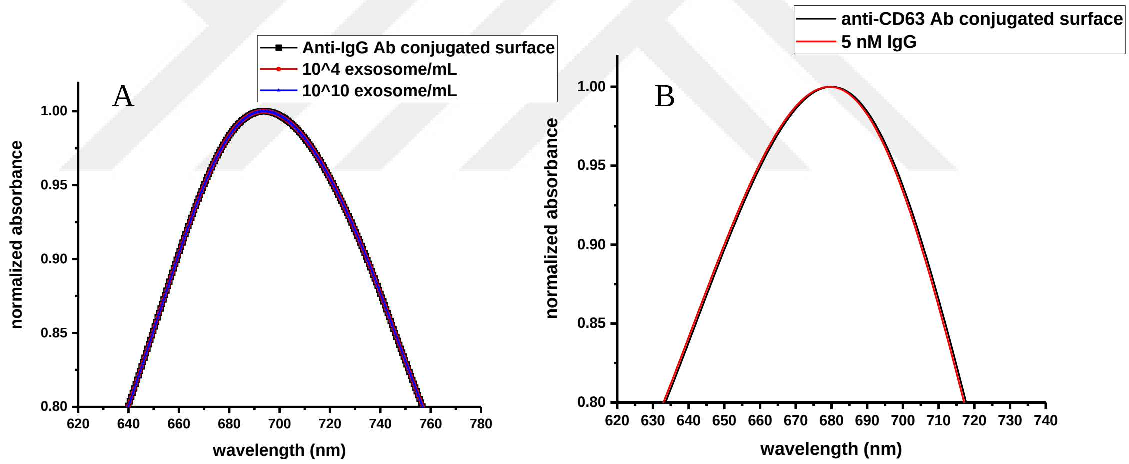

Figure A4. Control experiments: anti-IgG antibody conjugated surface before and after interaction with exosome solution at 10^4 and 10^{10} exosomes/mL concentrations (A) and anti-CD63 antibody conjugated surface before and after interaction with 5 nM IgG solution. There were no detectable non-specific binding events, suggesting that the exosome detection by surfaces functionalized with anti-CD63 antibodies happened through specific binding events.

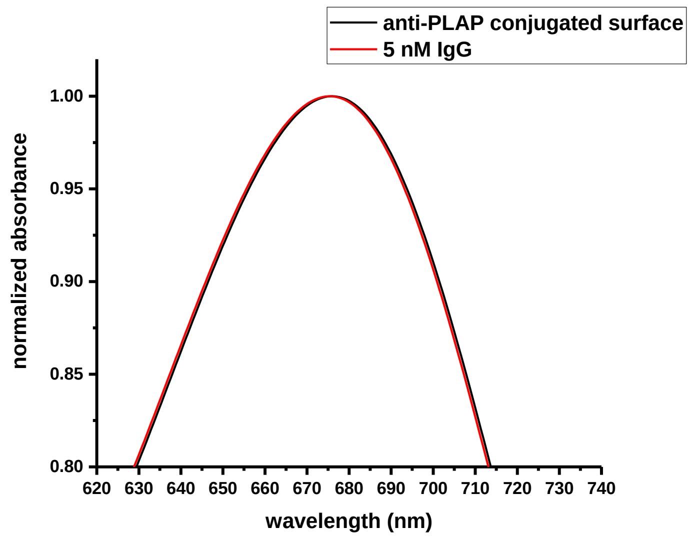

Figure A5. Specificity control experiments with anti-PLAP antibody conjugated surface before and after interaction with 5nM IgG solution.

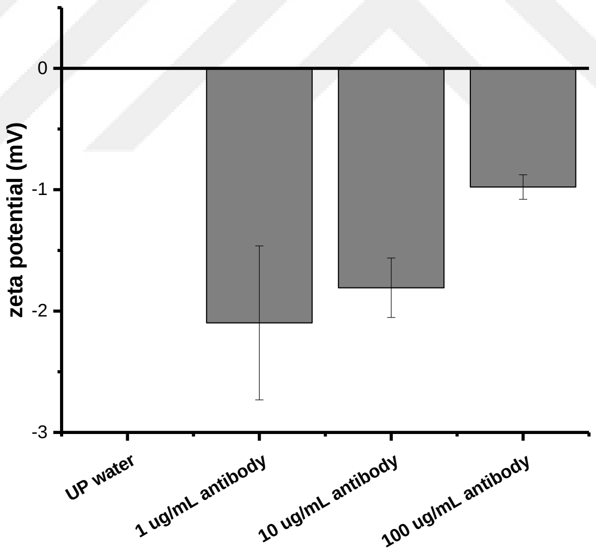

/

Figure A6. Zeta potential of antibodies in UP water at 1 µg/mL, 10 µg/mL and 100 µg/mL concentrations.

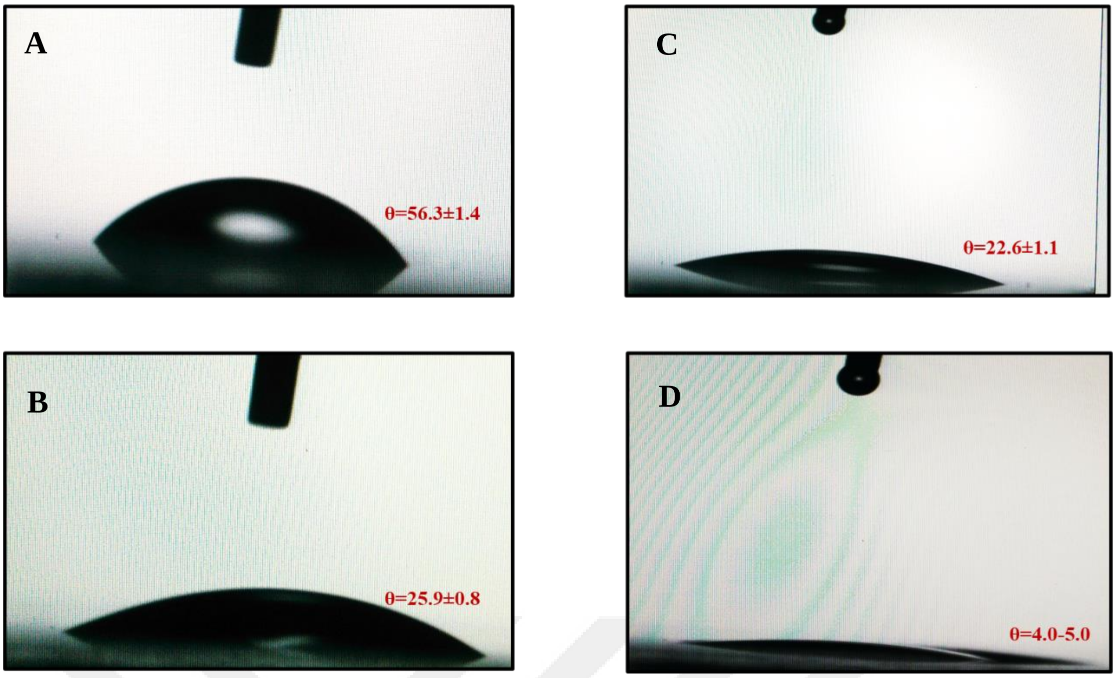

Figure A7. Contact angle measurements of microscope slides before any treatment at time zero (A), and after 5 seconds (B), after piranha treatment at time zero (C) and after 5 seconds (D)

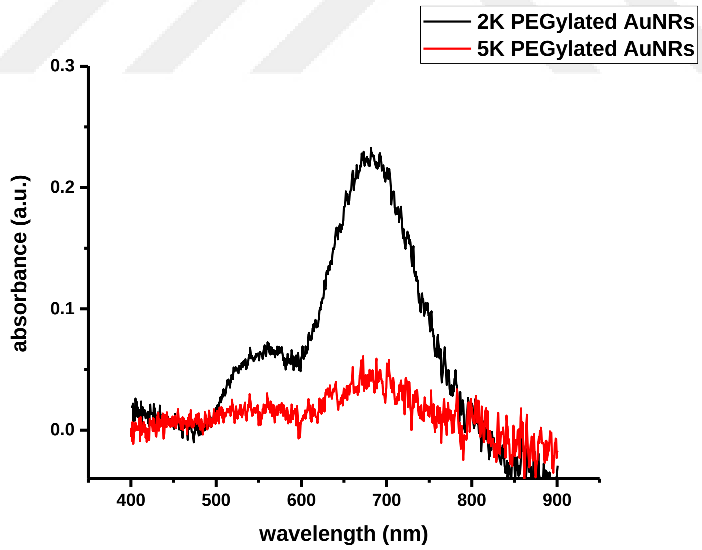

Figure A8. Raw LSPR data for 2K PEGylated and 5K PEGylated AuNRs patterned slides

CURRICULUM VITAE

1. PERSONAL INFORMATION

NAME/SURNAME	Damla Taykoz
BIRTHPLACE/DATE	Ankara/TURKEY - 28.08.1988
TEL	+90 505 655 32 90
E-MAIL	damlataykoz@gmail.com

2. EDUCATION

İzmir Institute of Technology Chemical Engineering, PhD, GPA: 3.93, Year: 2020
İzmir Institute of Technology Chemical Engineering, MSc, GPA: 3.71, Year: 2014
Hacettepe University Chemical Engineering, BSc, GPA: 3.10, Year: 2011

3. ACADEMICAL EXPERIENCE

İzmir Institute of Technology: Chemical Engineering, Research Assistant, Years: 2012-2020
University of Washington: Bioengineering, Research Fellow, Years: 2018-2019
von Karman Institute for Fluid Dynamics: Environmental and Applied Fluid Dynamics, Intern, 2010

4. PROJECT EXPERIENCE

PROJECT NAME	ORGANIZATION	TASK
Detection of Exosomes on Microfluidic Surfaces via LSPR Method	University of Washington / TUBITAK 2214/A	PI and Researcher
Preparation of Polymer-Peptide Conjugates for Biomedical Applications	İzmir Institute of Technology	Researcher
Curcumin Loaded Block Copolymer Micelles: Preparation, Characterization and Applications in Drug Delivery	İzmir Institute of Technology/Özel Ege High School	Researcher
Arginine Polymers for Gene Delivery	TUBITAK	Researcher
Synthesis of Biosynthetic Hybrid Polymers via RAFT Polymerization and *in vitro* Investigations of Polymers	TUBITAK	Researcher
Photosynthetic Biofuel cell for Energy Production	TUBITAK 2209/A	PI and Researcher

5. PUBLICATIONS

Articles:

Damla Taykoz, James Lai, Lucia N. Vojtech, Patrick Stayton and Volga Bulmus, "Highly Sensitive and Repeatable LSPR Chip Development for Improved Exosome Detection", *Submitted*
Damla Taykoz, Aykut Zelcak, Kadir Gul and Volga Bulmus, "Curcumin Loaded Micelles and Polymersomes", *Submitted*
Hajeeth Thankappan, Aykut Zelcak, **Damla Taykoz** and Volga Bulmus, "Efficient Synthesis of cRGD Functionalized Polymers as Building Blocks of Targeted Drug Delivery Systems", *European Polymer Journal, Volume 103, Pages 421-432,* 2018.

Posters and Oral Presentations:

Damla Taykoz, James Lai, Patrick Stayton and Volga Bulmus, "Development of LSPR Surfaces with High Sensitivity and Improved Antifouling Properties", **Oral Presentation** at 6th International Conference on Advances in Chemical Engineering & Technology, 02-03 March 2020 London/UK
Damla Taykoz, Deniz Uğur and Volga Bulmuş, "Synthesis, Characterization and in vitro Evaluation of Arginine Polymers", **Poster** presented at World Polymer Congress (*MACRO 2016*), 17-21 July 2016 İstanbul/TURKEY
Merve Kanargı, Gökmen Oğuzcan Hamza, **Damla Taykoz** and Volga Bulmuş, "Arginine Polymers for Gene Delivery" **Poster** presented at IZTECH *Chemical Engineering Competition*, 12 June 2015 İzmir/TURKEY
Damla Taykoz and Volga Bulmuş, "Development of Arginine Containing Well-defined Polymers and Investigation of Complexation with DNA", **Poster** presented at 20th International Biomedical Science and Technology Symposium (*BIOMED 2014*), 23-26 August 2014 Muğla/TURKEY

Thesis:

Damla Taykoz, "Development of Arginine-Containing Well-Defined Polymers" *MSc. Thesis*, 2014